TECHNISCHE UNIVERSITÄT WIEN
VIENNA UNIVERSITY OF TECHNOLOGY

Master Thesis

Elliptical method for time-domain quantification of the arterial baroreflex

by

Joana Barros de Brito

Registration Number 11831527

Submitted to the research group Biomedical Sensors

Institute of Electrodynamics, Microwave and Circuit Engineering

TU Wien

Supervised by

Univ.-Ass. Dipl. Ing. Babak Dabiri

&

Ao. Univ. Prof. Dipl.-Ing. Dr. tech.
Eugenijus Kaniusas

Vienna, May 2021

Acknowledgements

Firstly, I would like to thank Univ.Ass. DI Babak Dabiri for his constant guidance and support during this year. I would also like to thank Ao. Univ. Prof. Dipl.Ing. Dr.techn. Eugenijus Kaniusas, for the valuable opportunity to be a part of the Biomedical Sensing research group of the Institute of Electrodynamics, Microwave and Circuit Engineering. Finally, I would like to thank Univ.Ass. DI Klaus Zeiner for his patience and perfect waveform of biosignals.

Furthermore, I would like to express my profound gratitude to my parents, Cristina and Pedro, and grandmothers, Teresa e Júlia, who gave me everything and most importantly, every piece of love they had. I would also like to thank the people I have loved in the two cities between which I split my academic path and eventually my heart. To Lisbon. To Pipa, who is the closest I came to having a sister. To Cat and Carlos, with whom I hope to sit in a porch when I become old and grey. To each member of Shishando and the moments I regret having missed. To Afonso, who taught me the joy of dancing. To Vienna. To Paulina, and her art of making things blossom. To George, but never on Sundays. To Antonio, for doing stuff. To Martina, to Elena, to Dario, to Alice. To the improbable harmony of the old rocks group. To Anton, who taught me that penguins fly but not too far. To many others who although not mentioned, shaped the last two years of my life in Vienna. This accomplishment would not be possible without them.

Abstract

The quantification of the cardiovagal baroreflex sensitivity *BRS* over postural changes has been regarded as a valuable prognostic indicator for evaluation of the current state of autonomic functions. The usual time domain assessment is based on the linear regression of both systolic blood pressure values P_S and cardiac period values *RR* during segments of increasing or decreasing trend. These fluctuations can occur spontaneously or be induced, e.g. by vasoactive drugs.

This work proposes a novel method using image processing of the area defined by rise and fall segments. The best fit ellipse to this area corresponds to the bivariate normal distribution of the pixel area and characterizes the spontaneous *BRS*. These segments are analysed both individually and as cycles, which are composed of consecutive sequences of opposing trend. The cycle analysis allows the quantification and characterization of changes in the *RR*-P_S relation related to the direction of pressure change (hysteresis) behaviour as change in working point and steepness.

The study was performed on the EuroBaVar dataset (21 subjects in supine and standing positions during 10 to 12 minutes). The data was composed of the blood pressure signal in the finger artery and the 2 lead electrocardiogram. Additionally, a Graphical User Interface including both regression and ellipse method as well as spectral analysis was implemented, allowing the cardiovagal baroreflex computation for any dataset.

Ellipse method results as BRS_e were compared with results from the regression method BRS_r. BRS_e mean value accurately reflects the sensitivity decrease due to postural change (14.9 and 7.2 ms/mmHg, $p < 0.005$) verifying the results obtained for BRS_r (respectively, 14.8 and 6.8 mmHg, $p < 0.005$). *BRS* estimates from the two methods were correlated with $r > 0.98$ in both positions. The characteristic ellipse median inclination with respect to the P_S axis was steeper in supine position (86.4°) compared to standing (81.9°) and the median elongation was higher in supine by about 46%. The median magnitude of overall hysteresis was 48% superior in supine position.

With the proposed method, hysteresis can be characterized using spontaneous (i.e. not pharmacologically induced) changes in P_S, providing a potential tool for future baroreflex characterization. On the other hand, this characterization heavily relies on the number of cycles found (only 4 subjects in this dataset showed a significant number of cycles) and further approval with other datasets is necessary.

Kurzfassung

Die Quantifizierung der kardiovagalen Baroreflex-Sensitivität *BRS* über posturale Veränderungen wurde als wertvoller prognostischer Indikator für die Bewertung des aktuellen Zustands der autonomen Funktionen angesehen. Die übliche Bewertung im Zeitbereich basiert auf der linearen Regression sowohl des systolischen Blutdrucks P_S als auch der Werte der Herzperiode *RR* während Segmenten mit steigendem oder fallendem Trend. Diese Schwankungen können spontan auftreten oder z. B. durch vasoaktive Medikamente induziert werden.

In dieser Arbeit wird eine neuartige Methode vorgeschlagen, die die Bildverarbeitung des durch Anstiegs- und Abfallsegmente (Zyklen) definierten Bereichs nutzt. Die am besten passende Ellipse zu diesem Bereich entspricht der bivariaten Normalverteilung der Pixelfläche und charakterisiert den spontanen kardiovagalen Baroreflex. Diese Segmente werden sowohl einzeln als auch als Zyklen, d. h. als aufeinanderfolgende Sequenzen mit gegenläufigem Trend, analysiert. Die Zyklusanalyse ermöglicht die Quantifizierung und Charakterisierung von Veränderungen in der RR-PS-Relation in Abhängigkeit von der Richtung der Druckänderung (Hysterese), wobei zwischen Arbeitspunkt und Steilheit unterschieden wird.

Die Studie wurde mit dem EuroBaVar-Datensatz durchgeführt (21 Probanden in Rückenlage und im Stehen während 10 bis 12 Minuten). Die Daten setzten sich aus dem Blutdrucksignal in der Fingerarterie und dem 2-Leiter-Elektrokardiogramm zusammen. Zusätzlich wurde eine grafische Benutzeroberfläche implementiert, die sowohl die Regressions- und Ellipsenmethode als auch die Spektralanalyse beinhaltet und die Berechnung des kardiovagalen Baroreflexes für jeden Datensatz ermöglicht.

Die Ergebnisse der Ellipsenmethode für die kardiale *BRS* (BRS_e) wurden mit den Ergebnissen der üblichen Methode (BRS_r) verglichen. Der BRS_e -Mittelwert spiegelt die Sensitivitätsabnahme aufgrund von Haltungsänderungen genau wider (14.9 bzw. 7.2 ms/mmHg, $p < 0.005$) und bestätigt die für BRS_r erzielten Ergebnisse (14.8 bzw. 6.8 mmHg, $p < 0.005$). Die beiden Methoden waren in beiden Positionen mit $r > 0.98$ korreliert. Die mediane Neigung der charakteristischen Ellipse in Bezug auf die P_S -Achse betrug 86.4° in Rückenlage und 81.9° im Stehen, wobei sie steiler und länglicher war (um etwa 46%). Die mediane Größe der Gesamthysterese war in der Rückenlage um 48% größer.

Mit der vorgeschlagenen Methode kann die Hysterese anhand von spontanen (d. h. nicht pharmakologisch induzierten) P_S-Änderungen charakterisiert werden, was ein potenzielles Werkzeug für die zukünftige Charakterisierung des Baroreflexes darstellt. Andererseits hängt diese Charakterisierung stark von der Anzahl der gefundenen Zyklen ab (nur 4 Probanden in diesem Datensatz zeigten eine signifikante Anzahl von Zyklen) und eine weitere Bestätigung mit anderen Datensätzen ist notwendig.

Abbreviations

AV	atrioventricular valves
BRS	cardiovagal baroreflex sensitivity
BRS	values of BRS
ECG	electrocardiogram
f_C	value of heart period
HF	high frequency
HR	heart rate
HRV	heart rate variability
HRV	values of HRV
IQR	interquartile range
LF	low frequency
p	P-value, null hypothesis likelihood according to the paired student's t-test
P	(intraarterial) blood pressure
P	values of P
<P>	mean (intraarterial) blood pressure
P_D	diastolic blood pressure
P_D	values of P_D
P_S	systolic blood pressure
P_S	values of P_S
PNS	parasympathetic nervous system
PPG	photoplethysmogram
RR	inter beat interval from electrocardiogram
RR	values of RR
R_T	values of total peripheral resistance
SA	sinoatrial
SL	semilunar valves
SNS	sympathetic nervous system
SPV	systolic pressure variability
SPV	values of SPV
V_S	(left) ventricular stroke volume

Contents

CHAPTER **1.**

Introduction

The baroreflex mechanism is the most important mechanism involved in the mid-term regulation of blood pressure, achieving a resolution of < 5 mmHg (Zemaityte, 1997) in only a few cardiac cycles. This mechanism is governed by the autonomic nervous system, and its cardiovagal component is an indicator of the balance between parasympathetic (PNS) and sympathetic (SNS) activities in the modulation of heart rate (Kaniusas, 2012). Thus, the quantification of baroreflex has for decades been regarded as a highly valuable diagnostic tool. Indeed, several studies have shown that the sensitivity of the cardiovagal baroreflex (BRS) may have a prognostic value in myocardial infarction (La Rovere *et al.* 1998), heart failure (Benarroch, 2008) and diabetes (Chapleau, 2012).

Over the last 20 years, techniques have been developed to perform BRS estimation on non-invasive recordings of spontaneous fluctuations of cardiac interval *RR* and systolic blood pressure P_S (Malberg *et al.* 2002, O'Leary *et al.* 2003). In older experimental settings, it was common to induce pressure changes for example by administration of vasoactive drugs, known as modified Oxford maneuver (La Rovere *et al.* 1988, Rudas *et al.* 1999). Although the estimates obtained using modern techniques show correlation with estimates from the Oxford method, there are differences between those estimates and several parameters can influence the computational implementation of each technique. Among the commonly used techniques to analyze the fluctuations found, the time domain sequence method applies linear regression to consecutive sequences of P_S rise accompanied by *RR* increase or P_S fall accompanied by *RR* decrease while the frequency domain method presupposes the calculation of the spectral power of both P_S and *RR* time series in frequency bands of interest (Laude *et al.* 2004).

Cardiovagal baroreflex seems to be dependent on the direction of pressure change, usually exhibiting higher gain and lower setpoint for pressure rise in comparison with pressure fall. This hysteresis behavior may reflect fine adjustment of the baroreflex mechanism with the purpose of preserving systemic pressure values and adequate organ perfusion. Hysteresis was thought to be dependent primarily on baroreceptor vessel mechanics (Bonhay *et al.* 1997) but recent studies have shown that it might reflect the integrated action of both mechanical and neural components since the direction of hysteresis seemed to vary across trials (Studinger *et al.* 2007). Ler *et al.* (2010) suggested an elliptical model to fit the *RR*-P_S characteristic pattern with ascending and

descending portion to non-invasive recordings of subjects with pressure fluctuations induced by the injection of vasoactive drugs. The same authors proposed the calculation of a hysteresis index as the ratio between the minor and major axes of this ellipse.

The goal of this work is to present a novel method to characterize the state-dependent *RR*-P_S pattern as the best fit ellipse to the pixel image generated by the area enclosed by spontaneous baroreflex time sequences. The method was applied to all the sequences of ascending or descending trend and the *BRS* estimates were compared with results of the regression method, obtained for the same dataset. The *BRS* provided by the two methods positively correlated.

The dataset used in this work was provided by the E. W. Group of the European Society of Hypertension for BRS studies (2003), consisting of non-invasive blood pressure and 3 lead electrocardiogram recordings, both in supine and standing positions. Postural change has been reported to influence *BRS*, namely that there is a sensitivity decrease in standing position (Steptoe & Vögele 1990, Choy *et al.* 2006, Taylor *et al.* 2013). This is due to PNS withdrawal resulting in reduced available vagal activity for baroreflex regulation of heart rate. The ellipse method proved as effective in identifying changes in sensitivity due to postural change as other methods.

In addition to providing accurate *BRS* estimates for single sequences, the introduced method in this work allows the characterization of spontaneous cardiovagal baroreflex cycles, which are constructed from time consecutive sequences of opposite trend. Since these cycles have an ascending and descending portion, information on the hysteresis behavior can be extracted from parameters of the fitting. Thus, the method allows the quantification of hysteresis and the determination of its direction without any induced pressure changes. The hysteresis characterization is only possible if a significant number of consecutive sequences are found, which is the case for 7 out of 21 subjects in this dataset. Further development of the method and approval with other datasets is necessary.

The structure of this work is defined in the following way. The theoretical foundation of the project is laid out in section 1.1. Starting from the basics, with presenting a typical electrocardiogram recording and its parameters for characterization of the heartbeat signal. Following with the characterization of the blood pressure waveform during a cardiac cycle, and identification of the parameters that influence it, as well as the mechanisms of cardiovascular interrelation in play, the most important one being the baroreflex. The working of this mechanism is described in detail, as well as its hysteresis pattern and a look is taken into how cardiovascular conditions might be correlated with an impaired baroreflex. The usual time and frequency methods used for *BRS* estimation are explained. An overview of how *BRS* is affected during the respiratory cycle and by postural changes is also given during this chapter. In chapter 2, the dataset used in this project is characterized, as well as the used signal processing methods. Furthermore, the elliptical method proposed is described in detail and differentiated from the usual methods used for baroreflex sensitivity estimation. All the statistical analysis applied to the results obtained is described. The chapter ends with the presentation of the user-friendly GUI app, which was implemented to allow users to apply all the methods for BRS estimation described in this work, in particular the ellipse method to any dataset and without needing previous knowledge about their computational implementation. The results obtained for the above-mentioned EuroBaVar dataset (E. W. Group, 2003), and their statistical analysis are presented in chapter 3 and discussed in chapter 4. This work is concluded in chapter 5 with an outlook on the value of this method as a baroreflex assessment tool.

1.1. Theoretical background

In this section all the fundamentals of anatomy, physiology and signal analysis which are relevant to the understanding of this work are explained.

1.1.1. Heartbeat

The heartbeat corresponds to the periodic contractions and relaxations of the heart muscle serving its function of pumping blood throughout the entire body, transporting nutrients and oxygen to cells, and excreting unwanted substances generated during their metabolism, as well as regulating pH and temperature levels. The mechanical contractions of the heart are prompted by his electrical activity.

The electrical depolarization of the heart is initiated by the sinoatrial (SA) node and propagates through fibres on the wall of the atria towards the atrioventricular (AV) node, generating atrial systole. Blood enters the ventricles, which are in diastolic phase and fill rapidly. AV valves, which separate atria and ventricles, are open and semilunar (SL) valves, which are located at the point of attachment between ventricles and arteries, are closed. Once the action potential arrives to the AV node, which is the only electrical bridge between atria and ventricles, all the atrial wall is fully depolarized. The electrical excitation is forwarded to the ventricular walls through the Bundle of His and down Purkinje fibres, which are located at the separation between the two ventricles (interventricular septum). The ventricles start to contract, and atria enter diastolic phase. Once the pressure in the contracting ventricles is higher than the pressure in the atria, the AV valves close to prevent backflow of blood into the atria (see Figure 1).

During ventricular systole, SL valves open and the stroke volume V_S, which is around 2/3 of the heart blood volume leaves the heart towards the arteries. The blood output from the left ventricle travels to the aorta and continues to the whole body, bringing oxygen and nutrients to cells (arterial blood) and blood output from the right ventricle travels to the pulmonary artery and continues to the lungs, carrying excretion products (venous blood). Arterial blood flow oscillates with heart rate (section 1.1.2).

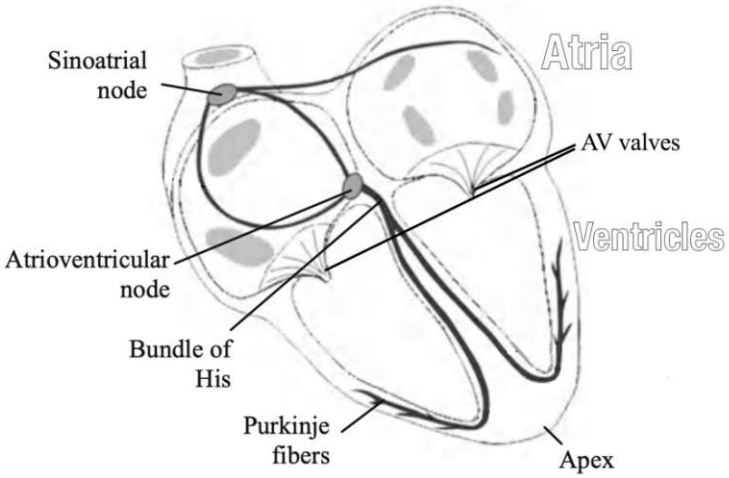

Figure 1 – Illustration of the heart and identification, on the right, of the main components of its electrical impulse conduction system. Taken and modified from Plonsey (1995).

As the ventricles relax, ventricular pressure falls behind arterial one and there is some backflow of blood right before SL valves close which is translated into the dicrotic notch at the arterial blood pressure waveform (Kaniusas, 2012). The arterial blood pressure waveform is described in section 1.1.2.

An easy and reliable way to register a heart cycle, with corresponding heart rate level f_C is an indispensable diagnostic tool. In the present day, the most widely used method to record electrical activity of the heart during cardiac cycle in the present day is the electrocardiogram ECG. In section 1.1.1.1, an ECG recording is shown, and its main characteristics explained in the light of the working of cardiac electric impulse conduction system described above.

Myocardial tissue cells themselves determine f_C in the SA node but is subjected to regulation by efferent PNS and SNS nervous system fibres. The working of this regulation is explained in detail in section 1.1.3.1. as it generates fluctuations in *RR* (and consequently f_C) which can be quantified as heart rate variability HRV. HRV relevance as a prognostic indicator of cardiovascular health, as well as its assessment methods are explained in detail in section 1.1.1.2.

1.1.1.1. Electrocardiogram

A typical ECG wave is shown in Figure 2 and its main characteristics are marked. The ECG wave shape (peak or deflection) is determined by the spread and direction of depolarization in the myocardium (heart muscle tissue).

- P wave: corresponds to atrial depolarization form the SA node towards the apex of the heart. At the end of this wave, there is an isoelectric line because the atrial wall is equally depolarized.
- QRS complex: corresponds to the moment of depolarization of the ventricles. Propagation from the interventricular septum to the wall of the left ventricle generates a small negative deflection in the ECG, the Q wave, while depolarization towards the apex of the heart generates the positive R peak. The R peak marks the end of atrial systole and beginning of ventricular contraction. When depolarization propagates towards the basal part of the ventricles, its direction changes again upward, and the negative S deflection appears. The isoelectric line at the end of what is designated by QRS complex of the ECG marks full ventricular depolarization.

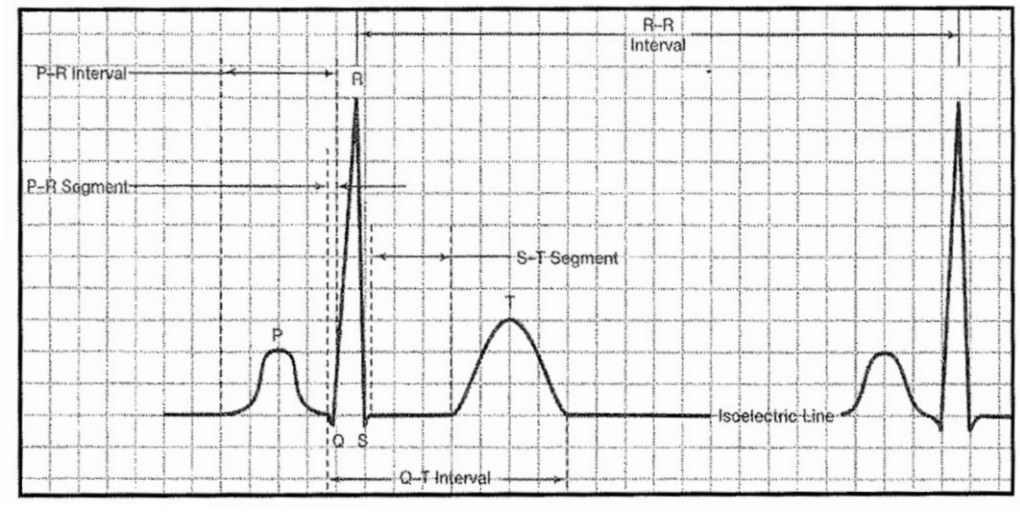

Figure 2 - Typical ECG wave during one cardiac cycle and its main characteristics. Image taken from Pflanzer *et al.* Each square represents 40 milliseconds in the horizontal direction and 0.1 mV in the vertical direction.

- T wave: corresponds to ventricular repolarization and at its end, ventricular systole ends.

The value of heart period ($1/f_C$) is usually defined as the interval of time between consecutive R peaks RR of the ECG, and it corresponds to the inverse of the heart rate (f_C). f_C assessment is reliable for an ECG sampling frequency higher than 500 Hz (Kaniusas 2012).

1.1.1.2. Heart Rate Variability

HRV corresponds to the variations in both instantaneous *RR* and f_C. It is considered a relevant clinical indicator of the integrity of autonomic functions and HRV perturbations are linked to early onset of cardiovascular diseases pathologies, like acute myocardial infarction (La Rovere *et al.* 1998) or diabetic neuropathy (Task Force, 1997).

Quantification of HRV can be performed in time domain, as the standard deviation of consecutive *RR* or in frequency domain, as spectral analysis of the *RR* beat-to-beat series (Kaniusas, 2012).

Conversion methods of *RR* time series into the frequency domain include fast Fourier transform, power spectral density calculation and parametric autoregressive modelling (Choy *et al.* 2006). In the resulting spectrum, three main frequency bands can be distinguished: very low frequency (**VLF**), low frequency (**LF**) and high frequency (**HF**), discriminated in Table 1.

Table 1 - Frequency bands in the HRV spectrum. Values taken from Choy et al. (2006).

VLF	0.01-0.04 Hz
LF	0.04-0.15 Hz
HF	0.15-0.4 Hz
Total power	0.02-0.4 Hz

The area of spectral peaks in each one of those bands can be calculated and it has been assumed to reflect autonomic regulatory activity. The values are given in ms^2, usually. The HF power reflects efferent vagal output, and correspondingly, parasympathetic nervous system (PNS) rapid modulation during respiration, including respiratory sinus arrythmia which has a frequency of about 0.2 Hz (see section 1.1.3.2 Effect of normal respiration). On the other hand, LF power is be related to mid-term regulation, for example by the baroreflex and thought to be associated both with SNS and PNS activities (Task Force, 1996). Given this assumption, the ratio LF/HF is a measure of the sympathovagal balance. Oscillations in the VLF range are related to long-term regulation mechanisms like changes in body temperature or adaptation to the task situation (Robbe *et al.* 1987, Kaniusas, 2012).

1.1.2. Arterial blood pressure waveform

The arterial pressure *P* waveform during the cardiac cycle is divided into systolic phase and diastolic phase, as illustrated in Figure 3. Ventricular systole corresponds to the moment when V_S exits the heart. It prompts a quick rise in pressure till the first peak. The secondary optional peak occurring during systole is due to constructive interference with the reflected wave (there is blood backflow during ventricular systole before closing of SL valves as explained in section 1.1). P_S is defined as the maximum of one of these two peaks, which is dependent on age (typically, from the age of 30, the second peak becomes more prominent than the first one, Kaniusas 2012).

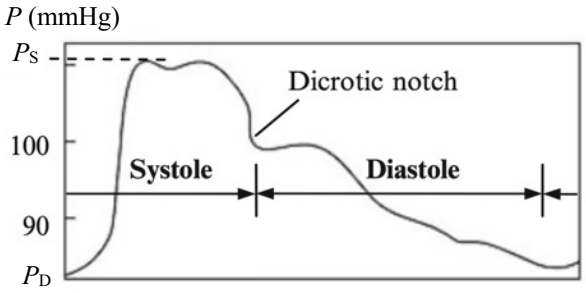

Figure 3 – Arterial blood pressure waveform during the cardiac cycle. Taken and modified from Kaniusas (2012).

A dicrotic notch occurs at the closing of the aortic valve, marking the separation of the two phases of the ventricular cardiac cycle and the beginning of the diastolic wave. The diastolic wave is characterized by an exponential decreasing curve. At the foot of this curve, diastolic blood pressure P_D is defined, as the lowest arterial pressure value measured during the cardiac cycle. The value of P_D is directly proportional to the rate of the decay and inversely proportional to its duration (cardiac period or $1/f_C$). The rate of the decay is proportional to the total peripheral resistance of arterial capillaries R_T, to the initial level of pressure P_S and to the arterial compliance.

In summary, the most important parameters to consider when studying blood pressure fluctuations are both of vascular nature (R_T) and cardiac nature (V_S and f_C). Their influence in the blood pressure waveform is summarized in equation (1-1) for mean arterial blood pressure $<P>$.

$$<P> \approx V_S \cdot f_C \cdot R_T \quad (1\text{-}1)$$

Increases in these parameters, left untended, will lead to an increase in P. To counteract them and bring P back to the desired target value, which is determined in the central nervous system, there are regulation mechanisms. These mechanisms will compensate for an increase in one of the parameters with a simultaneous decrease in another. They can be passive, like the blood reservoir effect of large arteries, which explains the exponential drop in P during diastole, or active mechanisms, like the baroreflex, a feedback-based control mechanism explained in detail in section 1.1.3.

There are several non-invasive methods to continuously record blood pressure, including the volume clamp method, first suggested by Penáz (1973). According to this method, a miniaturized finger cuff with an optical transmission sensor registers the radius of the finger artery, which increases proportionally to the pressure (blood volume) in the artery. The cuff pressure waveform then mirrors the blood pressure waveform.

1.1.3. Baroreflex

The changes in P manifest as changes in the amount of tension applied to the walls of blood vessels, which are sensed by mechanosensitive nerve endings, called baroreceptors, present in those walls. The more stretched the wall is, the higher is the frequency of firing action potentials of these nerve endings and the information is transmitted to the central nervous system. Arterial baroreceptors innervate large arteries (primarily, aortic arch and carotid sinuses) while cardiopulmonary baroreceptors are present in venous blood compartments (primarily, the heart, the vena cava, and the pulmonary vasculature), as illustrated in Figure 4.

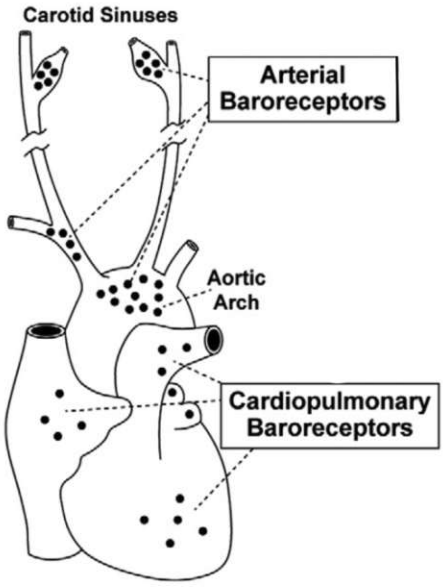

Figure 4 – Main locations of baroreceptors in the cardiovascular system. Partly taken from Chapleau (2012).

In the venous blood compartments, pressure is low, and the baroreceptors here present are often called "volume-receptors". Changes in the activity of cardiopulmonary baroreceptors mostly triggers changes in intrathoracic blood volume. On the other hand, increased activity of arterial baroreceptors, which happens when there is a sudden rise in *p*, triggers a negative-feedback mechanism that rapidly counteracts these changes (Chapleau, 2012). This mechanism is explained in detail in section 1.1.3.1.

1.1.3.1. Arterial baroreflex mechanism

The firing frequency of arterial baroreceptors increases when *P* rises and decreases when *P* falls. This feedback is forwarded to the central nervous system, which compares the current level of *P* to the target value and senses differences, activating modulation mechanisms throughout the efferent autonomic nervous system activity (neurogenic control) and smooth muscles activity (myogenic control). A schematic representation of the functioning of the baroreflex mechanism can be found in Figure 5.

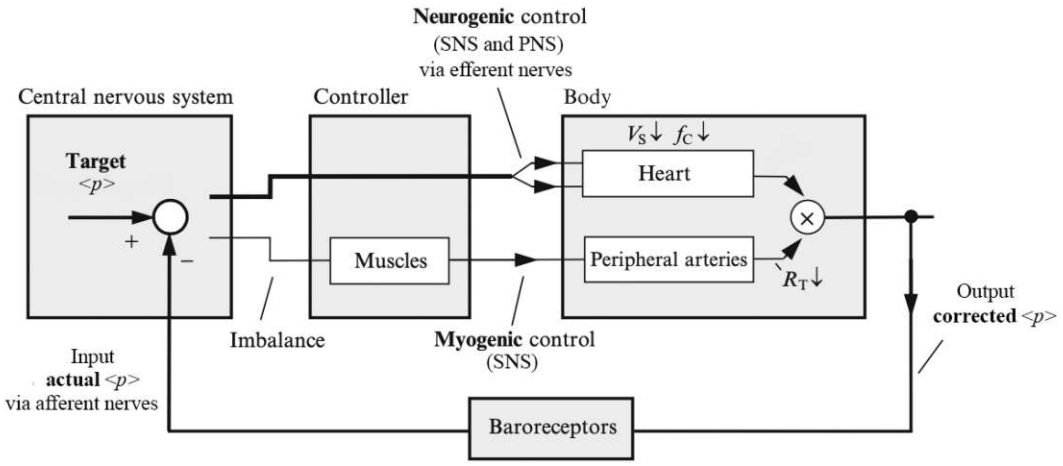

Figure 5 – Schematic representation of the baroreflex mechanism. Taken and modified from Kaniusas (2012).

Myogenic control, and therefore R_T, is exclusively modulated by SNS activity, and mainly determines the level of P_D. On the other hand, neurogenic control is a result of the complex interaction between SNS and PNS activities, adjusting V_S and, therefore, determining the level of P_S. PNS efferent pathways modulate the SA node of the heart, via the vagus nerve, decreasing f_C while SNS pathways have both ionotropic effect on heart muscle, increasing V_S and on smooth muscles of peripheral vessels, increasing R_T and chronotropic effects on the SA node, increasing f_C. There is a delay in the chronotropic regulation of the SA node between the two control pathways, being that SNS activity is slower in the increase of f_C than PNS activity in its lowering (Kaniusas, 2012). This delay has some impacts in the baroreflex mechanism sensitivity, described in section 1.1.3.2.

Activation of baroreceptors in response to a sudden rise in P causes an increase in vagal output to the SA, complemented by a decrease in SNS activity. As a result, there will be a decrease in all f_C, V_S and R_T. Ultimately, P is lowered back to its target value. The reverse occurs when there is a sudden fall in P, with increased SNS activity and decreased vagal tone, leading to an increase in all three above mentioned parameters leading finally to an increase in P back to its target value. The pressure fluctuations around the target value are of about ± 5 mmHg (Zemaityte, 1997).

Abnormalities in the baroreflex function have been linked to neurological diseases that affect the control pathways or to cardiovascular diseases that affect the heart structures. Some examples are denervation of the heart muscle in the case of heart transplant patients (Raczak *et al.* 2004), diabetes which causes damage to the vagal nerve from early stages (Chapleau, 2012) or non-treated hypertension (Parati *et al.*, 1988). Baroreflex disfunction may manifest as orthostatic hypotension, the inability to compensate for a pressure drop caused by standing up. In fact, baroreflex regulation during postural change has been a subject of various studies (Choy *et al.* 2006, Taylor *et al.* 2013). This mechanism is described separately in (v) in section 1.1.3.2. because of its relevance in the scope of this work since the dataset used is acquired for an experimental setup of postural change.

The further study and characterization of the baroreflex mechanism might shed some light on how to handle such conditions pharmacologically (Benarroch, 2008). Thus, baroreflex quantification can be regarded as a clinically relevant tool, as it provides a measure of the current state of the autonomic response. This quantification is usually done by means of its gain, denominated baroreflex sensitivity (La Rovere *et al.* 1998).

Two types of sensitivity can be obtained, depending on the experimental setup: sympathetic sensitivity, defined as the change in R_T per unit change in P_D, or cardiovagal sensitivity (BRS), defined as the change in cardiac period (= $1/f_C$) per unit change in P_S (Kaniusas, 2012). BRS is explained further in section 1.1.3.2.

1.1.3.2. Cardiovagal baroreflex sensitivity

BRS corresponds to the vagally mediated baroreflex response, having as input a pressure drop or rise and as output an increase or decrease in vagal outflow, respectively. The level of vagal outflow relates directly to *RR* (Ler *et al.* 2010), by SA modulation, and typically *BRS* is estimated from the characteristic *RR*-P_S curve.

Experimental setups for the BRS assessment can record spontaneous pressure changes, during respiratory cycle for example (cf. (iv) in section 1.1.3.2), or induced pressure changes. Inducing methods include administration of vasoactive drugs like phenylephrine (Rudas *et al.* 1999), physical exercise (Incognito *et al.* 2019), neck suction (Rea and Eckberg 1987, Parati *et al.* 1988), cold pressor test (Hughson, 1993). The use of vasoactive drugs to provoke human baroreflex is

referred to as the modified Oxford method. Modern techniques aim to obtain BRS estimates from the analysis of spontaneous fluctuations. Induced or spontaneous fluctuations in P_S can be correlated with correspondent *RR* values via the sequence method, explained in (i) in section 1.1.3.2.

Rea and Eckberg (1987) measured changes of muscle sympathetic nerve activity generated by changes in the carotid distending pressure induced via neck suction and managed to characterize the sympathetic myogenic control exerted by the baroreflex over a wide range of pressures. In the same study, the cardiac vagally-mediated baroreflex is determined to have a linear range of about 60 mmHg and higher gain at resting pressure levels. The characteristic cardiovagal baroreflex curve exhibits three zones: threshold, linear and saturation in the pressure range, which was suggested by the same authors to be fitted by a logistic sigmoid, as shown in Figure 6. Usual experiments are conducted in the pressure range corresponding to the linear portion of the sigmoid curve.

Baroreflex function is dependent not only on the level of *P* but also on the rate and direction of change. The mechanism is more accurate for faster *P* changes and for rising rather than falling pressures (Chapleau, 2012). This leads to a hysteresis behavior of the *RR*-P_S relation, which will be explained below (see (iii) in section 1.1.3.2).

(i) Time domain estimation

The usual time domain procedure for BRS estimation starts with identifying spontaneous or induced sequences of common, either increasing or decreasing, trend both in arterial pressure using either the value of <*P*> or P_S and in *RR*. Linear regression is applied to these sequences (considering that we are in the pressure range corresponding to the linear portion of the sigmoid curve described in section 1.1.3.2) and the gain of the regression line quantifies the cardiovagal regulation sensitivity, with typical values of 10 ms/mmHg (Kaniusas, 2012).

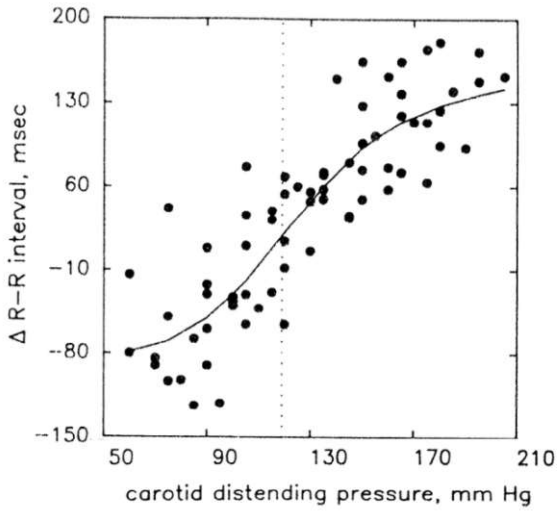

Figure 6 – Fitting of a 4-parameter logistic sigmoid to the characteristic pressure-*RR* relation. X-axis denotes the carotid distending pressure in response to neck suction in mmHg. Y-axis denotes the *RR* change. The linear part of the curve extends from 103 to 152 mmHg. Maximum gain at ~120mmHg. Taken and modified from Rea & Eckberg (1987).

Several parameters have been reported to affect the performance of the time domain method, such as the coefficient of correlation of the regression (typically, sequences with a correlation coefficient of at least 0.8 are validated), the minimum beat duration of the sequence (typically, at least two beats) or the minimum beat-to-beat pressure or *RR* variation (up to 1 mmHg for pressure and up to 5 ms for *RR*). The Pearson's coefficient of correlation of the linear regression measures the strength of the *RR*-P_S relation in a way that 0 corresponds to no dependence between the variables and 1 to maximum positive correlation.

Laude *et al.* (2004) investigated the effect of these parameters on spontaneous sequences identified in the EuroBaVar dataset (E. W. Group, 2003) (in section 2.1 a detailed description of this dataset is found). The use of <*P*> instead of P_S was shown to lower the accuracy of the estimates. In the same study, it was determined feasible to associate a lack of BRS estimates in some subjects with impaired baroreflex in those subjects and the sequence method proved efficient in detecting baroreflex impairment when a minimum of three beats were used to validate a sequence and even if no restrictions to the minimum variations of *RR* and P_S are applied.

In different publications the effect of applying a lag of one, as illustrated in Figure 7, or two beats to validate a sequence has also been investigated (Steptoe & Vögele, 1990) since it was argued that for HR superior to 75 bpm, baroreflex might only influence the length of the next heartbeat relative to current pressure (Pickering & Davies, 1973).

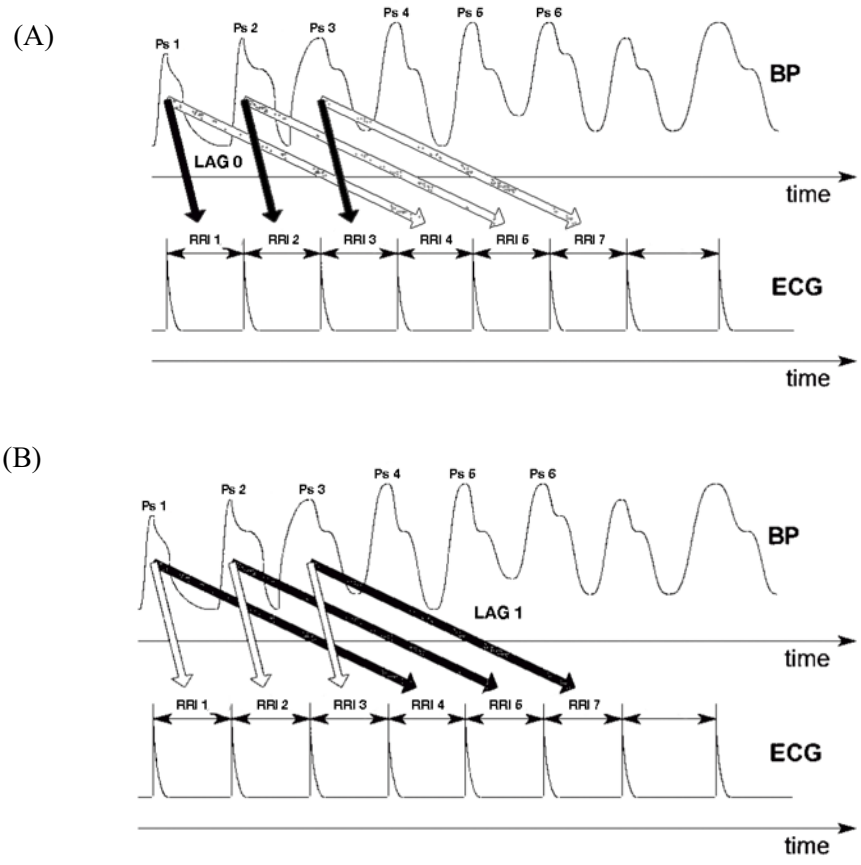

Figure 7 – Time correspondence between systolic pressure peaks and cardiac interval in spontaneous baroreflex measuring in (A) synchronous and with (B) a lag of one beat between the two bio signals. Taken and modified from Malberg *et al.* (2002).

A gold standard method for the obtention of BRS estimates does not exist and the choice of which restrictions to apply to the sequence method heavily depends on the dataset being handled.

(ii) Frequency domain estimation

For spectral analysis, the beat-to-beat *RR* and P_S are resampled into equidistantly spaced time series. These interpolated time series are then transformed from the time domain to the frequency domain either by Fourier transform or power spectral density calculation. There are two approaches to the *BRS* estimation in frequency domain (Choy *et al.* 2006), the α coefficient, defined as the square root of the ratio between the spectral powers P_{RR} and P_{P_S} of *RR* and P_S respectively, in HF or LF bands (the ranges of frequencies of these bands are discriminated in 1.1.1.2), and the square root of the magnitude of the cross-spectrum of *RR* and P_S in the LF band (Robbe *et al.*, 1987). The values of magnitude are unreliable if the bands have a low coherence. The magnitude squared coherence between two signals in the frequency domain is a measure of the correlation between them, comparable to the regression coefficient in time domain, at each frequency value (Robbe *et al.*, 1987). The coherence in the band of interest can be calculated using the Porges *et al.* (1980) formula for weighted coherence magnitude C_W in equation (1-3). The frequency band of interest, in the case LF, is limited by the frequencies θ_1 and θ_2 and $\rho^2(\theta)$ corresponds to the magnitude squared coherence at each frequency of the two signals of interest, in this case *RR* and P_S, which have a respective spectral density of $f_H(\theta)$.

$$\alpha \mathrm{HF, LF} = \sqrt{\frac{P_{RR}}{P_{P_S}}}\Bigg|_{HF,LF} \quad (1\text{-}2)$$

$$C_W = \frac{\sum_{\theta_1}^{\theta_2} \rho^2(\theta) f_H(\theta)}{\sum_{\theta_1}^{\theta_2} f_H(\theta)} \quad (1\text{-}3)$$

(iii) Hysteresis behaviour

Hysteresis in the cardiovagal baroreflex means that there is a change in the vertical position of the sigmoidal curve (setpoint) and in the linear portion gain (*BRS*) between ascending and descending sequences (Studinger *et al.* 2007). This difference is not observed for sympathetic sensitivity (Rudas *et al.* 1999). In terms of setpoint, higher values have been observed for falling pressure due to longer *RR* and in terms of BRS, generally higher values are estimated for rising rather than falling pressures (Studinger *et al.* 2007, Kaniusas 2012, Incognito 2020).

It was hypothesized that this behaviour might be explained by the compliance of the arterial vessels where baroreceptors are located. Changes in diameter of the arterial vessels in response to a pressure change result in vessel wall strain which is translated in a change in the frequency of baroreceptor firing. The activity of myelinated afferent baroreceptor fibres correlates linearly with vagal outflow which, in its turn, correlates linearly *RR* length (Eckberg and Sleight, 1992). Bonhay *et al.* 1997 observed a nonlinearity in the carotid artery diameter-P_S curve in response to phenylephrine injection, which exhibits steeper slope for falling rather than rising pressure, trend expressed also in the P_S-*RR* relation. However, this hypothesis doesn't seem to satisfy all the aspects of baroreflex hysteresis.

A smaller carotid diameter for rising P_S would imply unresponsiveness of the carotid artery in the lower end of a physiological range of pressures or a rigid behaviour (lower distensibility) in this range. Myers et al. (2002) determined that carotid distensibility is in fact higher for lower

pressure, within a physiological range and Studinger *et al.* (2007) observed a higher systolic carotid diameter for rising pressures across cardiac cycles. Moreover, several studies demonstrated that the expected hysteresis pattern is not always verified. The previously mentioned authors found 4 out of 18 trials while Ler *et al*. (2010) found 52 out of 104 trials where the setpoint for the rising portion of the curve was higher. These discrepancies indicate that vessel mechanics alone is not sufficient to predict the magnitude and direction of hysteresis. It has been suggested that there might be a neural origin to these differences. One of the hypotheses is that there are unmyelinated afferent baroreceptor fibres that begin to fire at higher pressures and provoke slowing of f_C (O' Leary *et al.* 2003). Another explanation of neural origin suggested is central resetting of the baroreflex at the end of the increasing sequence (Ler *et al.* 2010).

Hysteresis can be geometrically modelled by an elliptical pattern (Eckberg & Sleight, 1992) that encompasses the two sigmoidal *RR*-P_S curves for rising and falling pressure put together, with a trajectory of specific direction defined in this pattern. Ler *et al.* (2010) modelled the 3D relation between carotid diameter, *RR* and P_S and extracted the 2D *RR*-P_S relation was obtained from principal component analysis, obtaining a planar ellipse trajectory as shown in Figure 8. The same authors proposed the ratio between minor and major axes of the resulting ellipse as a hysteresis index.

Considering the description of the hysteresis behaviour, with generally higher *BRS* for the ascending portion of the ellipse, it should be noted that the *BRS* varies slightly over the respiratory cycle, as will be described in the section below.

(iv) Effect of normal respiration

The levels of P_S and $<P>$ fluctuate during the respiratory cycle, activating the baroreflex mechanism.

During inspiration, the respiratory muscles contract and the diaphragm lowers, allowing space for air to enter the lungs. The intrathoracic pressure is decreased and consequently, venous return to the heart is enhanced which leads to increased right ventricular volume of blood. This causes a deviation in the interventricular septum and a decrease in space in the left heart. Thus, V_S decreases during inspiration by about 10% (Kaniusas 2012) leading to decreased P_S by 5%.

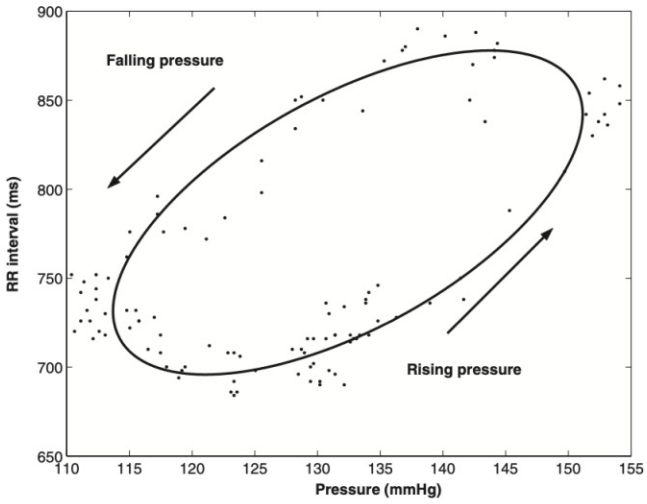

Figure 8 – Example of elliptical fitting by principal component analysis of *RR*-P_S data. The arrows indicate the trajectory of the pressure change. Taken from Ler *et al.* (2010).

On the other hand, the SA rate increases during inspiration due to inhibited vagal activity, effect which may on the one hand improve pulmonary gas exchanges in the lungs (Yasuma & Hayano, 2004) and is on the other hand potentiated by baroreflex control, activated to compensate for the decreased V_S. Therefore, f_C is also increased, compensating for the decreased V_S and the level of P_D does not change. The SA rate modulation is known as respiratory sinus arrythmia, and it has a frequency of about 0.2 Hz (included in the LF range from section 1.1.1.2).

During expiration the reverse occurs, with increased vagal activity leading to decreased f_C to compensate for the P_S increase due to respiratory movements. *BRS* is decreased in inspiration, by comparison with expiration (Kaniusas, 2012), due to the hysteresis of the baroreflex control.

It seems feasible that the respiratory cycle might be characterized by spontaneous consecutive segments of opposing trend in the *RR*-P_S relation, with common decrease during inspiration and common increase during expiration.

The respiratory modulation of f_C is decreased in standing position as will be explained in the section below.

(v) Effect of postural changes

Suddenly standing up causes a momentary drop in pressure, which is due to the gravity action impeding venous return. A reduced venous return leads to a decrease on the amount of V_S that is available to the heart to pump out (Lowry *et al.* 2016). As a compensatory mechanism, the baroreflex mechanism is activated to increase f_C, inhibiting the vagus nerve. The respiratory sinus arrythmia modulation of expiration becomes less pronounced in this position due to the pre-inhibited vagus nerve (Choy *et al.* 2006).

Several heart diseases can lead to disruption of baroreflex regulation during postural changes, leading for example to orthostatic hypotension. Thus, *BRS* assessment during pressure changes induced by postural changes is a common practise (Taylor *et al.* 2013, Choy *et al*. 2006). Cardiovagal *BRS* decreases when moving from supine to standing position, similarly to the effect that is achieved with the administration of some drugs, like phenylephrine. Steptoe & Vögele determined a *BRS* decrease from 17.5 ms/mmHg in supine to 7.65 ms/mmHg in standing position by regression analysis of spontaneous fluctuations. Laude *et al.* (2004) determined a mean 2.1 supine to standing ratio of sensitivity estimates between the two positions for the EuroBaVar dataset (described in section 2.1) by using several different calculation methods, in the time and frequency domains. Analogously to what is observed for the hysteresis behaviour, the dissociation between cardiovagal and sympathetic sensitivity is also observed for postural changes and standing up appears to increase sympathetic reflex gain (O'Leary *et al.* 2003).

CHAPTER **2.**

Methods

In this chapter, the methodology used to obtain the results of this work is presented. The dataset used is described extensively, as well as the methods used to obtain the three time domain and two frequency domain BRS estimates. The ellipse method is included in this description and the obtention of other parameters from the analysis of the ellipses is explained, namely the strategy used to quantify hysteresis of the *RR*-P_S pattern. The GUI app implemented to run the analyses on other datasets is also introduced.

2.1. The EuroBaVar dataset

The EuroBaVar dataset is provided by the Working Group on Blood Pressure Heart Rate Variability of the European Society of Hypertension (2003), consisting of 42 recordings of 21 subjects, divided in two groups (8 subjects from group A and 13 subjects from group B). The recordings last 10-12 minutes, in both supine and upright positions, and were obtained using non-invasive monitoring devices: a 3-lead electrode ECG recorded using a Datex cardiocap II monitor (Datex Engstrom, Helsinki, Finland) and a *P* waveform recorded using a Finapres 2300 device (Ohmeda, Helsinki, Finland, continued as Finometer supplied by FMS, Arnheim, The Neatherlands), (Laude *et al.* 2004). The Finapres is a recently developed blood pressure measurement instrument based on the volume clamp principle (Penáz, 1973), that showed good agreement between *P* readings and intraarterial recordings both at rest and in a stress situation, namely postural change (Steptoe & Vögele, 1990). The demographic data of the subjects can be found in **Erro! Autorreferência de marcador inválida.**. Informed consent was obtained, and the study was approved by the Paris-Necker committee for the protection of human subjects in biomedical research.

Table 2. Demographic data of the subjects. Taken from Laude *et al.* (2004).

Age (years)	38.4 ± 3.3
Height (m)	1.65 ± 0.02
Weight (kg)	64.1± 2.4
Body mass index (kg/m^2)	23.3 ± 0.8

The heterogenous pool of subjects included: 4 healthy subjects, 1 patient which had been through a heart transplant recently, 1 diabetic patient showing impairment in cardiac autonomic regulation, 3 hypertensive patients (1 treated with medication and 2 non medicated) and 12 normotensive patients (including 1 diabetic patient without evident impairment in cardiac autonomic regulation, 2 treated hypercholesterolemic subjects and 1 three months pregnant woman) (Choy *et al.* 2006). The entire curves of ECG and *P*, sampled at 500 Hz with a 16-bit resolution, were used for analysis, in detriment of the beat-to-beat based recordings.

2.2. Signal processing

For an accurate computation of the cardiovascular interrelations is important to precisely extract parameters of interest, being those R peaks and *RR* for ECG and P_S and P_D peaks for *P*, from the curves. No peaks (or beats) should be missing, since the baroreflex time sequences are dependent on the instantaneous beat-to-beat fluctuations of those quantities and missing one beat might imply missing a whole sequence. For that purpose, the built in MATLAB R2020b (The MathWorks Inc., Natick, MA, USA) function *findpeaks* was used with specific detection settings. Minimum peak prominence was restricted to 0.6 times the mean R peak height found in a preliminary unrestricted analysis. Minimum distance between consecutive peaks was restricted to 0.4 seconds. Results are found in Figure 9.

A manual correction was added after detection to ensure that the first P_S value occurs after the first detected R peak.

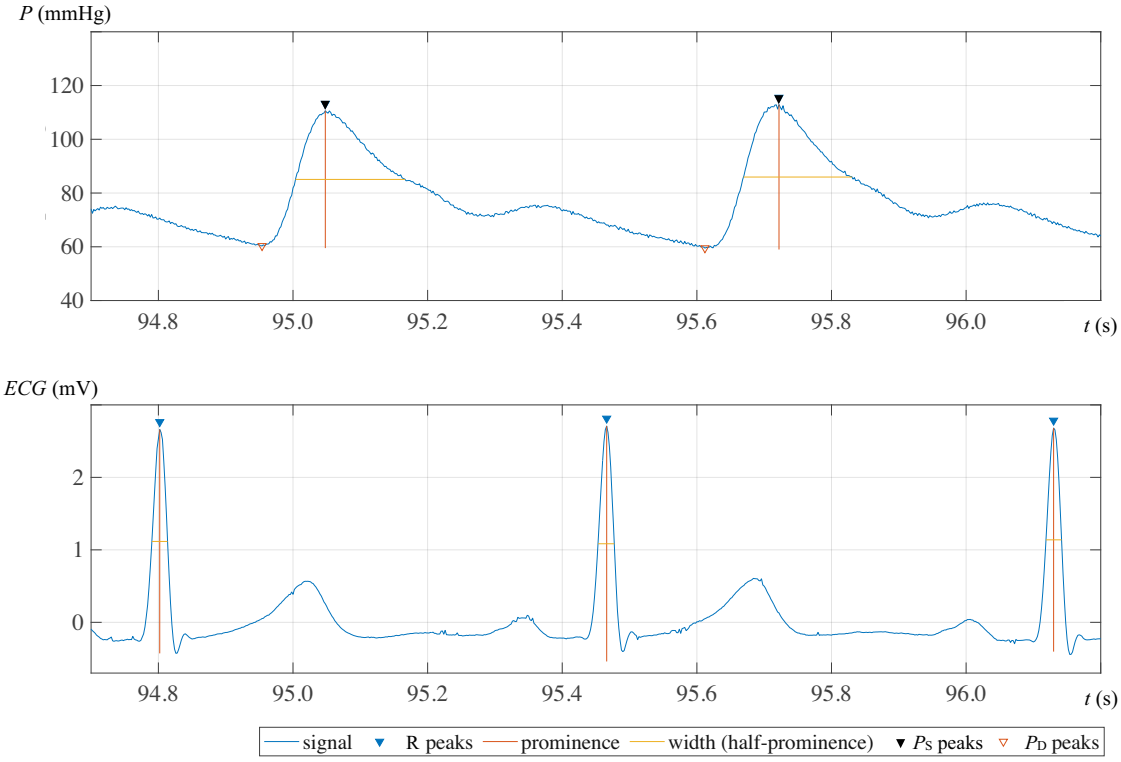

Figure 9 - ECG and *P* curves with detected peaks. The prominence of a peak is defined as the height of the peak relative to the highest local minimum in the two intervals extending from the peak to the right and left of the signal to a higher peak or to the end of the signal (MathWorks, *findpeaks Documentation*). Peak prominence is marked in both curves. Data from subject A1 in supine position.

2.3. Cardiovagal baroreflex sensitivity estimation

The BRS estimates obtained included three time domain procedures, two based on the sequence method (section 2.3.2) and one based on the ellipse method (section 2.3.1), and one spectral analysis procedure (section 2.3.3). All the procedures used P_S and *RR* values. The estimates have unit of millisecond per millimetre mercury and their statistical significance was investigated (section 2.3.4).

2.3.1. Ellipse method

According to Feller (1957) or Kendall and Stuart (1977), the k-th moment μ_k of a unidimensional random variable *x* with a probability distribution function *f (x)* about a value *c* is a quantitative measure related to the shape of its graph and is defined according to Riemann integrals by equation (2-1). This moment defines the bivariate normal distribution of variable *x* which is centred at *c*. If *c* is the mean μ_x of *x* in the previous equation, the moments defined are called central moments, resulting in equation (2-2). From this equation follows that the first central moment of a unidimensional data *x* is its expected value *E*, and the second central moment of that data is its variance. For the case of bidimensional data X_{ij}, the second central moment is the covariance matrix, $cov[X_i, X_j]$, according to equation (2-3). The contour line of a bivariate normal distribution is an ellipse. The directions and lengths of the axes of the ellipse are given by the eigenvalues and eigenvectors of the covariance matrix (Santos-Fernández 2012, Wang *et al*. 2015).

$$\mu_{\mathrm{k}} = \int_{-\infty}^{\infty} (x - c)^k \, f(x) \, dx \tag{2-1}$$

$$\mu_x^{\mathrm{k}} = E\left[(X - \mu_X)^{\mathrm{k}} \right] = \int_{-\infty}^{\infty} (x - \mu_x)^{\mathrm{k}} \, f(x) \, dx \tag{2-2}$$

$$\mu_{X_i X_j} = cov[X_i, X_j] = E[\, (X_i - E[X_i]\,)\,(X_j - E[X_j])\,] \tag{2-3}$$

where:
μ_{k}: k-th moment of a variable *x* centered at a value *c*
f(x): probability distribution of *x*
μ_x^k: k-th central moment of a variable *x*
E: expected value
$X_i X_j$: bidimensional data
$cov[X_i, X_j]$: covariance matrix

The ellipse method for baroreflex assessment which is proposed in this work finds the ellipse that has the same normalized central moment as the black and white image defined by the points enclosing a baroreflex region, which can correspond to a single sequence of common trend, same as is used for regression method, or defined by two consecutive sequences of opposing trend.

For spontaneous consecutive ascending-descending or descending-ascending sequences, baroreflex cycles can be defined in the shape of a closed polygon that has vertices in the points that form the two sequences, as illustrated in Figure 10. Values of the vertices for this polygon are, for P_S and in mmHg, (104.7, 106.5, 107.2) and (106.3, 105.7, 105.2) and for *RR* and in ms, (628, 644, 670) and (666, 656, 642), respectively for the ascending and descending portions of the cycle.

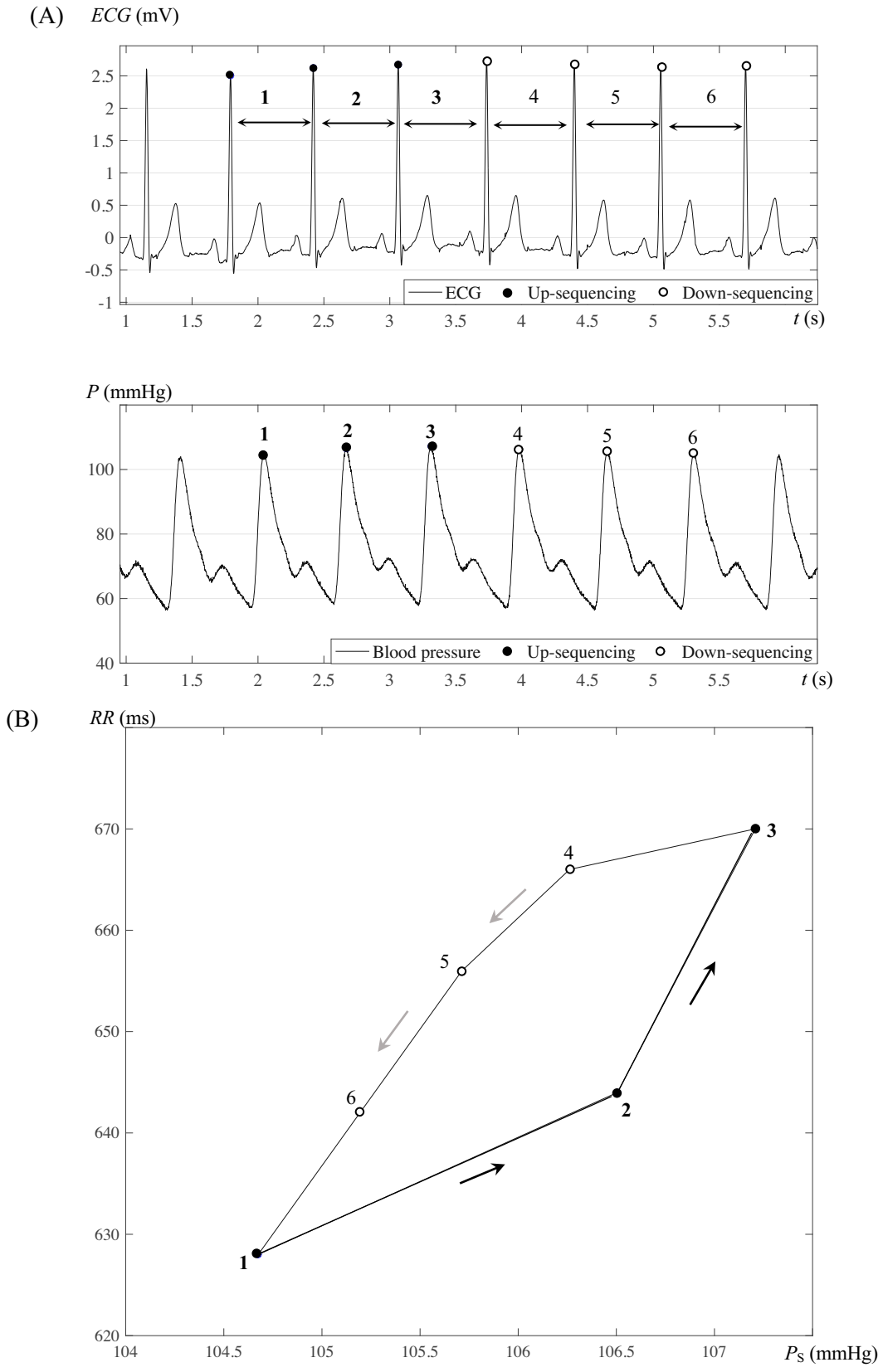

Figure 10 – Representative example of (A) consecutive ascending-descending trend forming the (B) baroreflex cycle. Data from subject A1 in supine position.

When the input vertices produce boundary intersections or improper nesting, the original border of the polygon is maintained but the polygon is divided into several distinct regions (MathWorks, simplify Documentation). An example of a cycle in such conditions can be found

in Figure A-2 (A) (Appendix A). There is redundancy in the cycle computation method for the cases in which an odd number of consecutive sequences are found. In this case, all the possible cycles are defined, meaning that some sequences are simultaneously part of two distinct cycles. An example of this situation is found in Figure A-1 (Appendix A).

The characteristics of the best-fitted ellipse to the area defined by the cycle are used to estimate values for cardiovagal sensitivity and hysteresis magnitude. The ellipse is calculated by the MATLAB R2020b (The MathWorks Inc., Natick, MA, USA) built in function *regionprops*, which also extracts its relevant characteristics, namely length of semi major axis a, length of semi minor axis b, area, centroid coordinates x_c and y_c, and orientation θ. This function receives as input a binary image. A binary image is a storage of pixels of a single bit, 0 or 1, in a matrix. Consequently, the first step of the ellipse method is the conversion of the coordinates of the vertices of the baroreflex region to pixel values. The resulting image is denominated $BW[u, v]$.

The range of P_S and RR in which baroreflex regions were detected was, for EuroBaVar dataset, 75-175 mmHg and 500-1500 ms, respectively. The pixel size of 1000×10000 was chosen for BW_{uv} as standard for all the cycles, proportional to the width of the ranges of P_S and RR by a factor of 10, which results in a pixel resolution of 0.1 mmHg × 0.1 ms. An illustration of the process and resulting image can be found in Figure A-3, Appendix A.

Since the data is digitized, the integral in the equations (2-2) and (2-3) must be replaced by a summation over the domain covered by the data, resulting in equations (2-4) and (2-5). The extracted axes lengths a and b and centroid coordinates x_c and y_c were scaled back to the original coordinate system and an example of the resulting ellipse is found in Figure 11. The ellipse is centred at (106.0 mmHg, 650.6 ms), has $a = 38.2$ and $b = 1.24$, in $(\text{mmHg}^2 + \text{ms}^2)^{1/2}$, $\theta = 87.4°$ and area of 11.9 ms·mmHg. The *BRS* estimate for this cycle is 21.8 ms/mmHg. The *BRS* value corresponds to the tangent of the orientation θ. In this way, estimates of *BRS* were obtained for all sequences and cycles of all subjects, in both supine and standing positions.

$$\mu_{u,v} = \sum_{(u,v)\in I}(u - u_c)^p (v - v_c)^q \, BW[u,v] \tag{2-4}$$

$$cov(\, BW[u,v]\,) = \begin{bmatrix} \mu'_{20} & \mu'_{11} \\ \mu'_{11} & \mu'_{02} \end{bmatrix} \tag{2-5}$$

where:
$BW\,[u, v]$: binary image, corresponding to the distribution of pixel coordinates (u, v)
$\mu_{u,v}$: central moment for digitized data
(u, v): pixel coordinates in the image
(u_c, v_c): centre of the bivariate distribution
μ'_{ij}: expected value in the ij direction

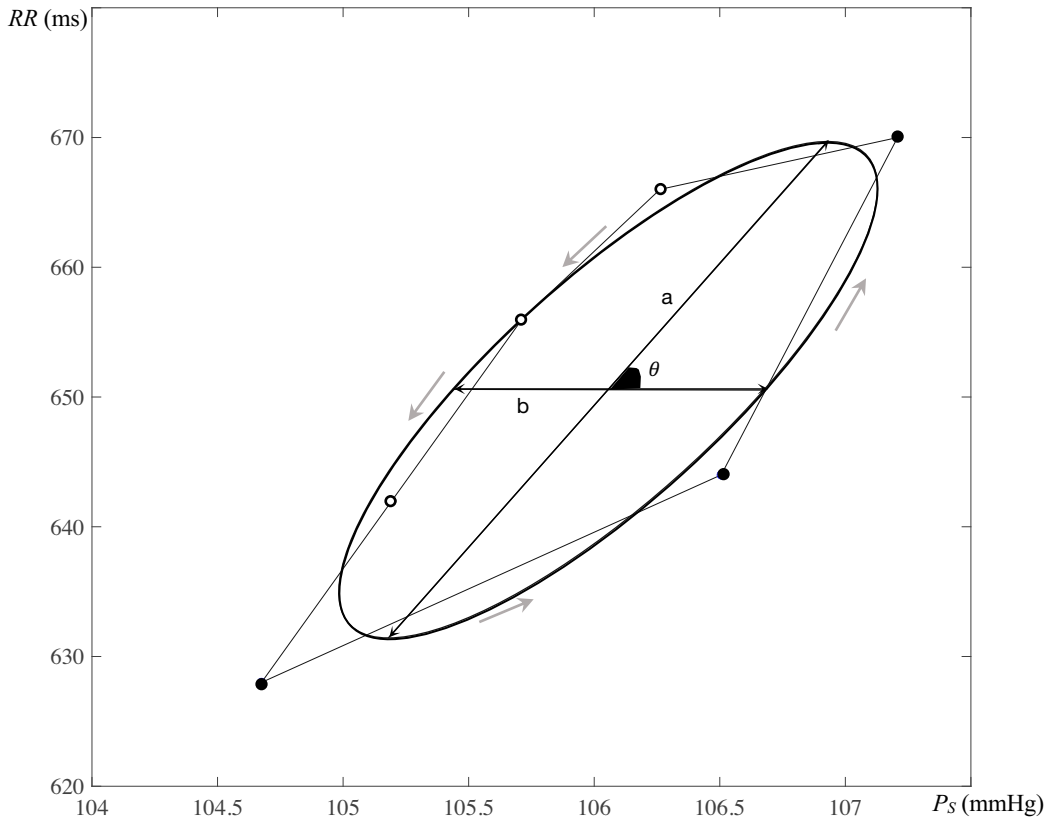

Figure 11 - Representative example of the best fitted ellipse to a baroreflex cycle using the ellipse method. Data from subject A1 in supine position.

In the cases when the polygons corresponding to the baroreflex cycles were composed of several regions, *regionprops* returns as many ellipses as regions, and each of them is the best fit of the corresponding region. An illustration of a cycle in these conditions and of the fitting process in that case can be found in Figure A-2, Appendix A. The best fit ellipse of the whole region is calculated by the weighted, by the area of each region, summation of the parameters (centroid, minor axis length and orientation) obtained for each region. Given that the orientation of the separate regions only varies by $\pm 1\%$, the total length of the major axis is a simple summation, without weights, of the lengths of the major axes of each region, unlike the other parameters. A representative example of the best fit ellipse to a cycle with several regions can be found in Figure 12. The ellipse is centred at (124.8 mmHg, 661.3 ms), has b = 1.46 and a = 125.2, in $(\text{mmHg}^2 + \text{ms}^2)^{1/2}$, θ = 81.6° and area of 43.3 ms·mmHg. The *BRS* for this cycle is 6.7 ms/mmHg.

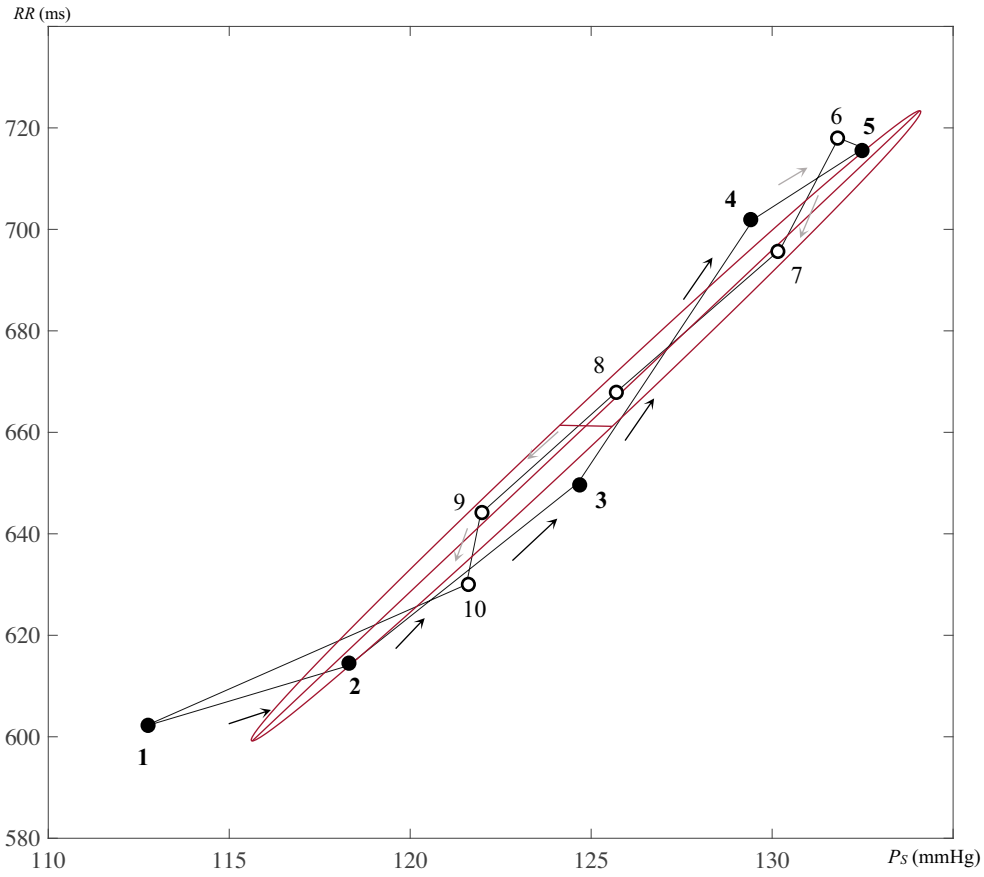

Figure 12 - Representative example of the best fit ellipse to a baroreflex cycle with five regions using the ellipse method. Data from subject A1 in supine position.

The ellipse method was applied both to the sequences, allowing the obtention of a BRS value directly comparable to the results from the regression, and to the cycles, allowing the characterization of hysteresis. An example of the ellipse method applied to a sequence region is found in Figure 13. The ellipse is centered at (106.1 mmHg, 647.3 ms), has semi major and minor axes lengths of 17.2 and 0.41, in $\sqrt{\text{mmHg}^2 + \text{ms}^2}$, orientation of 86.7° and area of 7.1 ms·mmHg. The BRS estimate for this sequence using the ellipse method is 17.4 ms/mmHg.

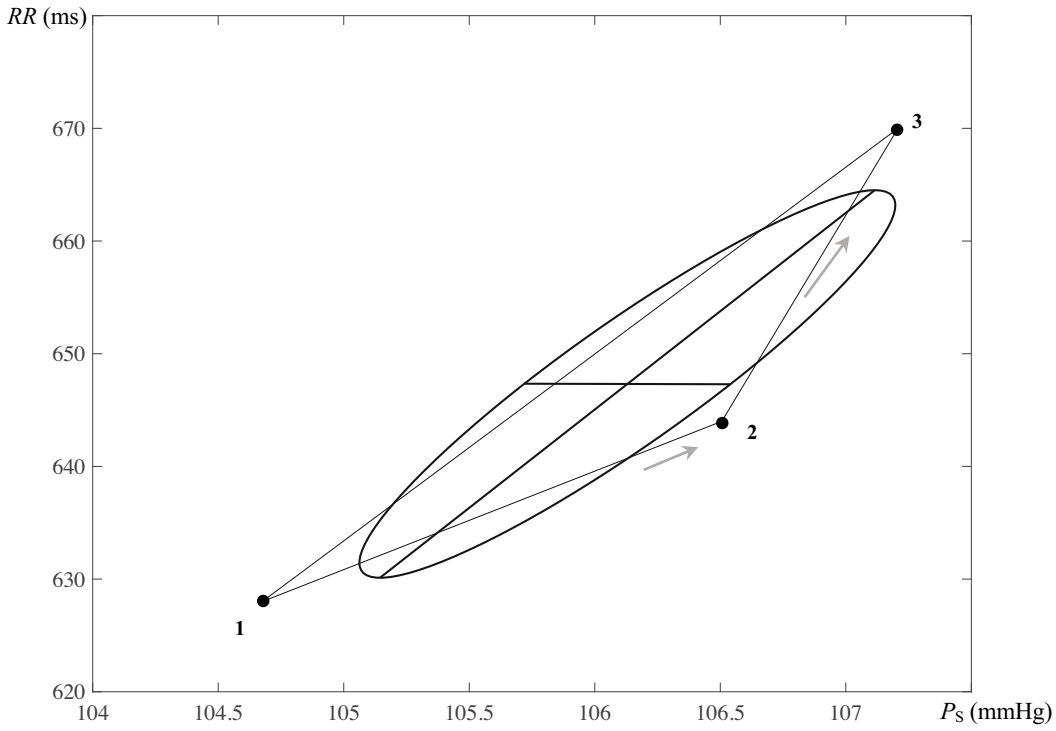

Figure 13 - Representative example of the best fit ellipse to a baroreflex (ascending) sequence using the ellipse method. Data from subject A1 in supine position.

Considering sequence analysis with this method, the only relevant parameter to extract is the θ since it provides the BRS estimate for that sequence. However, when the ellipse method is applied to cycles, the ratio between axes of the ellipse can provide information about the hysteresis behaviour of the *RR*-P_S curve (see section 2.3.1.1). Additionally, it was investigated how did the area and centroid of the ellipse vary across the dataset and if these parameters, by determining the shape of the *RR*-P_S pattern, can be relevant to the understanding of the dynamics of the baroreflex mechanism. The ellipse area is calculated as $\pi \cdot a \cdot b$ and given in $ms \cdot mmHg$.

2.3.1.1. Hysteresis characterization

Hysteresis for each cycle was obtained as a ratio between the length of the major axis and the length of the minor axis of the best fit ellipse to that cycle, according to Ler *et al.* (2010). This ratio was defined as the hysteresis index *H* according to equation (2-6) and one value was obtained per cycle and when *H* equals 1 the *RR*-P_S relation is a circle.

$$H = \frac{b}{a}, \quad 0 \leq H \leq 1 \quad (2\text{-}6)$$

Parallelly, to investigate the possible integrated (neural and mechanical) modulation of baroreceptor firing, values of setpoint difference Δ*Setpoint* and slope difference Δ*BRS* between ascending and descending portions was calculated for each cycle as shown in Figure 14. These quantities correspond to the qualitative and quantitative assessment of hysteresis, respectively. Δ*BRS* was calculated as a difference between *BRS* obtained as the slope of ascending and descending portions of the cycle using the regression method. Δ*Setpoint* corresponds to the maximum vertical distance that can be defined within each ellipse, as illustrated in Figure 14.

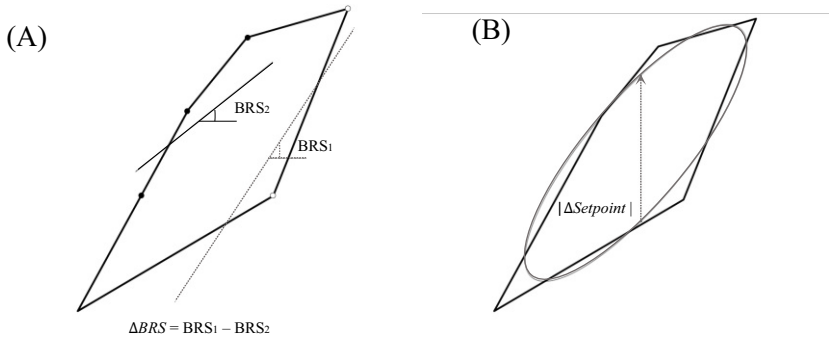

Figure 14 - Illustration of calculation of values of (A) ΔBRS and (B) Δ*Setpoint*.

The sign of Δ*Setpoint* was attributed according to the polygonal shape of the cycle since the best fit ellipse will always show a positive value of Δ*Setpoint* derived from its own geometrical shape. Cycles with intersection of ascending and descending sequences, resulting in several regions, were determined to have a positive Δ*Setpoint*. In all the other cases, the hysteresis value as Δ*Setpoint* is negative since *RR* is longer along the whole descending portion of the curve, comparing to the ascending portion.

The weight γ_{Up} and γ_{Dn} of each ascending and descending, respectively, portions in the total hysteresis were estimated per cycle as the ratio between the minor axis length of the ascending/descending sequence and half of the minor axis length of the cycle.

2.3.2. Sequence method

For time domain cardiovagal BRS estimation in time domain a function was created that identifies consecutive sequences of opposite common trend in P_S and *RR*. A linear regression fit, in the least-squares sense, is applied to each sequence and the *BRS* of the sequence corresponds to the slope of that regression line. In this way, *BRS* estimates were obtained for all sequences of all subjects in the dataset, in both positions. A visual example of the regression method is presented in Figure 15.

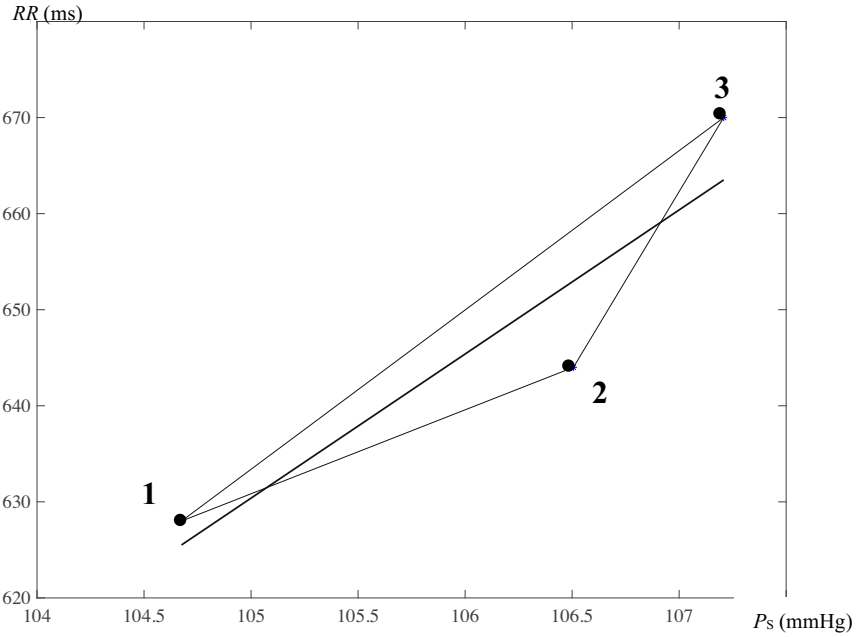

Figure 15 - Representative example of the regression method applied to one sequence of ascending trend. Data from subject A1 in supine position.

P_S and *RR* of the sequence are, in mmHg and ms respectively, (104.7, 106.5, 107.2) and (628, 648, 670). The *BRS* obtained for this sequence is 15.0 ms/mmHg.

The parameters reported to affect the performance of the sequence method are sequence beat duration, coefficient of correlation of the linear regression, minimum instantaneous variation of P_S or *RR* and application of a lag of few beats between *RR* and corresponding P_S (Laude *et al.* 2004). In this work, it was chosen to validate sequences with a minimum of two beats and consider BRS estimates as faithful representatives of the cardiovagal sensitivity only if the Pearson coefficient of correlation between P_S and *RR* values of the sequence is superior to 0.85. No restrictions were applied to the minimum instantaneous variation between P_S or *RR* values. The effect of applying a lag of one beat between P_S and the corresponding *RR* was investigated. In lagged sequences, beat 1 of P_S time series is corresponded with beat 2 of *RR* time series, in the sequence illustrated in Figure 10 (A) and successively for all P_S values of the sequence. Additionally, the beat-to-beat systolic pressure variability (*SPV*), *HRV* and *BRS* of each sequence were also investigated (cf. section 3.2).

2.3.3. Spectral analysis

Beat-to-beat series of *RR* and P_S were resampled at 4 Hz by linear interpolation to construct equidistantly spaced time series. The mean value was subtracted from both signals to eliminate the DC component, corresponding to nonharmonic components in the VLF region.

The power spectra of both time series were calculated by means of fast Fourier transformation. In the power spectral analysis of short-term fluctuations of *RR*, three main frequency bands can be distinguished, as explained in section 1.1.1.2: VLF in the range of 0.01-0.04 Hz, LF in the range of 0.04-0.15 Hz and HF in the range of 0.15-0.4 Hz. The spectral powers were obtained by simple summation, across each frequency band, of the squared spectral peaks. In this way, values for VLF, LF and HF spectral powers were obtained in absolute units (ms^2) and in normalized units, normalization by the total spectral power value. The ratio LF/HF was obtained as an indicator of sympathovagal balance. The values were used for obtaining the BRS estimates in the form of the ratios αLF and αHF, one per subject in each position.

As an alternative frequency method to obtain BRS estimates, mean values of magnitude of the cross spectrum in the LF frequency bands (csBRS) were calculated and their coherence was investigated. The cross spectrum was computed using Welch's averaged, modified periodogram method of spectral estimation.

2.3.4. Statistical analysis

A paired t-test was used to compare mean values of all results between supine and standing positions and those values were considered statistically significant for a $p < 0.005$. The p-value p corresponds to the probability that the mean difference between the two sets of observations being compared is zero. If this hypothesis is verified, all the observable differences can be explained by random variation. If not, the differences between observations have statistical significance.

The results of *BRS* estimates obtained using different methods were presented as median (mean ± SE). Results were obtained for all sequences, allowing the comparison between regression and ellipse method estimates. In addition, results of only sequences which are part of cycles were also obtained, allowing the comparison with ellipse method BRS estimates for cycles. Cross correlation between methods was calculated as a Pearson coefficient of BRS estimates, for results of all sequences.

The median, 25th and 75th quartiles of the characteristics, namely major axis length a, minor axis length b, and orientation θ, of all ellipses in the dataset were obtained separately for supine and standing positions to get an overview of how the shape of the baroreflex cycle is affected by postural change. The resulting ellipses were subjected to a simplified version of dual axis fourier shape analysis (Moellering & Rayner, 1981). The digitized best fitted ellipse is periodic and generates two orthogonal time series, RR and P_S that can be subjected to harmonic analysis individually to obtain values for the phase shift between RR and P_S values in the cycles. Cross correlation between ellipse shapes and actual polygonal cycle shapes was calculated as a Pearson coefficient of values for area.

2.4. Graphical User Interface

A multi window Graphical User Interface (GUI) was implemented using MATLAB R2020a (The MathWorks Inc., Natick, MA, USA), allowing easy cardiovagal baroreflex computation using all the methods described in this work for any dataset. In this section, this GUI is presented.

The app creation was inspired by the EuroBaVar dataset, so it is prepared to run a comparative analysis of data from both supine and standing positions. However, single position data can also be processed.

In terms of data upload, files with any extension are accepted if the data is formatted in a $m \times n$ matrix with m samples and n biosignal recordings (channels). A maximum of $n = 4$ channels is accepted, and the recordings can be ECG (in mV or in V), mechanic barocardiogram (in mmHg), pulse plethysmogram or PPG (in mV) or mechanic respirogram RESP-belt (in mV). Logically, there should not exist any channels measuring the same bio signal but if there are then the last specified channel is taken for processing, e.g. in the case where both channels 1 and 4 are specified as ECG, channel 4 is taken for processing.

A commented flowchart describing the working of the windows *Main*, *Data Upload*, *Data visualization* and *Cardiovagal BRS* of this GUI app is presented in Figure 16-19.

The goal was to make the GUI app as user friendly as possible and the several protections and pop-up messages were implemented to concretize that goal.

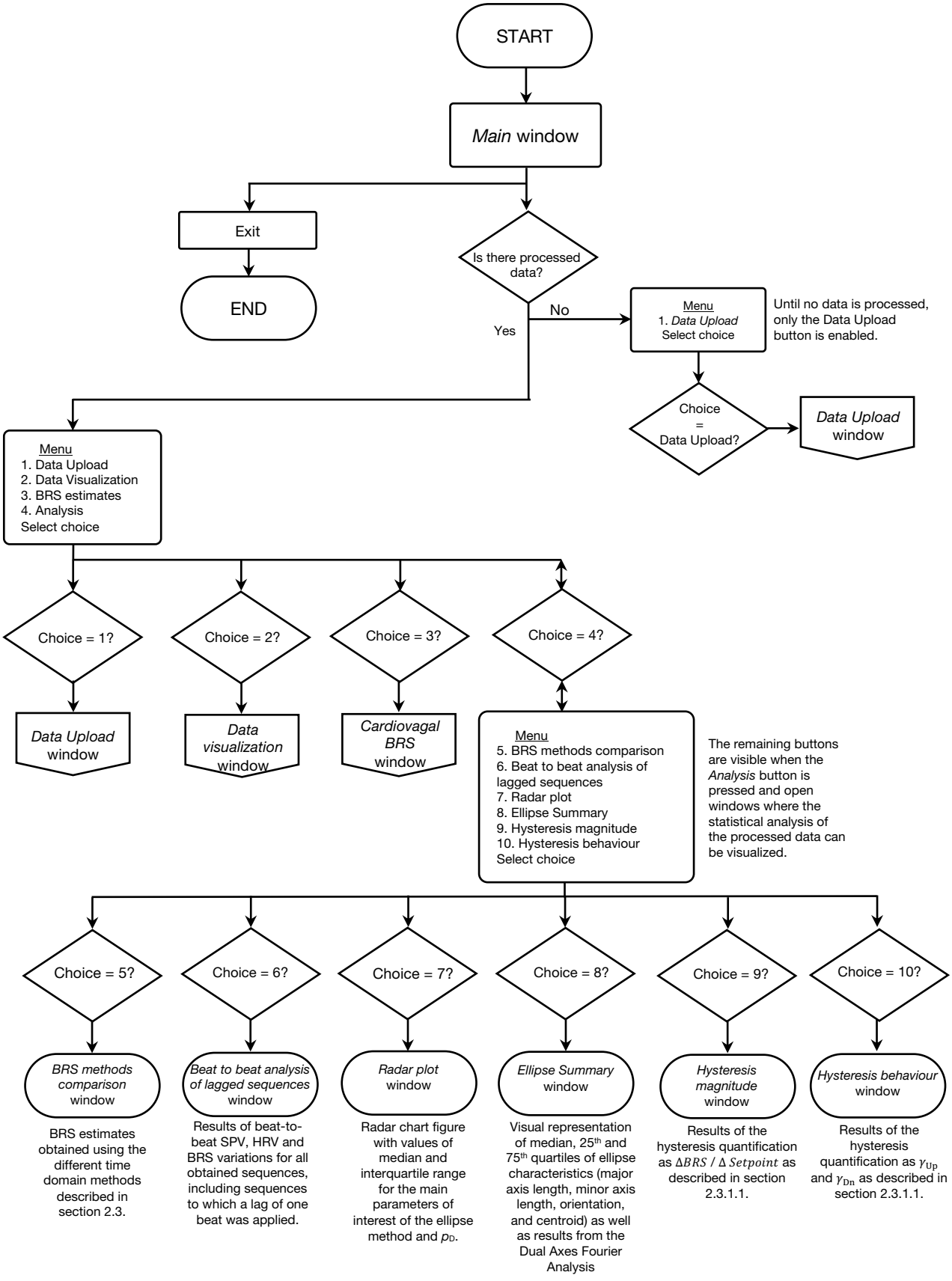

Figure 16 - Flowchart describing the working of the *Main* window of the GUI app

.

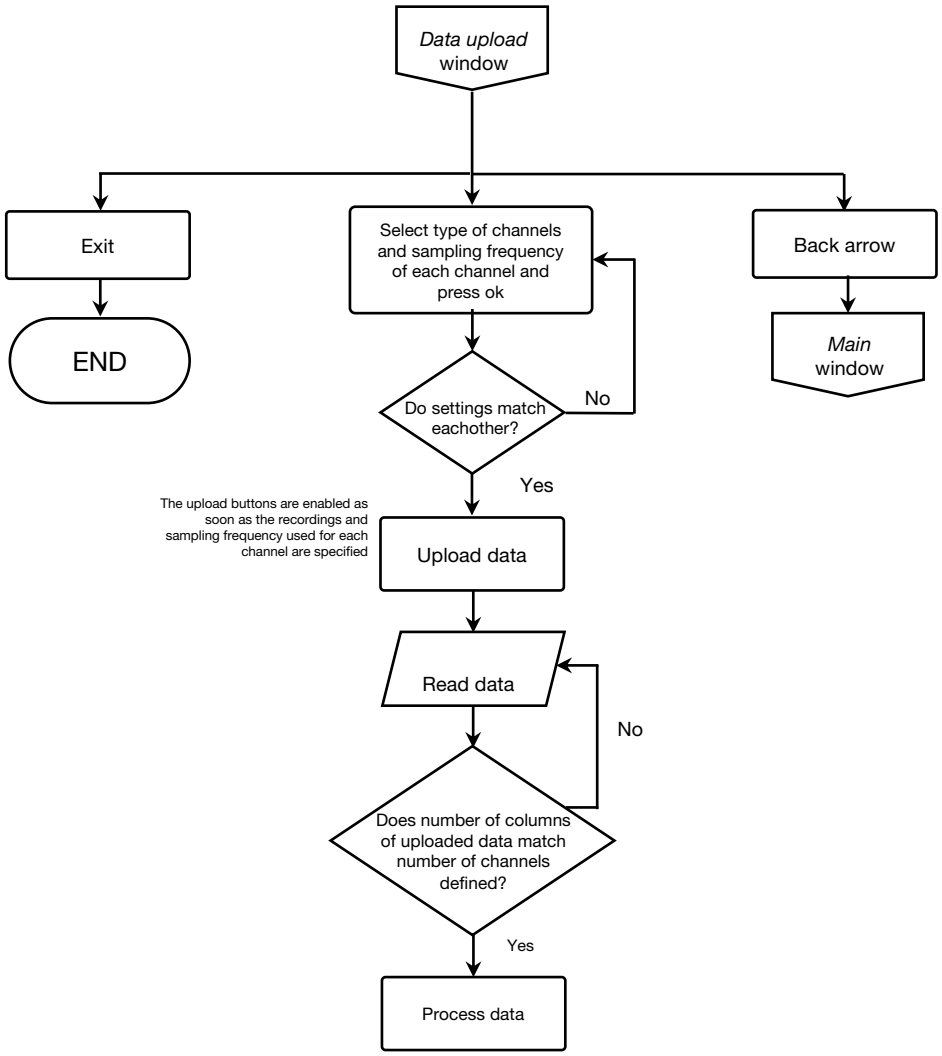

Figure 17 - Flowchart describing the working of the *Data Upload* window of the GUI app

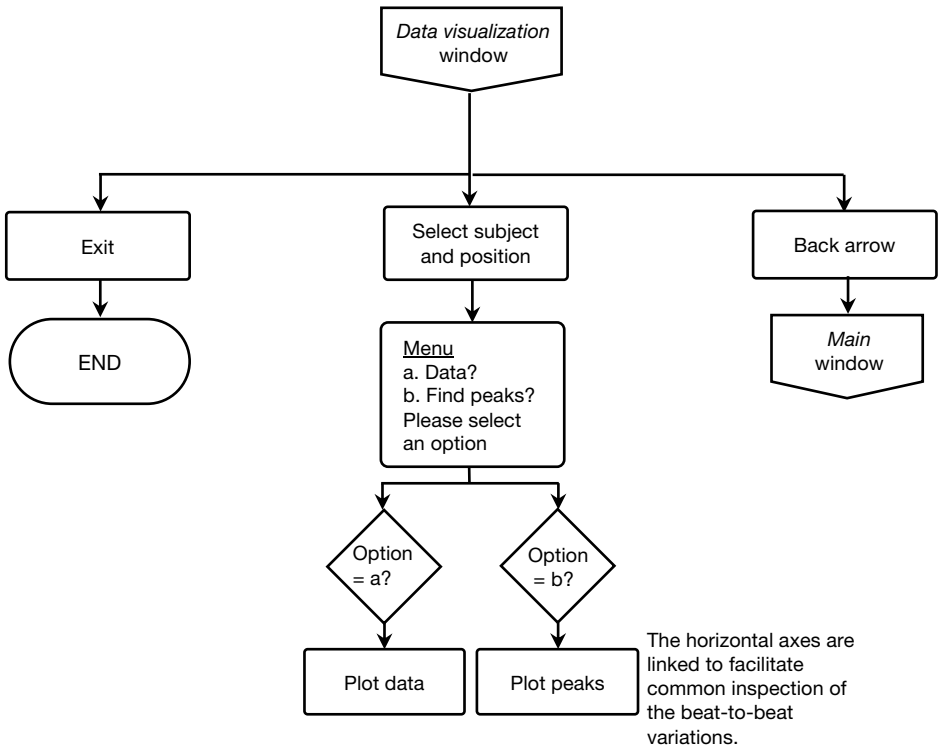

Figure 18 - Flowchart describing the working of the Data visualization window of the GUI app.

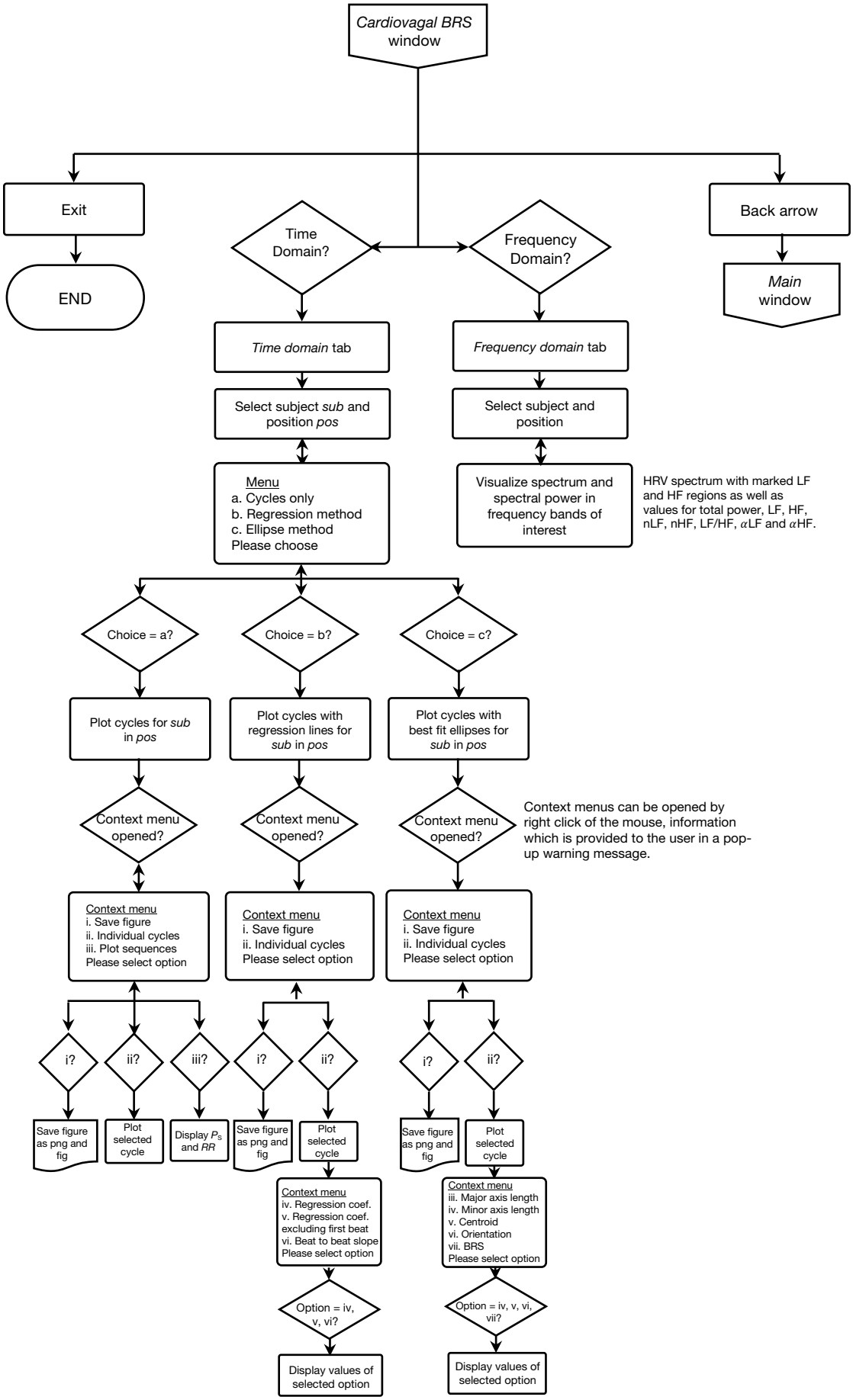

Figure 19 - Flowchart describing the working of the *Cardiovagal BRS* window of the GUI app.

CHAPTER 3.

Results

In this chapter, the results obtained in this work are presented. These results include *BRS* from spectral method and time domain regression and ellipse methods, results of hysteresis assessment as an index *H*, quantitative and qualitative results of hysteresis assessment as Δ*BRS* and Δ*Setpoint* respectively, values for weight of each ascending or descending sequence in the total hysteresis, γ_{Up} and γ_{Dn}, as well as parameters obtained from the ellipse analysis of the cycles, such as area and centroid position.

3.1. Ellipse method

Results for *BRS* estimates obtained using this method were chosen to be presented in section 3.4 as IQR values along with the estimates of the regression method to allow direct comparison between results of both methods. The coefficient of cross-correlation between best-fit ellipses and polygonal shapes, calculated by comparison of area values for both shapes, was 0.99.

In Figure 20, the summary plot of characteristics of the median and IQR ellipses found in the dataset is presented. The inner ellipse corresponds to the 25th quartile of axes lengths and orientation, the middle ellipse to the 50th quartile (median value) and the outer ellipse to the 75th quartile of these quantities. The shaded area corresponds to the IQR. The ellipses are centred in the median centroid position value for each position.

In Table 3, the major axis *a* of the ellipse decreases by 32% of the median value, from 70.8* to 48.4* while the minor axis *b* increases by 61% of the median value from 3.6* to 5.8* from supine to standing position. There is also a 62% decrease in *BRS* (from 13.6 to 6.7 ms/mmHg) due to the smaller angle of orientation θ in standing position. The position of the centroid does not vary significantly in P_S value, but the *RR* value is higher by 154.1 ms in supine position.

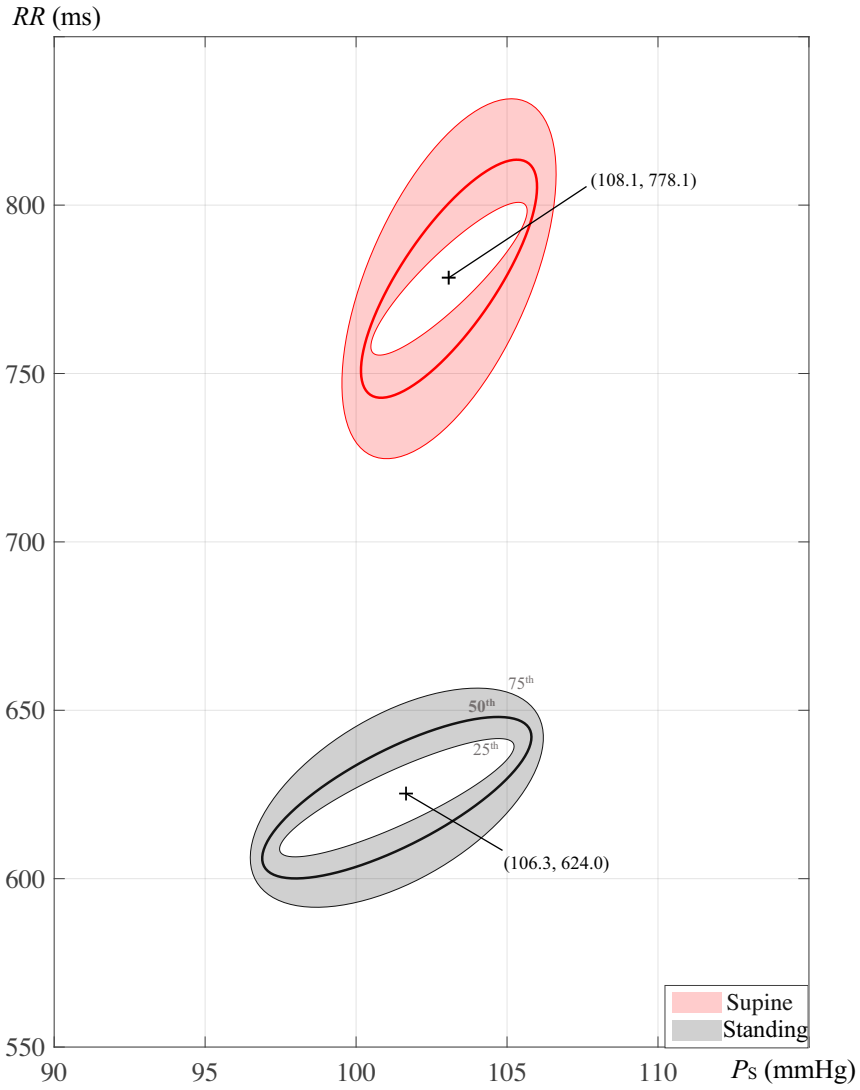

Figure 20 – Summary plot of the median and IQR ellipses fitted to the baroreflex cycle. The inner contour ellipse corresponds to the 25th quartile of data, the middle one to the 50th (median) and the outer one to the 75th. To simplify visualization, the IQR ellipses are relocated at the median value of the centroids obtained for the dataset.

Table 3 – Values of quartiles of main characteristics of the best fit ellipses obtained.

	Major axis length a^*		*Minor axis length* b^*		*Orientation* θ *(°)*	
	Supine	Stand.	Supine	Stand.	Supine	Stand.
25th	45.6	35.8	2.4	3.8	83.9	79.0
Median	70.8	48.4	3.6	5.8	85.8	81.5
75th	107	65.2	5.8	8.0	87.4	85.2

* $(ms^2 + mmHg^2)^{1/2}$

In Figure 21, IQR and median curves of Δ*RR*, the vertical difference in ms, and ΔP_S, the horizontal difference in mmHg, calculated at equidistant points along the ellipses. The maximum magnitude of Δ*RR* for the median curve, corresponds to median value of Δ*Setpoint* in Figure *28*. This value is 45.6 ms (occurring at a P_S value of 108.0 mmHg) in supine position, superior by 35.3% than the value of 33.7 ms (occurring at a P_S value of 106.0 mmHg) obtained for standing position. Reciprocally, the maximum magnitude of ΔP_S for the median curve decreases by 36.2% from 3.7 mmHg (occurring at a *RR* value of 768 ms) in supine position to 5.8 mmHg (occurring at a *RR* value of 627 ms) in standing position. Reciprocally, the maximum magnitude of ΔPS for the median curve increases by 36.2% from 3.7 mmHg (occurring at a RR value of 768 ms) in supine position to 5.8 mmHg (occurring at a *RR* of 627 ms) in standing position.

In Figure 22, the decomposition of *RR* and P_S series of values in cycles is presented through IQR and median curves. The inner curve corresponds to the 25th quartile, the middle curve corresponds to the 50th quartile (median) and the outer curve to the 75th quartile of those values. The shaded area represents the IQR of these series. From Table 4, the phase shift increases by 1.9° of the median value in standing position, while the *RR* deflection decreases by 32% (from 70.7 to 47.9 ms) and the P_S deflection increases by 35% (from 5.8 to 8.9 mmHg) of the median, compared to supine.

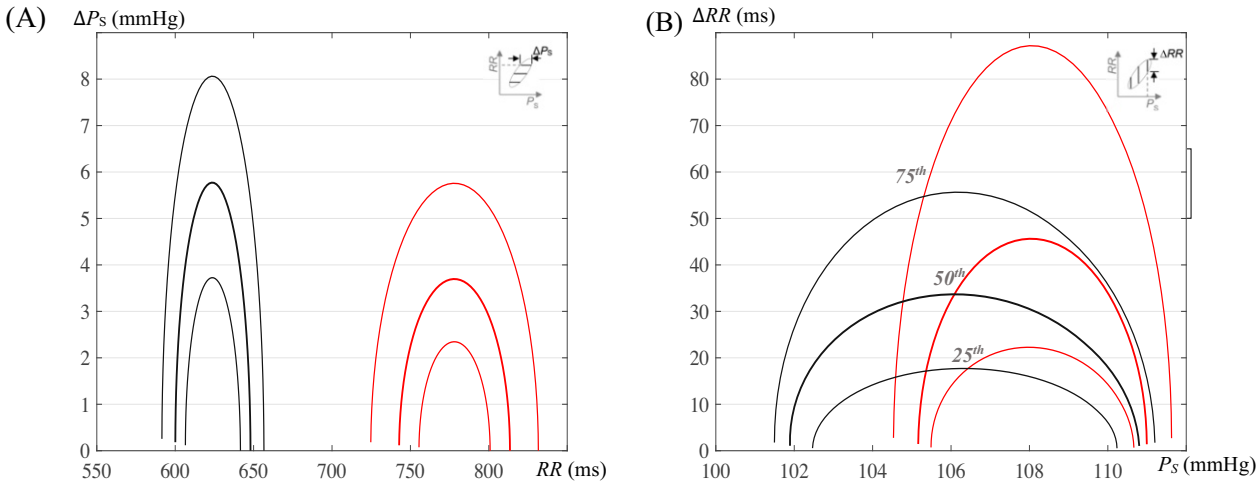

Figure 21 – IQR values of (a) Δ*RR* in the best fitted ellipses as a function of P_S and of (b) ΔP_S as a function of *RR*.

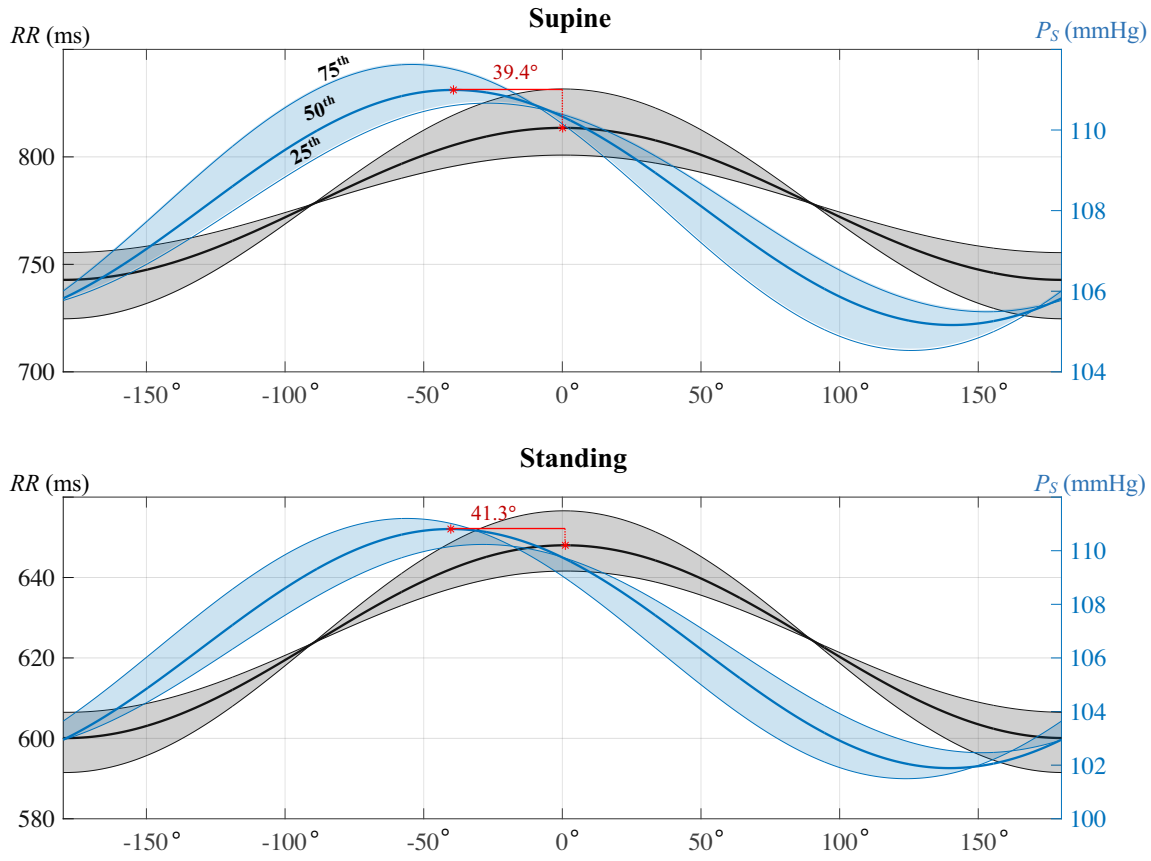

Figure 22 - Phase shift between *RR* and P_S series of values in cycles. The respective maxima and delays are marked between median-related curves of P_S and *RR*.

Table 4 – Values of phase shift and deflection between decomposition curves of *RR* and P_S series.

	Phase shift (°)		*Deflection of RR (ms)*		*Deflection of Ps (mmHg)*	
	Supine	Standing	Supine	Standing	Supine	Standing
25th	27.3	29.8	45.4	35.1	5.2	7.7
Median	39.4	41.3	70.7	47.9	5.8	8.9
75th	54.3	56.7	106.9	65.1	7.1	9.7

The radar chart in Figure 23 allows the direct comparison of IQR and median values obtained for ellipse parameters, being that the area, *BRS*, x_c (centroid values of P_S), y_c (centroid values of *RR*) and *H* (hysteresis index). Additionally, values for diastolic pressure P_D across the dataset are also presented in this summary. In standing position median values of y_c (from 778.1 to 624.0 ms) and *BRS* (from 15.7 to 7.0 ms/mmHg) are decreased while the median *H* (from 0.05 to 0.11) and P_D (from 61.3 to 64.8 mmHg, $p < 0.005$) are increased and median values of area and x_c show no significant difference.

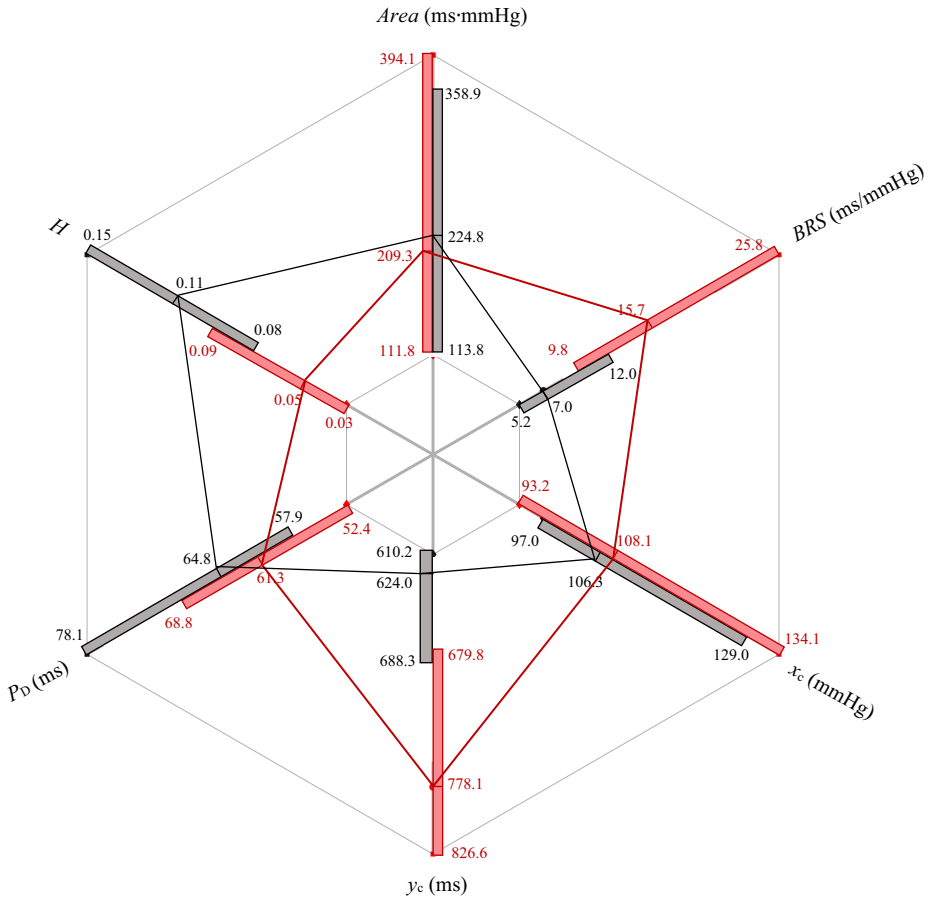

Figure 23 - Radar chart of the IQR values of parameters of the best fitted ellipses found.

In Figure 24, the trajectory formed by the positions of the centroids of the best fit ellipses is found, for each subject with a significant number of cycles (superior to 10) of the dataset. The pressure range of these centroids is highly variable from subject to subject but as a general trend, for similar P_S range higher values of RR are found in supine position, reflecting the higher efficiency of the baroreflex mechanism in this position. The range of P_S varies between 85-180 mmHg and the range of RR between 550-1000 ms.

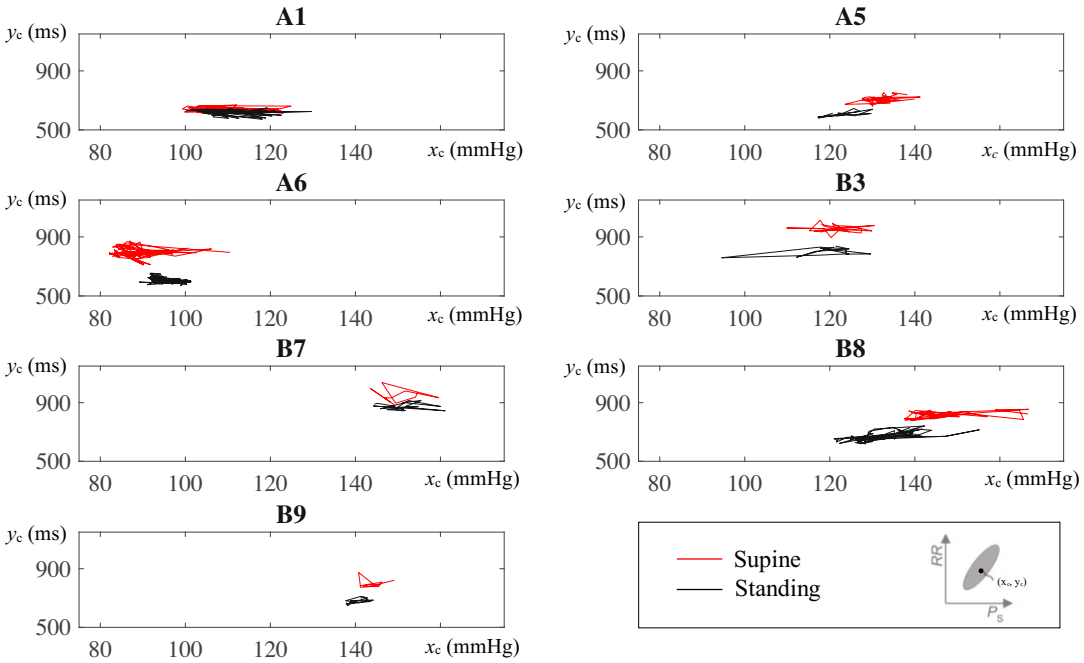

Figure 24 – Trajectory formed by the centroids of the ellipses for each subject. Only subjects with cycles superior to 10 in number are shown.

In Figure 25 the probability distribution of centroid values (x_c, y_c) of the best fitted ellipses in the dataset is presented. Each point of this distribution corresponds to the operating point of the baroreflex for each cycle if it would be reduced to a point in space (its centre of mass). The range of P_S in which the baroreflex sequences are found is mainly 90-140 mmHg. For *RR*, the range is mainly 550-900 ms. In terms of mean, the postural differences between P_S are not significant, from Table 5, but mean *RR* is decreased by 14% in standing position. This leads to the location of the standing IQR ellipse at a lower *RR* (624.0 ms) than the supine IQR ellipse (778.1 ms) in Figure 20.

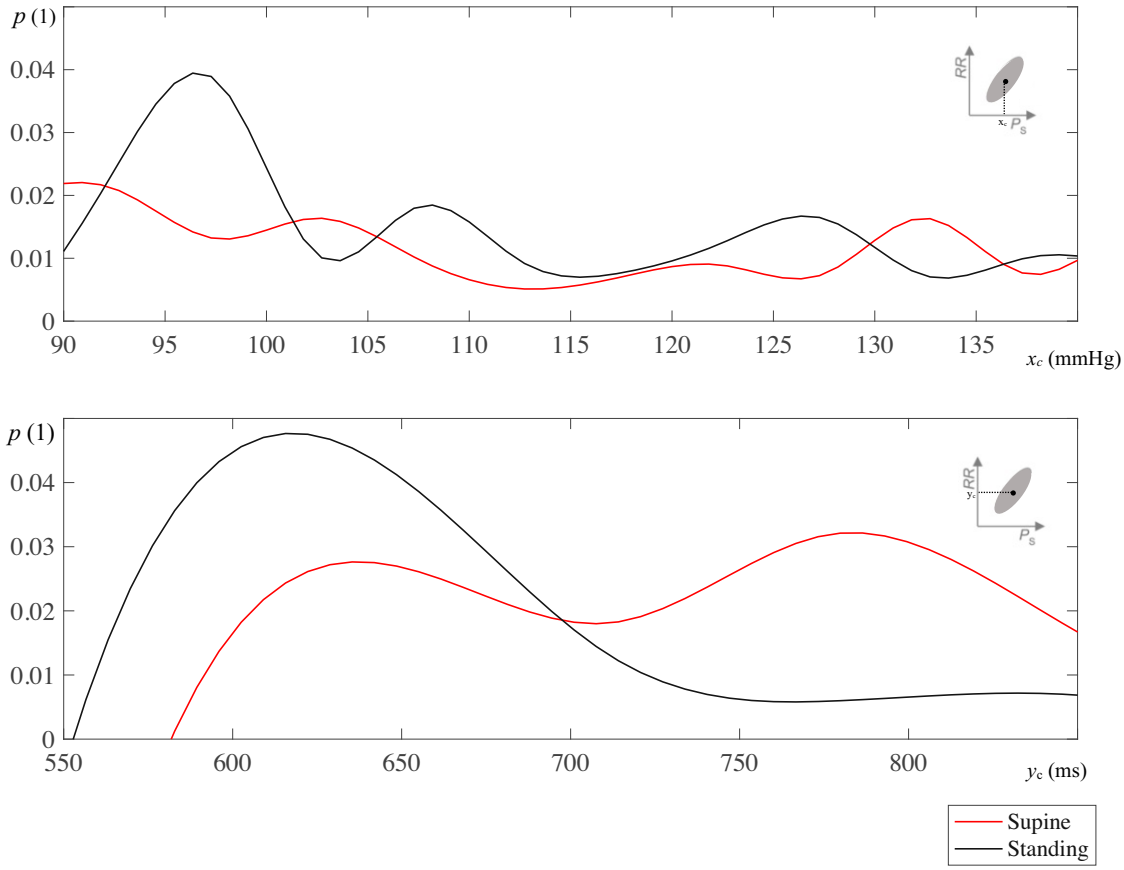

Figure 25 - Distribution of *RR* and P_s of centroids of best fitted ellipses in the dataset.

Table 5 - P_S and *RR* of centroids of best fitted ellipses.

	Supine	Standing	*p*
x_c (mmHg)	109.2 (114.3 ± 23.2)	109.1 (114.3 ± 19.1)	n.s.
y_c (ms)	779.0 (771.5 ± 104.7)	628.7 (663.2 ± 82.3)	< 0.005

In Figure 26 the probability distribution of the values of area for the best fit ellipses to the baroreflex cycles is presented, differentiating between supine and standing positions. From Table 6, it can be concluded that no significant differences between values of area of the ellipses exists between supine and standing positions.

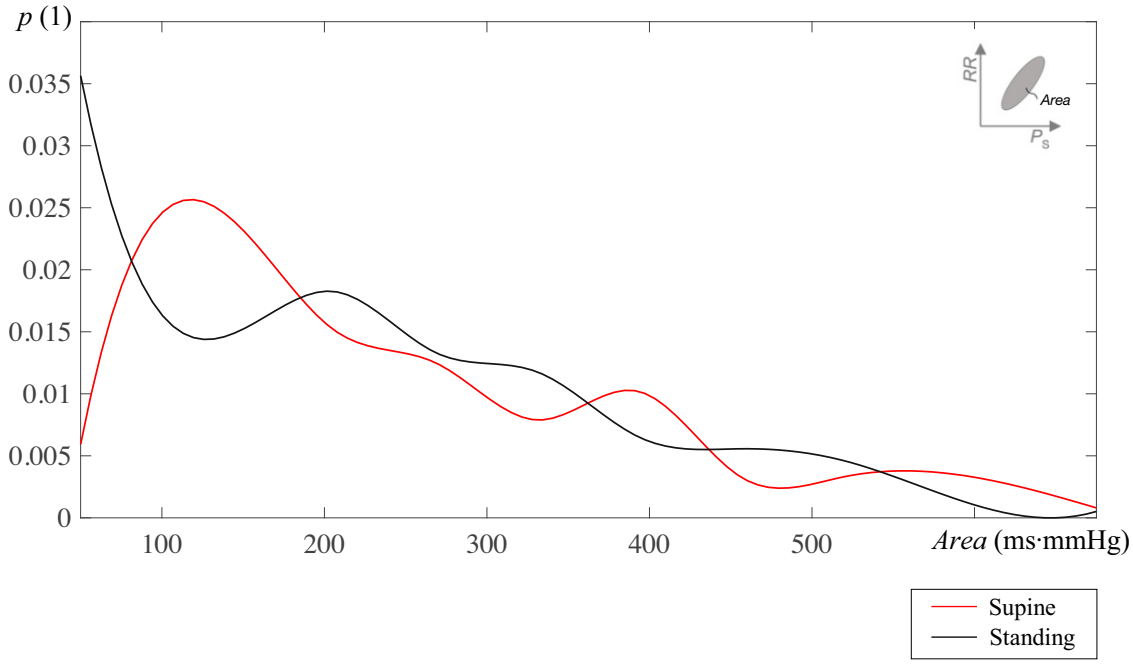

Figure 26 - Distribution of values of area in the best fit ellipses to the baroreflex cycles.

Table 6 - Values of area of best fit ellipses to the baroreflex cycles found.

	Supine	Standing	*p*
Area (ms · mmHg)	209.3 (339.9 ± 516.4)	224.8 (346.6 ± 527.7)	n.s.

3.1.1. Hysteresis quantification

In Figure 27 the probability distribution *p* for values of the hysteresis index *H* is presented. In Table 7, *H* is presented by median (mean ± SE). The mean *H* in standing position was 0.11, increased by 71% percent from 0.07 in supine.

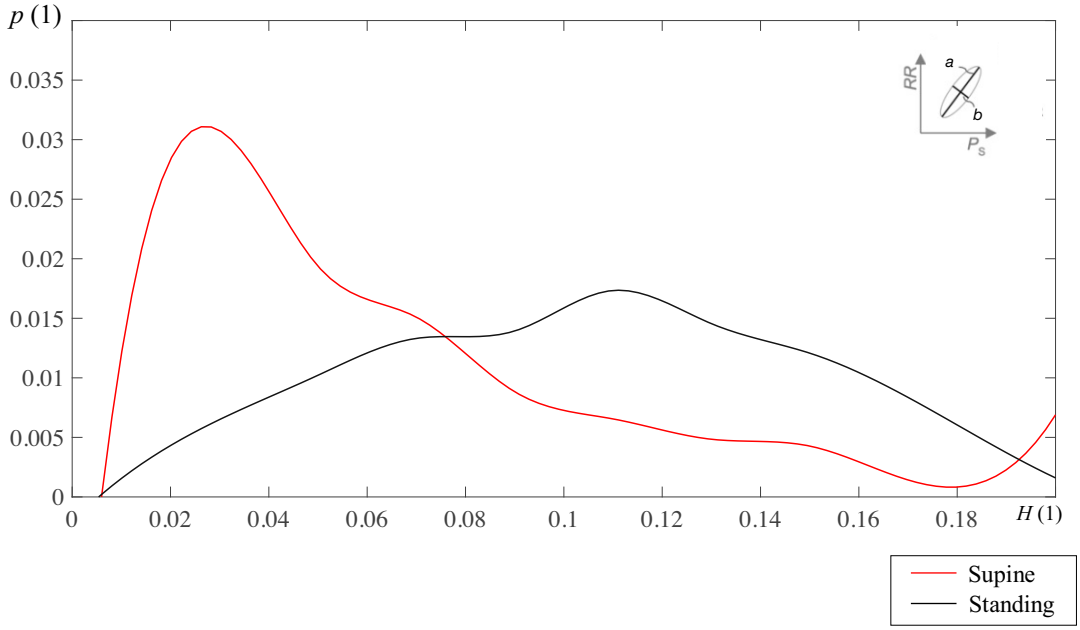

Figure 27 - Probability distribution of the index of hysteresis *H*.

Table 7 - Values of hysteresis index of best fitted ellipses to the baroreflex cycles.

	Supine	Standing	*p*
H	0.05 (0.07 ± 0.06)	0.11 (0.12 ± 0.08)	< 0.005

In Figure 28, the boxplot graphs with values of Δ*BRS* and Δ*Setpoint* across trials are found, with distinction between supine and standing positions. As explained previously (section 2.3.1.1), these quantities will be positive if the *BRS* and setpoint value of the ascending sequence of the cycle is higher than the *BRS* and setpoint value of the descending sequence, respectively. The mean value of Δ*BRS* decreased with postural change by 114% from 4.2 ms/mmHg in supine to -0.6 ms/mmHg in standing position, with $p < 0.005$. In terms of Δ*Setpoint*, the mean value varied from -68.1 to -50.3 between supine and standing, decreasing by 26%. The estimate of Δ*Setpoint* for most trials verified the expected trend, with negative value expressing larger *RR* for falling pressures, but 24 out of 386 for supine and 28 out of 346 for standing trials showed the opposite trend. On the other hand, values of Δ*BRS* were positive according to expected in 247 out of 386 cases for supine position but only in 139 out of 374 cases for standing position.

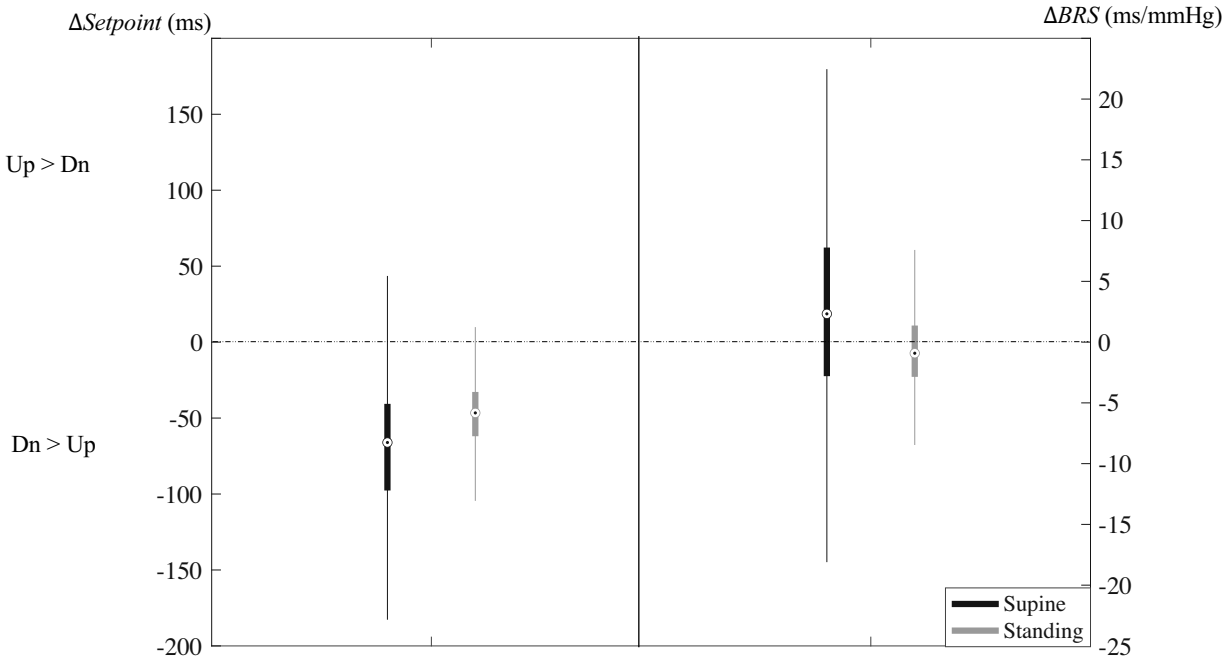

Figure 28 – Hysteresis quantification by values of Δ*Setpoint* and Δ*BRS* between ascending and descending portions of the baroreflex cycles.

In Figure 29, the weight γ of each sequence in the total hysteresis of the cycle is presented, differentiated between ascending and descending sequences and between supine and standing positions. The mean variation of γ_{Up} and γ_{Dn} between standing and supine positions did not have a statistically significant value of p and neither did the mean differences between γ_{Up} and γ_{Dn} for the same position.

The probability distribution of the weight γ of each sequence in the hysteresis of the best fitted ellipse to the cycle is presented in Figure 30, without differentiation between Up/Dn portions. By definition, γ will have a value superior to 1 if there is overlap between Up and Dn portions of the cycle. This happens if the sequences that compose that cycle are highly non-linear resulting in a broad minor axis (b_{Up} or b_{Dn} in Figure *29*) The probability p of this occurring is lower (it only happens in 17.4% of sequences which are part of cycles) than the case where $\gamma \leq 1$ and the sequences do not overlap in the overall hysteresis of the cycle.

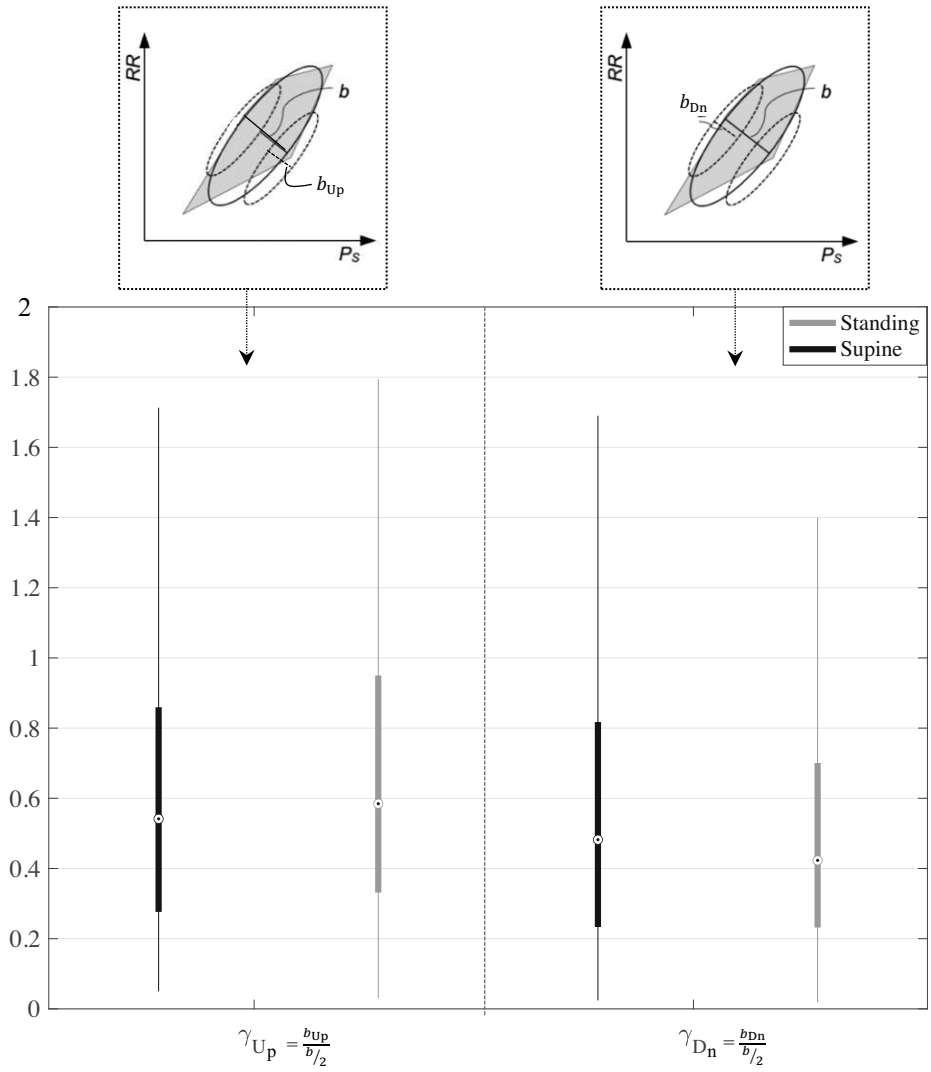

Figure 29 – Contribution of each ascending (γ_{Up}) and descending (γ_{Dn}) sequence to the total hysteresis of the cycle.

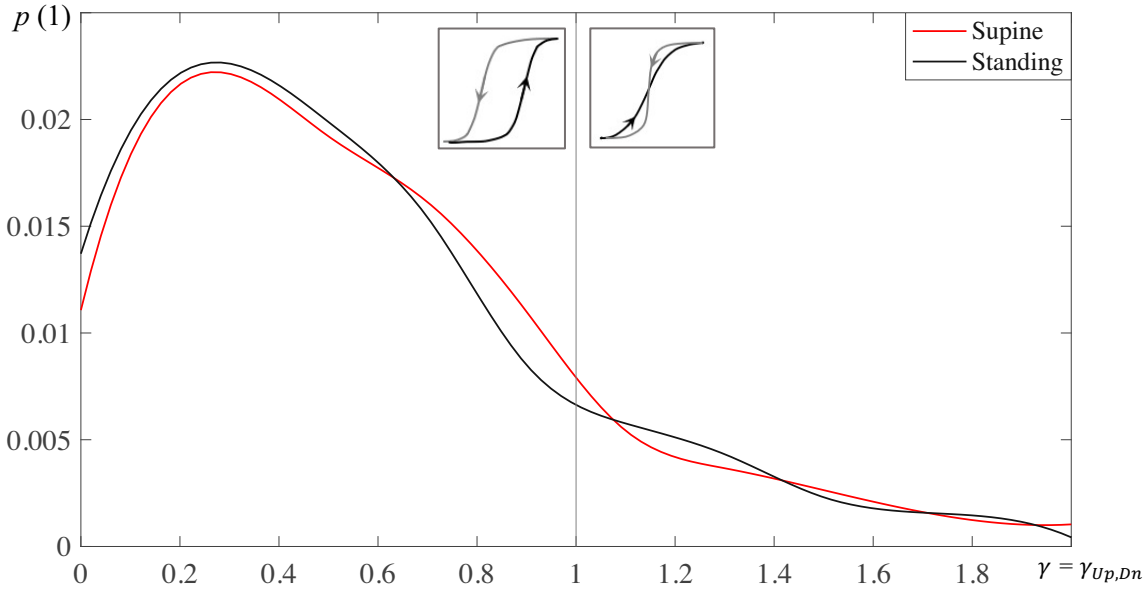

Figure 30 – Probability distribution of γ.

3.2. Sequence method

Results for *BRS* obtained using this method were chosen to be presented in section 3.4 as interquartile range (IQR) values along with the estimates of the ellipse method to allow direct comparison between results of both methods.

Values of *SPV*, *HRV* and *BRS* for the first three beats of each sequence were obtained to understand in which range are these instantaneous variations for the dataset. Values of beat-to-beat *BRS* are calculated as the ratio of beat-to-beat values of *HRV* and *SPV*. Additionally, the effect of applying a lag of one beat between P_S and the corresponding *RR* in the *SPV*, *HRV* and *BRS* was investigated. The results are presented in this section.

In Figure 31, results for beat-to-beat *SPV*, *HRV* and *BRS* are presented by mean ± SE obtained for the first three beats of sequences which are part of cycles. The cycles are composed by two consecutive portions of opposite trend and the spontaneous fluctuations of pressure which originate them can theoretically reflect a respiration cycle. The comparison with lagged sequences in this case does not make sense, since no further analysis in this work includes cycles composed of lagged sequences. Beats 1 to 3 correspond to the first three beats of the ascending portion (**Up**) and beats 4 to 6 correspond to the first three beats of the descending portion (**Dn**) of the cycle, according to A-3 A) (Appendix A). Bar graphs A-C present values in absolute units and the D-E present values in normalized units, normalization by the minimum value of each subtraction. The number of Up and Dn sequences which are part of cycles is not the same because one sequence can simultaneously belong to two baroreflex cycles, as mentioned previously (cf. Figure A-1, Appendix A).

The total *SPV* and *HRV* during a cycle can be found in Table 8 as mean ± SE, differentiated between the ascending (beats 1, 2, 3) and descending (beats 4, 5 6) portions. The maximum mean value of beat SPV is found at the onset of expiration (first beat of ascending sequence) for both positions, with a value of 2.67 mmHg for supine and 3.80 mmHg for standing. Reciprocally, this beat corresponds to the minimum mean of both *HRV* (23.6 ms and 12.3 ms, respectively) and *BRS* (8.8 ms/mmHg and 3.2 ms/mmHg, respectively). The mean *SPV* during the cycle is increased by over 40% in standing position, compared to supine position and reciprocally the mean *RR* is decreased by over 30%. There are no significant differences for the total variation of P_S and *RR* during the cycle between ascending and descending portions.

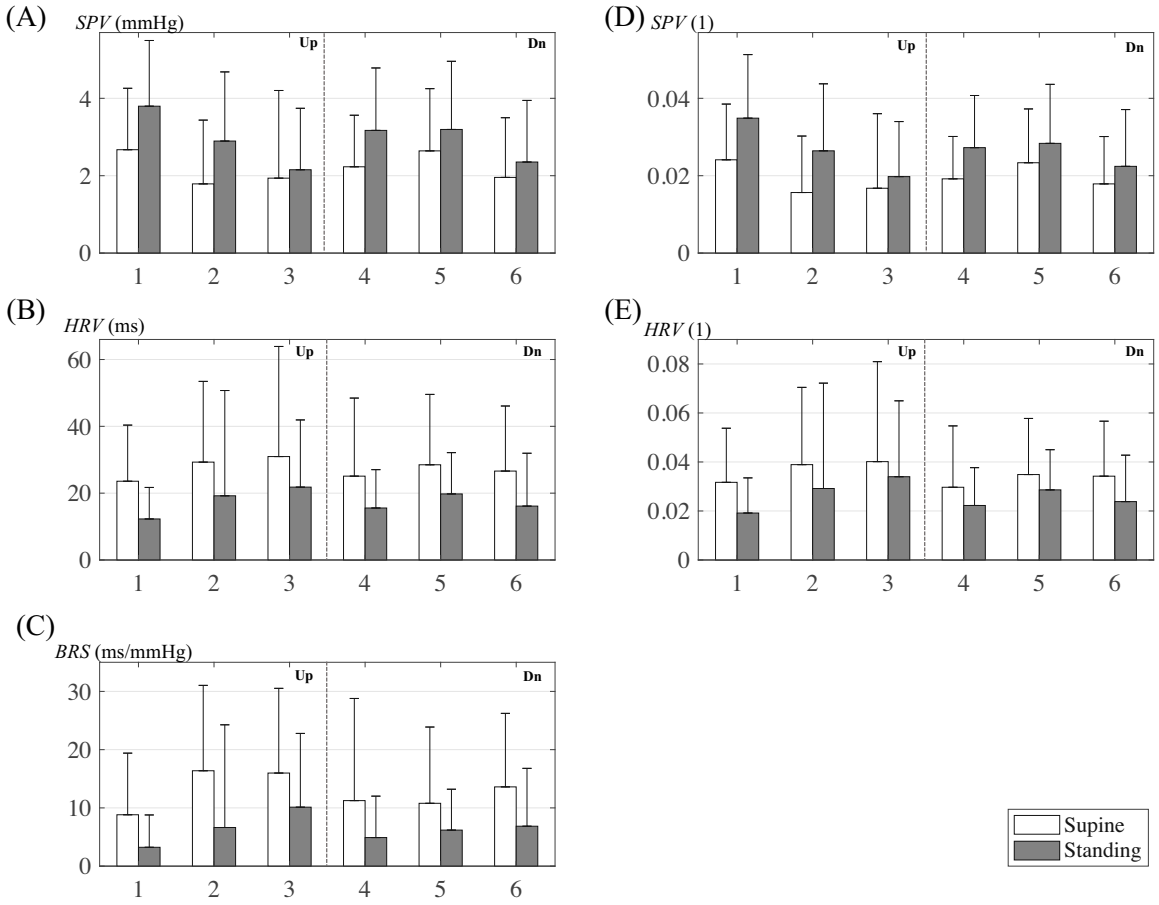

Figure 31 - Beat to beat mean *SPV*, *HRV* and *BRS*. The results shown in this figure are obtained for sequences which are part of cycles, obtained without any delay. For every instantaneous variation (*SPV*, *HRV*, *BRS*) and each beat, $p < 0.005$.

Table 8 - Total deflections during a cycle.

	Portion	**Supine**	**Standing**
SPV (mmHg)	1, 2, 3	5.4 ± 4.5	7.8 ± 4.0
	4, 5, 6	5.9 ± 3.2	7.9 ± 4.2
HRV (ms)	1, 2, 3	67.0 ± 45.1	45.1 ± 48.3
	4, 5, 6	66.6 ± 43.8	45.9 ± 27.8
SPV (%)	1, 2, 3	4.92 ± 4.35	7.36 ± 4.20
	4, 5, 6	5.06 ± 2.55	6.85 ± 3.62
HRV (%)	1, 2, 3	9.21 ± 6.32	7.15 ± 7.33
	4, 5, 6	7.91 ± 4.47	6.51 ± 3.32

In Figure 32, results for beat-to-beat *SPV*, *HRV* and *BRS* obtained for the first three beats are shown by mean + SE. The results are differentiated between sequences of common ascending trend (**Up**) and sequences of common descending trend (**Dn**) of *RR* and P_S. Bar graphs A-C correspond to the results of the sequence method without any lag and the bar graphs D-F correspond to the results of the sequence method applying one beat delay between P_S and

corresponding *RR*. The results are averaged for all sequences found in the dataset of each type. The exact number of sequences of each type can be found in Table 9.

The number of sequences decreases when applying the one beat delay because of the minimum beat duration required to validate a sequence. Sequences with only two beats are usually excluded from the lagged analysis, unless the *RR* value in the beat following the end of the sequence complies with the trend. In sequences longer than two beats, *SPV* are the same with or without delay, only the *RR* with which they are corresponded changes, by the lag definition itself (cf. Figure 7). The *BRS* obtained using the regression method for sequences without lag and lagged sequences, without differentiation between ascending or descending trend, is found in Table 10 as mean ± SE.

Table 9 - Number of sequences, lagged sequences and sequences which are part of cycles found in the dataset.

		Supine		**Standing**	
		# Up	*# Dn*	*# Up*	*# Dn*
Lag 0		745	903	776	1013
	> 2 beats	234	260	266	358
Lag 1		529	452	719	590
	> 2 beats	220	131	299	174
In cycles		298	310	277	305
	> 2 beats	155	166	175	200

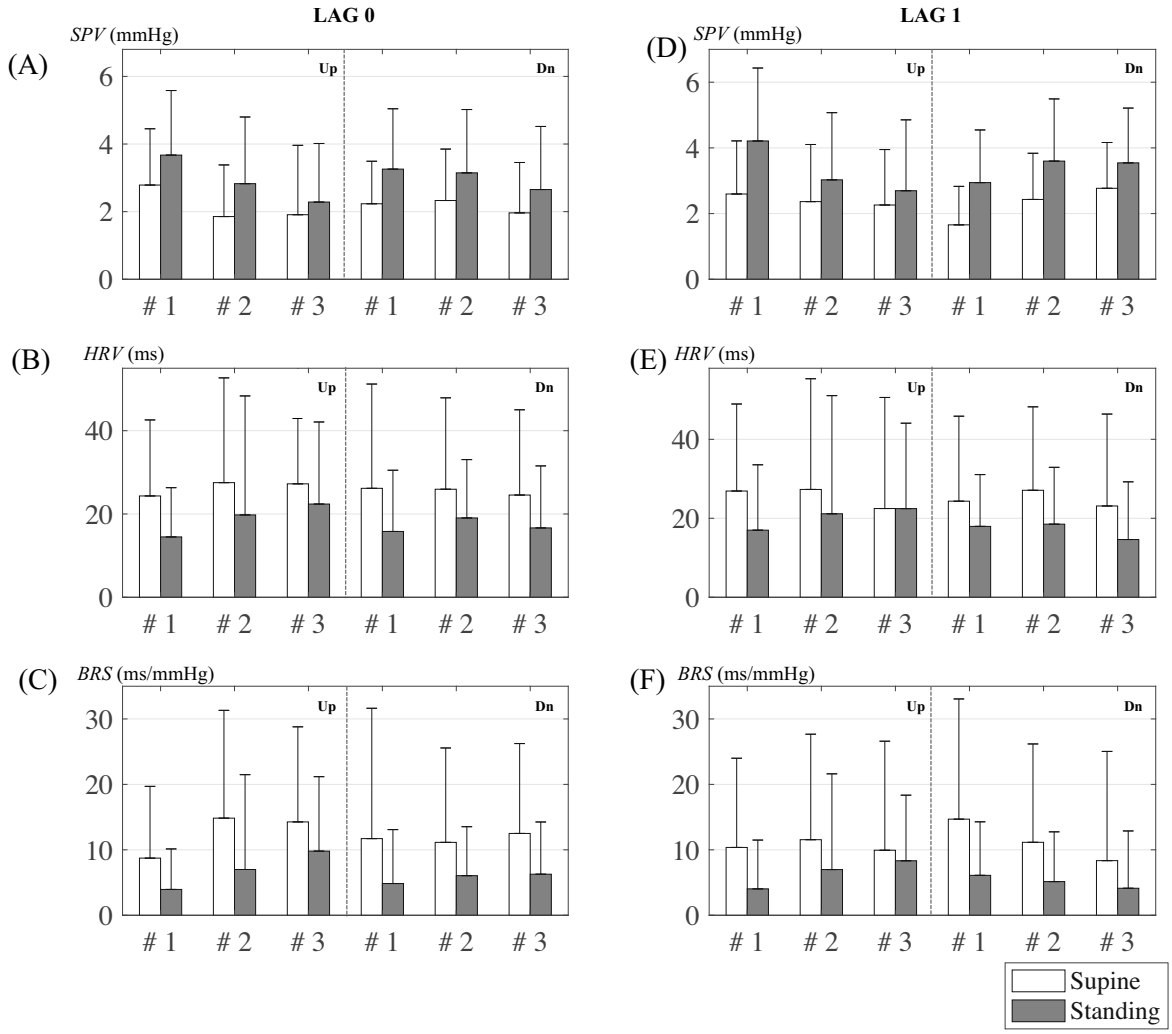

Figure 32 - Beat to beat mean of *SPV*, *HRV* and *BRS*. The results shown in this figure are obtained for all sequences of the dataset. For every instantaneous variation (*SPV*, *HRV*, *BRS*) and each beat, $p < 0.005$.

Table 10 - *BRS* of all sequences obtained using the regression method, without differentiation between ascending or descending trend. Comparison between sequences without delay and lagged sequences. Between supine and standing positions, $p < 0.005$.

	Supine	**Standing**
Lag 0 (ms/mmHg)	13.6 ± 12.7	6.5 ± 6.7
Lag 1 (ms/mmHg)	14.8 ± 19.7	6.6 ± 8.9

3.3. Spectral analysis

Results for spectral power obtained using the fast Fourier transform in the frequency bands of interest, both in absolute values (LF and HF), and normalized by the total power (nLF and nHF), as well as the *BRS* estimates as ratio αHF and αLF can be found on Table 11. Only the values of sympathovagal ratio (LF/HF) and αHF showed statistical significance. The LF/HF mean value was doubled in standing position, due to increased sympathetic outflow. BRS estimates as αHF

showed that a decrease of about 60% of mean happens when moving from supine to standing position (from 18.1 to 7.4 ms/mmHg).

The last row of Table 11 shows the *BRS* estimate obtained by calculation of the cross-power spectrum of *RR* and P_S. This value did not show statistical significance, despite having a coherence mean value superior to 0.5.

Table 11 - Frequency domain analysis using fast Fourier transform for the calculation of the spectral powers.

	Supine	Standing	*p*
Total power (ms^2)	1242.6 (2180.2 ± 2420.6)	1255.0 (1466.5 ± 1561.2)	n.s.
LF (ms^2)	657.1 (1230.0 ± 1322.6)	916.1 (1069.7 ± 1236.2)	n.s.
HF (ms^2)	506.4 (950.2 ± 1194.2)	277.0 (396.9 ± 397.9)	n.s.
LF/HF	1.49 (1.63 ± 1.03)	2.86 (3.25 ± 2.11)	< 0.005
nLF	0.60 (0.57 ± 0.16)	0.74 (0.70 ± 0.17)	n.s.
nHF	0.40 (0.43 ± 0.15)	0.26 (0.30 ± 0.17)	n.s.
αLF (ms/mmHg)	7.6 (10.6 ± 12.0)	1242.6 (2180.2 ± 2420.6)	n.s.
αHF (ms/mmHg)	14.7 (18.1 ± 14.3)	5.9 (7.4 ± 5.8)	< 0.005
cs*BRS* (ms/mmHg)	13.5 (14.9 ± 6.8)	17.5 (18.5 ± 8.9)	n.s.
Coherence	0.51 (0.55 ± 0.17)	0.51 (0.61 ± 0.20)	-

3.4. Statistical analysis

All the time domain *BRS* estimates obtained are presented in Figure 33 and the corresponding values can be found in Table 8 as median (mean ± SE), allowing a direct comparison between supine and standing positions, ascending (Up) or descending (Dn) portions and regression (R) or ellipse (E) methods. The subscript *a* or *c* corresponds to estimates from all sequences or from sequences which are part of a cycle, as illustrated in the figure. The coefficient of cross-correlation between regression and ellipse methods was 0.99.

A decrease of 50-60% in mean *BRS* when moving from supine to standing position is verified for all estimates, whether from regression or ellipse method, and whether analyzing all sequences or only sequences which are a part of cycles. The sensitivity mean value is increased for Up in comparison to Dn sequences, by 27% when using the regression method (16.9 and 13.3 ms/mmHg) and 17% when using the ellipse method (16.2 and 13.9 ms/mmHg) in supine position. This difference is accentuated when analyzing only sequences which are part of a cycle, and the sensitivity increase for Up is of 31% of mean value using regression (17.3 and 13.2 ms/mmHg) and of 25% of mean value (17.9 and 13.4 ms/mmHg) using best fitted ellipse. The *BRS* mean value dependence on the direction of pressure change is not verified for standing position and the differences between Up and Dn estimates for the same method are not significant.

The number of ascending and descending sequences which are part of cycles is not the same, as mentioned previously. The number of cycles is small in comparison to the number of sequences found in the dataset, 44% for supine and 39% for standing positions.

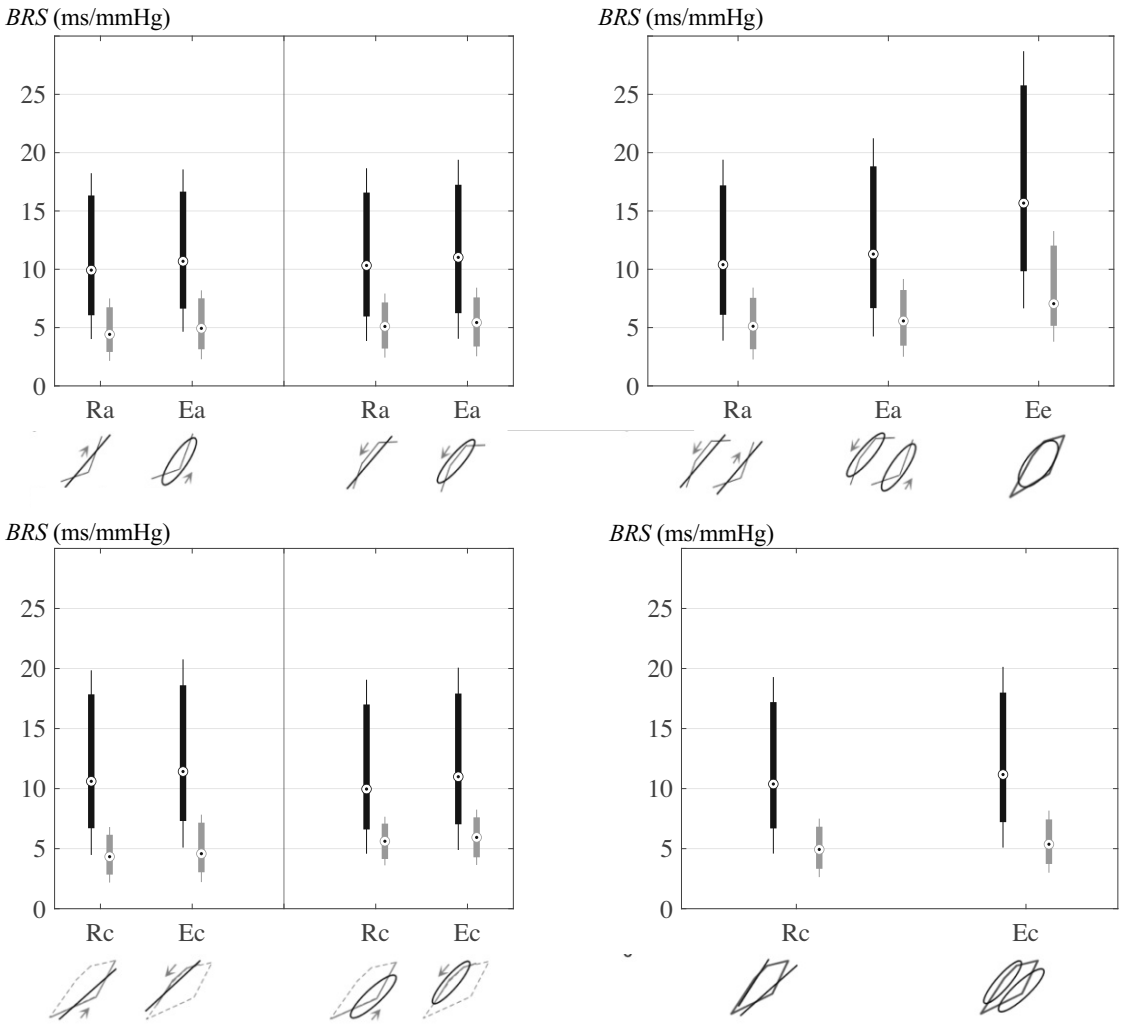

Figure 33 – Time domain *BRS* estimates.

Table 12 – Values of time domain *BRS* estimates

	# of Sequences	Supine	Standing	*p*
$R_{a,\,Up}$	680/609	10.5 (16.9 ± 42.6)	4.7 (6.8 ± 7.0)	< 0.005
$R_{a,\,Dn}$	870/951	10.6 (13.3 ± 11.9)	5.4 (6.8 ± 7.1)	< 0.005
R_a	1550/1560	10.6 (14.8 ± 29.6)	5.2 (6.8 ± 7.0)	< 0.005
$R_{c,\,Up}$	330/286	11.9 (17.3 ± 16.9)	4.4 (6.0 ± 6.3)	< 0.005
$R_{c,\,Dn}$	331/312	10.3 (13.2 ± 12.1)	5.8 (6.6 ± 4.7)	< 0.005
R_c	661/598	11.0 (15.2 ± 14.8)	5.3 (6.3 ± 5.5)	< 0.005
$E_{a,\,Up}$	631/575	11.5 (16.2 ± 17.0)	5.1 (7.4 ± 7.2)	< 0.005
$E_{a,\,Dn}$	809/908	11.2 (13.9 ± 11.9)	5.7 (7.1 ± 8.3)	< 0.005
E_a	1440/1483	11.3 (14.9 ± 14.4)	5.6 (7.2 ± 7.9)	< 0.005
$E_{c,\,Up}$	298/277	12.4 (17.9 ± 17.9)	5.0 (6.8 ± 7.0)	< 0.005
$E_{c,\,Dn}$	310/305	11.1 (13.4 ± 9.4)	6.1 (7.2 ± 5.1)	< 0.005
E_c	608/582	11.6 (15.6 ± 14.4)	5.2 (7.0 ± 6.1)	< 0.005
E_e	386/374	15.7 (29.6 ± 149)	7.0 (12.8 ± 25.5)	< 0.005

3.5. GUI app

In this section, windows of the GUI app are presented.

In Figures 34-33, the EuroBaVar dataset was used to illustrate the working of the four main windows of data processing and preparing for analysis. The *Main* window is designed to indicate to the user what is the logical order of buttons to press making the next logical button to press acquire a green colour (the logical order corresponds to the numbering in the flowchart below). In the *Data Upload* window, in Figure *35*, text warnings in green show up in the upper right corner to tell the user how to upload the data. After data has been processed, other buttons are enabled, e.g. *Data Visualization*, in Figure *36*. Context menus in the *Cardiovagal BRS* window in Figure *37* can be opened by right click of the mouse, information which is provided to the user in a pop-up warning message.

In Figures 34-37, this analysis is run on data acquired for this work, to test the efficiency of the app in evaluating different datasets. This data was acquired with the BioPac Student Lab (manufactured by BIOPAC Systems Inc., CA USA) and consisted of four signals: 3 lead electrocardiogram, blood pressure recorded with Finapres, pulse plethysmogram (PPG) and RESP-belt respirogram. The recording was acquired with a sampling frequency of 1000 Hz and lasted 10-12 minutes, in both supine and standing positions.

In the *Data Vis*ualization window in Figure 38, the peaks of the four signals are successfully identified for this subject. The respirogram is incorporated in the *Beat to beat analysis of lagged sequences* window in Figure 39, where a separate tab for analysis of sequences corresponding to moments of the respiratory cycle is found if the data includes this biosignal. The PPG is used to calculate PPG deflection[1] and this value is incorporated in the *Radar plot* window, as shown in Figure 41. The ellipse summary along with the decomposition of time series of *RR* and P_S for this subject is also illustrated in Figure 40.

[1] PPG deflection (ΔPPG) is defined as $\Delta PPG = \frac{p_S + 2 \cdot p_D}{3}$ where P_S and P_D are extracted from the PPG signal.

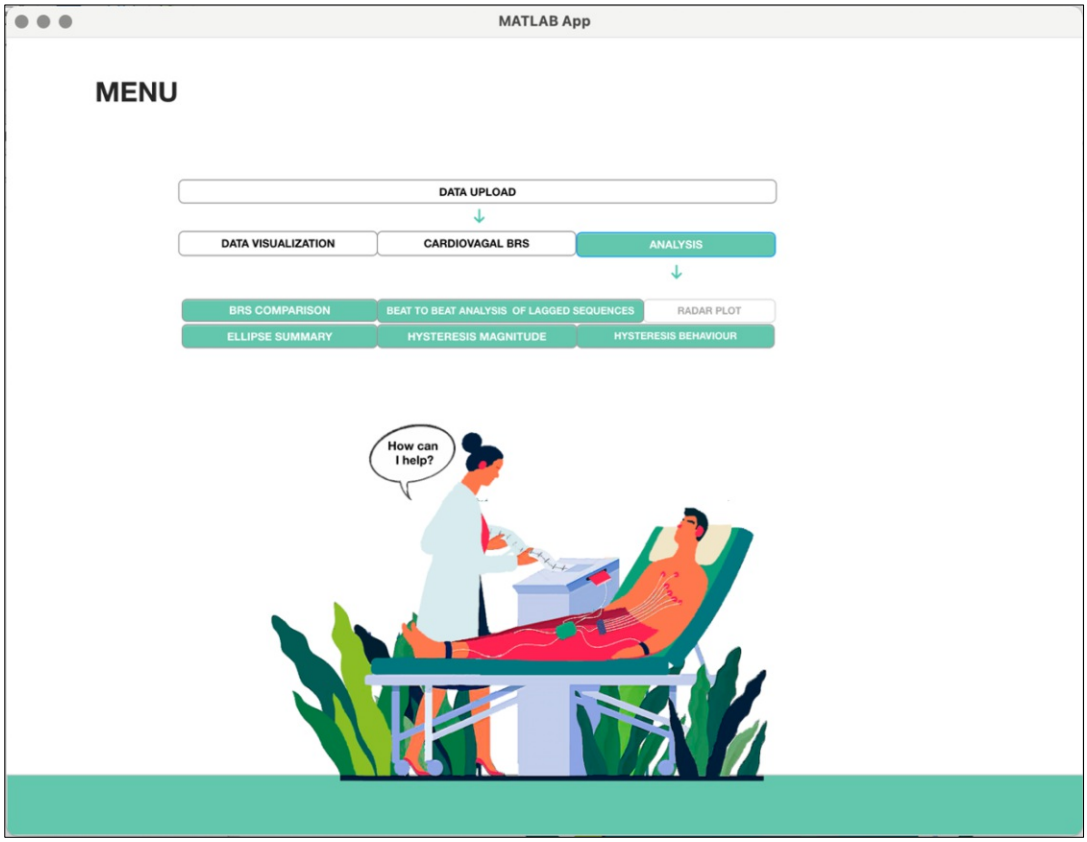

Figure 34 - *Main* window of the GUI.

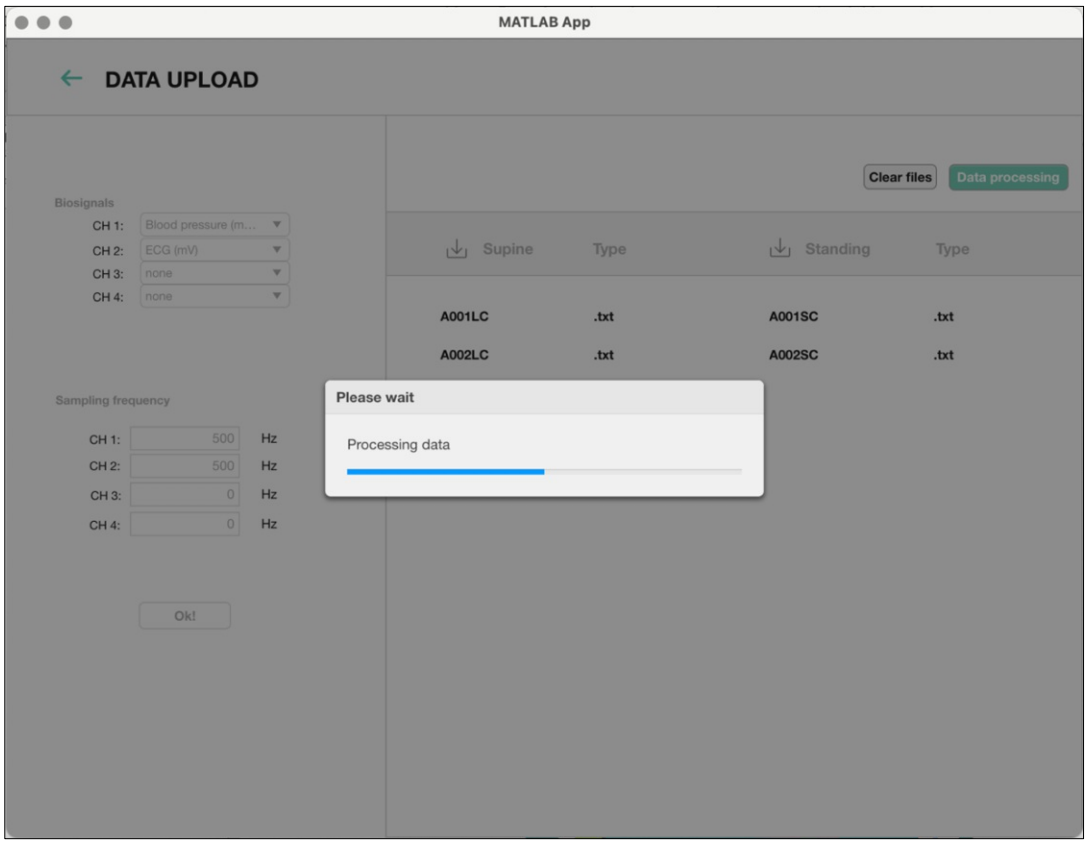

Figure 35 – *Data upload* window of the GUI.

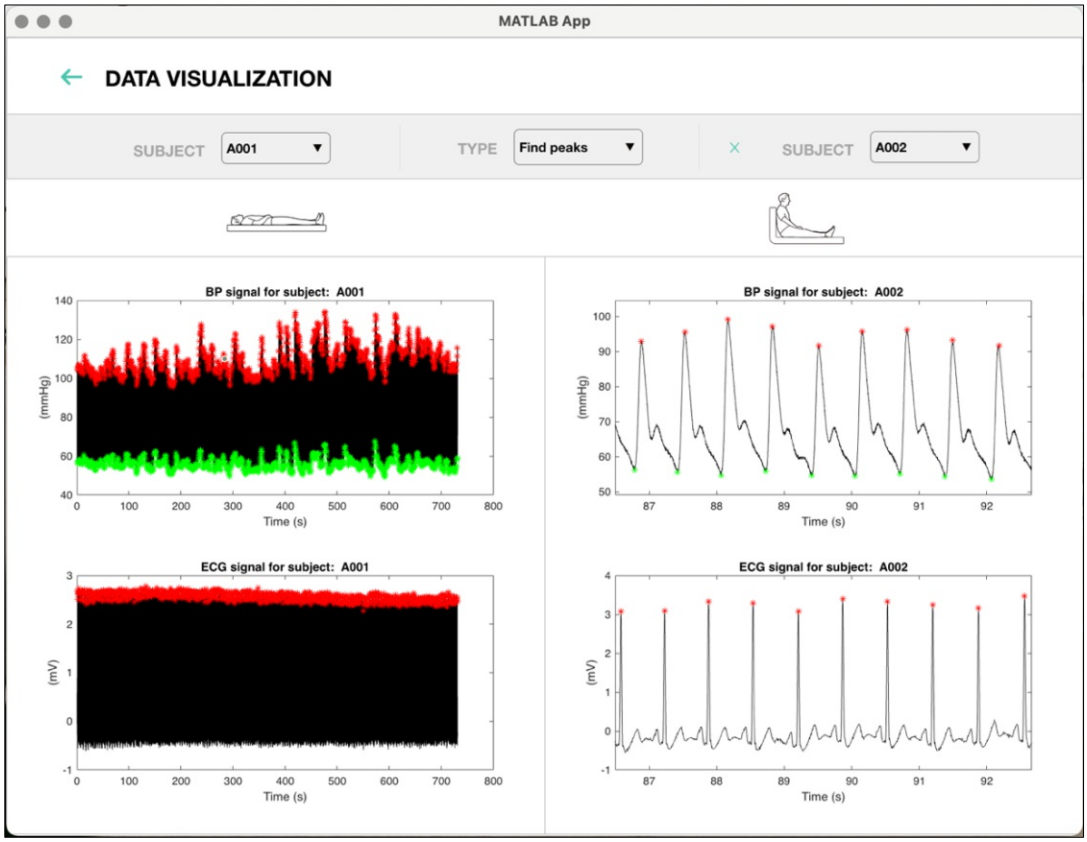

Figure 36 - *Data visualization* window of the GUI. The found peaks of ECG and *p* for subjects A1 in supine and A2 in standing positions can be inspected. Data for subject A2 was zoomed between 86 and 93 seconds of the total recording (600-720 seconds).

(A)

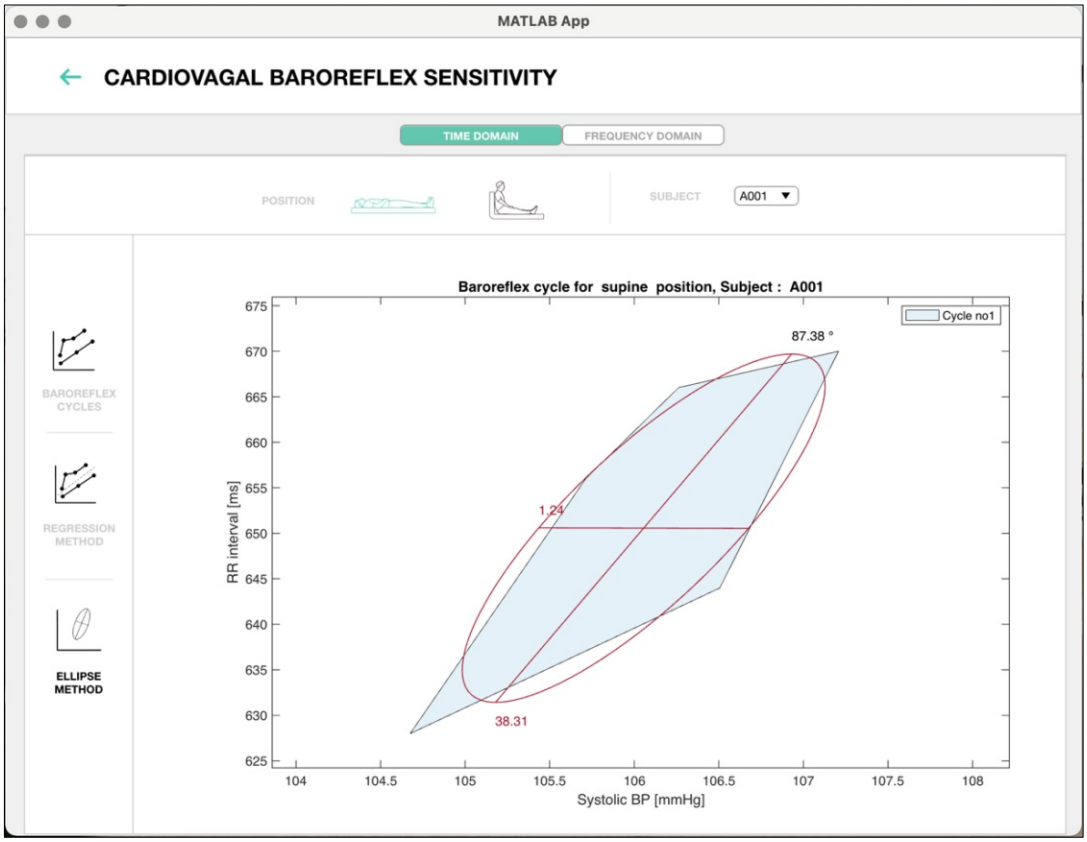

(B)

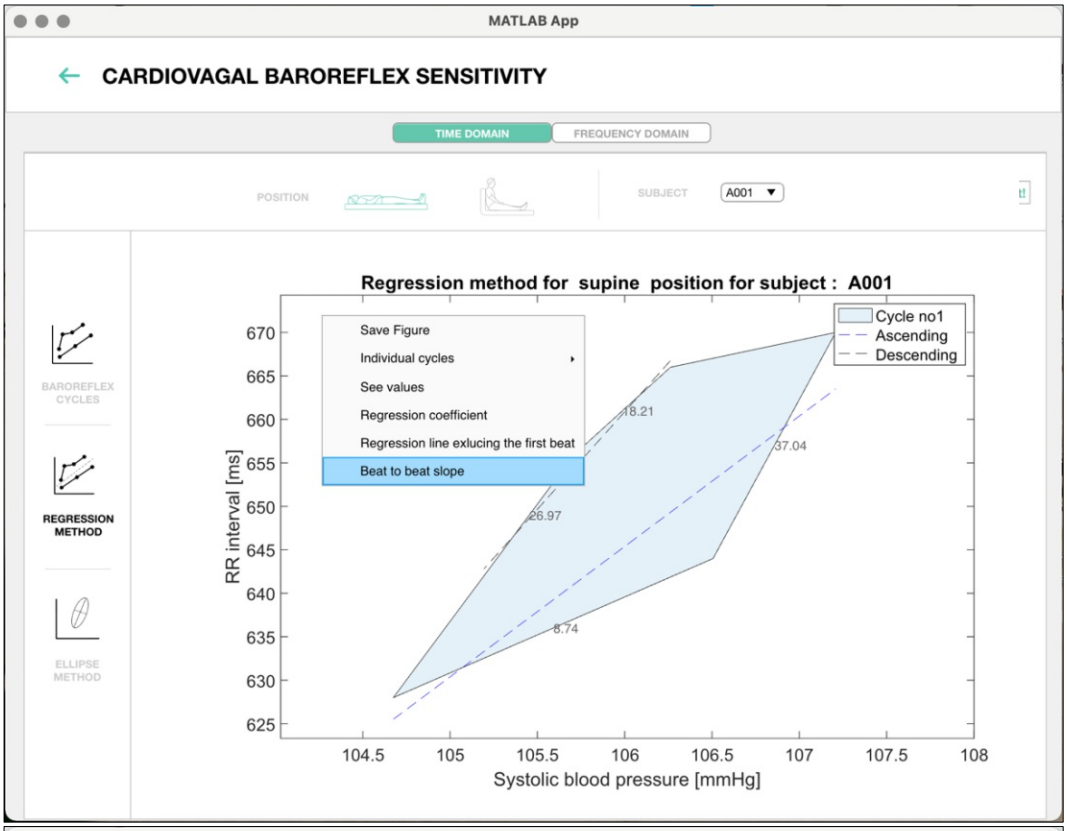

(C)

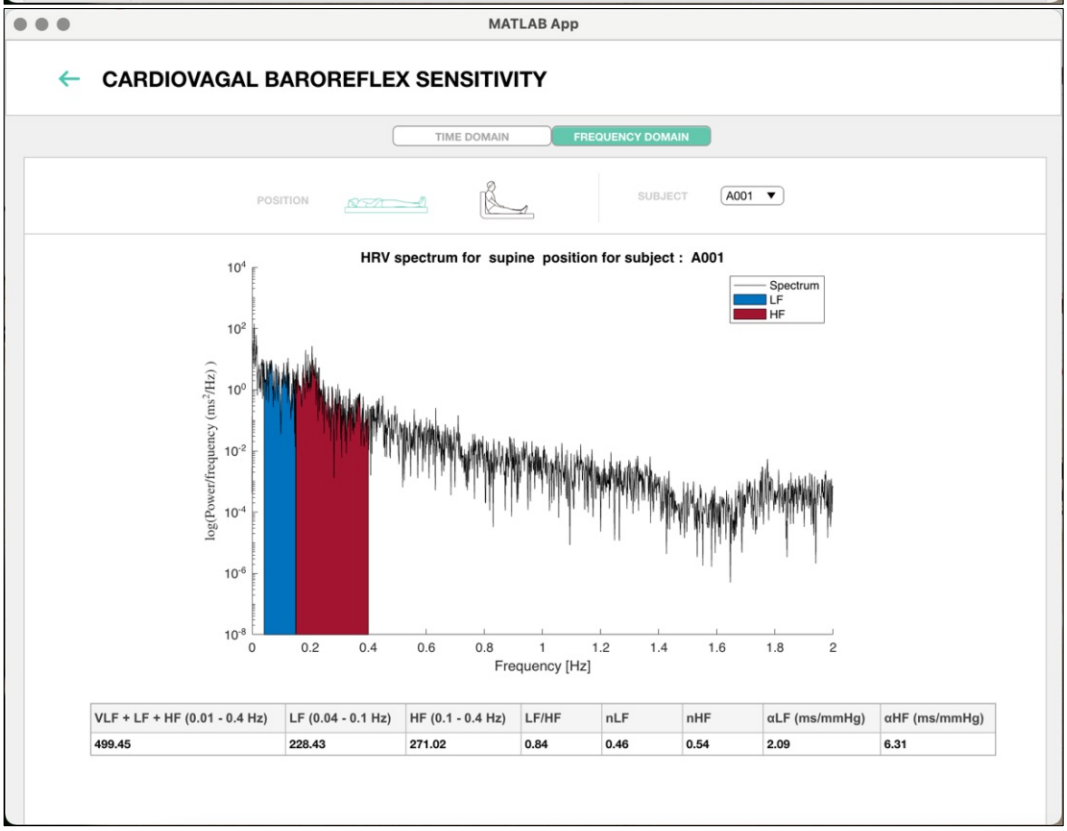

VLF + LF + HF (0.01 - 0.4 Hz)	LF (0.04 - 0.1 Hz)	HF (0.1 - 0.4 Hz)	LF/HF	nLF	nHF	αLF (ms/mmHg)	αHF (ms/mmHg)
499.45	228.43	271.02	0.84	0.46	0.54	2.09	6.31

Figure 37 - *Cardiovagal BRS* window of the GUI. In (A) and (B) the tab corresponding to the time domain *BRS* calculation is selected and in (C) the tab corresponding to the frequency domain *BRS*.

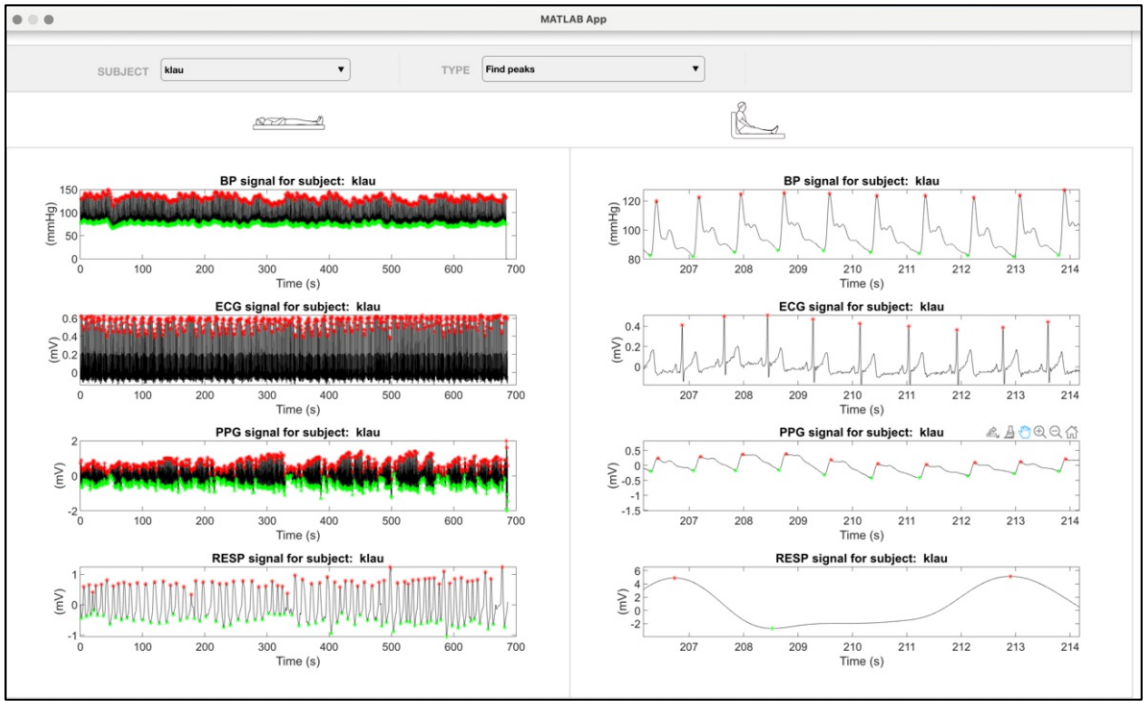

Figure 38 - *Data visualization* window of the GUI app with PPG and RESP-belt signals.

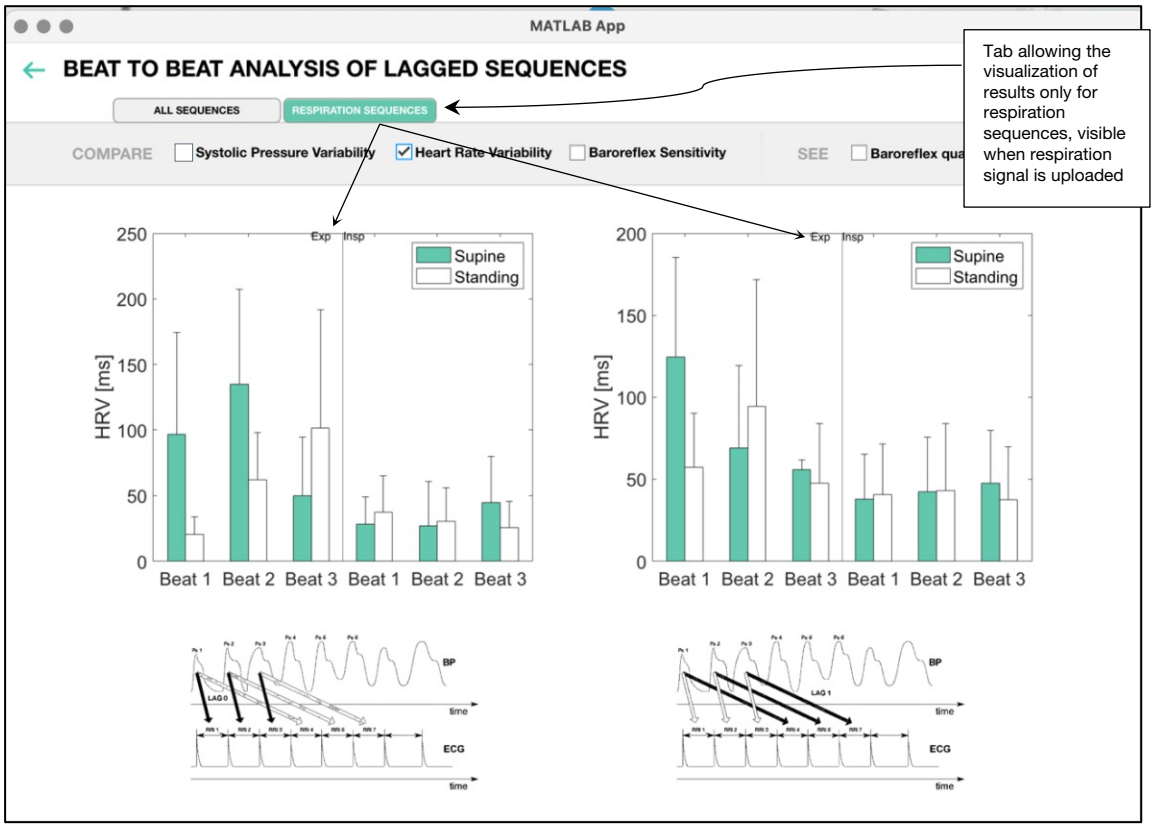

Figure 39 - Beat to beat analysis of lagged sequences window of the GUI app.

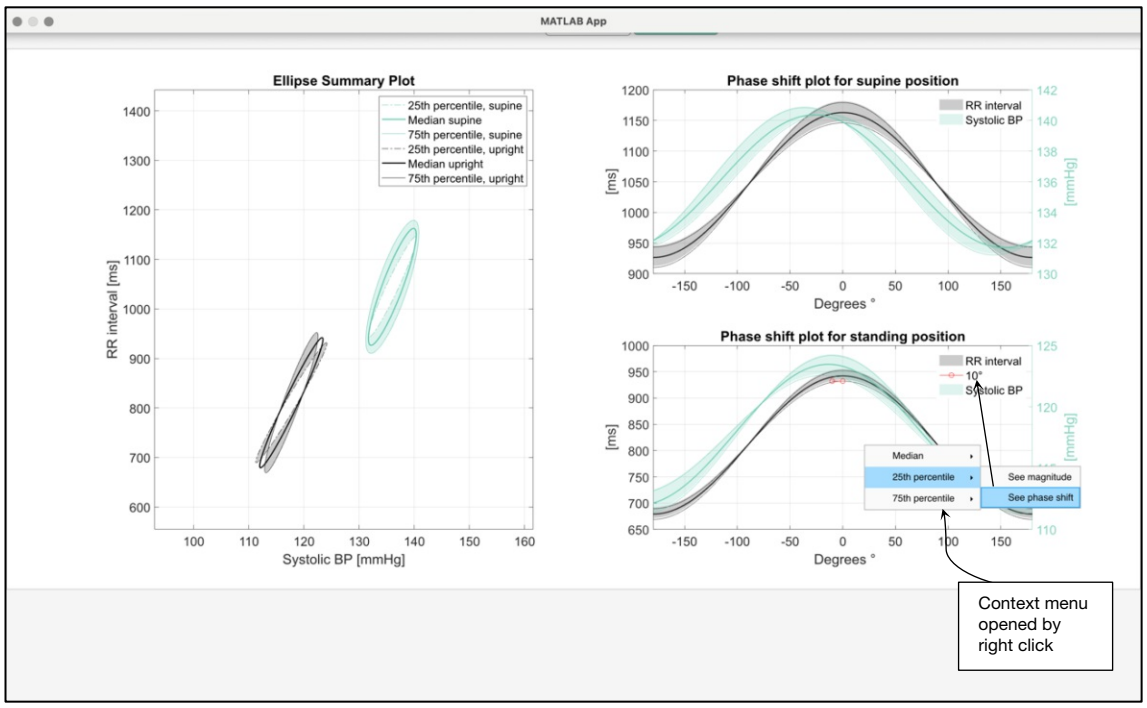

Figure 40 - *Ellipse Summary* window of the GUI app.

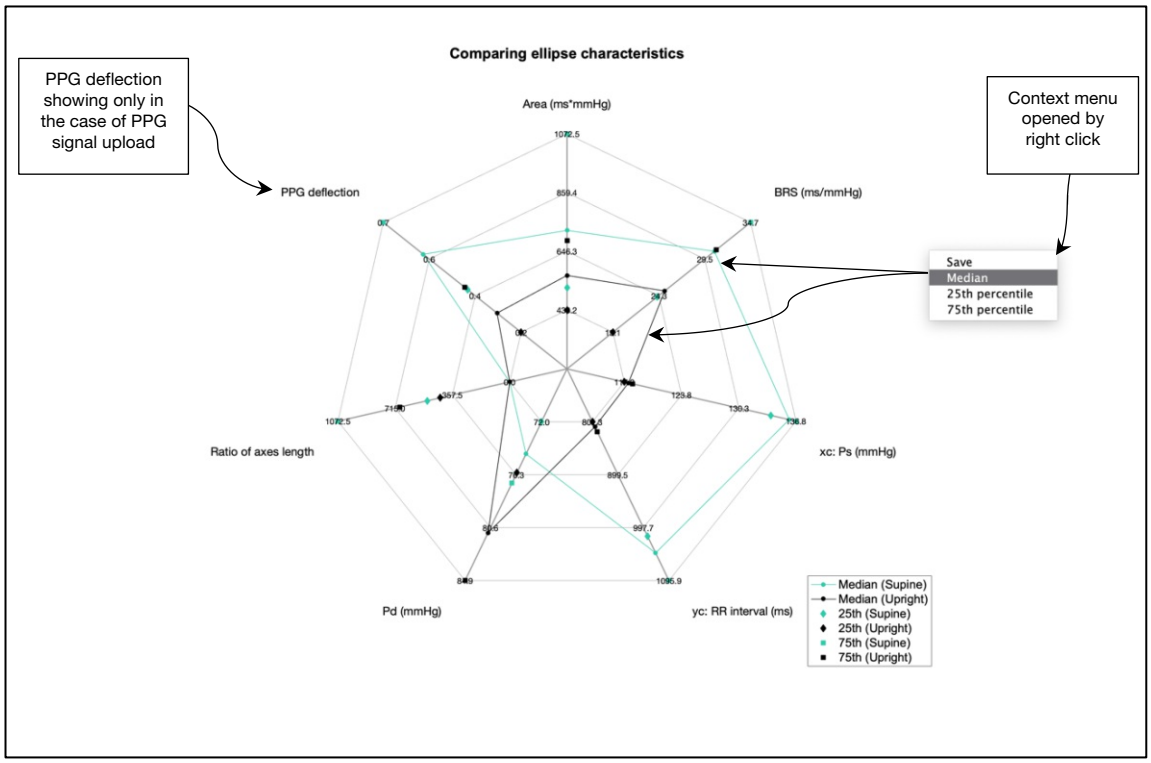

Figure 41 - *Radar plot* window of the GUI app.

CHAPTER **4.**

Discussion

The state-of-the-art techniques for assessment of baroreflex function aim to use spontaneous fluctuations of *RR* and P_S to extract sensitivity estimates, as opposed to the classical drug-infusion experimental setups. The advantage of using spontaneous sequences is that the recording is not limited in time by the inducing stimulus duration. Moreover, *BRS* from spontaneous fluctuations have been shown to reflect some pathologies more clearly by comparison with estimates from induced fluctuations (Millic *et al.* 2009). These techniques do not account for the dependence of the *RR*-P_S sigmoidal curve on the direction of pressure change, which creates a difference in the working point (quantitative) and slope (qualitative) of this curve between ascending and descending pressure values. An ellipse fit has been proposed to model the pattern formed by ascending and descending segments, in the case where the pressure changes are pharmacologically induced by the Oxford method (Ler *et al.*, 2010). Hence a reliable method that allows the characterization of the hysteresis behaviour from spontaneous pressure fluctuations can be regarded as a valuable tool for the understanding of the baroreflex.

This work presents a novel method based on the best-fit ellipse that characterizes the bivariate normal distribution of the pixel image formed by the *RR*-P_S pattern. The applicability of this method is investigated for the EuroBaVar dataset. Using this method individual sequences can be analysed and a *BRS* is obtained from the orientation of the best fit ellipse to that sequence that can be compared with the estimates from the usual regression method or spectral analysis. Furthermore, consecutive sequences of opposite trend representing the spontaneous variations observed during a respiration cycle can be analysed together and from the ellipse parameters, quantification of hysteresis can be performed. The coefficient of cross-correlation between the ellipses and the region formed by the consecutive sequences was 0.99.

The IQR and median ellipses for supine position are steeper and more elongated. The median ellipse suffers a decrease in orientation angle from 85.8° in supine to 81.5° in standing position or a 62% decrease in *BRS*. The decreased sensitivity means that for similar values of P_S, lower baroreflex outputs are achieved and the standing IQR ellipses are placed at a lower vertical position (y_c of 624.1 compared to 778.1 ms in supine).

The 50th ellipse in standing position has a major axis decrease of 32% and a minor axis increase of 61% in comparison with supine (Table 3), yielding the 70% increase in hysteresis index *H* (Table 7) even though no significant differences in area were found (Table 6). The cycles in

standing position are best fitted by a curve which closer in shape to the circle and in standing position by a more eccentric ellipse. The decreased PNS activity in standing position is accompanied by increased sympathetic outflow, which is verified by the increased value of P_D, leading to less linearity in the *RR*-P_S relation. Increased peripheral resistance by SNS activity is verified by the increased median value of P_D in standing position by 8% (Figure *23*).

In the drug-inducing method, the range of variation of P_S is around 10 mmHg (Taylor et al. 2013) while in the case of the spontaneous variations in this work were of 5.6 $\pm$ 3.7 for supine and of 7.9 $\pm$ 4.0 for standing positions (Table 8). The mean deflection of P_S is increased by over 40% in standing position and reciprocally the mean deflection of *RR* is decreased by over 30%. This trend is confirmed by the time series decomposition which shows a median value increase of P_S deflection over 2π (5.8 mmHg to 8.9 mmHg) and decrease of *RR* deflection over 2π (70.7 ms to 47.9 ms) and reflects the lowered cardiovagal sensitivity in standing position, due to gravity action on venous blood volume distribution. The lower baroreflex efficiency leads to an increased delay between the P_S and *RR* time series (from 39.4° to 41.3°).

The ellipse method proved as effective as other methods in identifying changes in sensitivity due to postural change and the percentage of sensitivity decrease (50-60%) in the estimates in standing position is the same as the one calculated for the regression estimates, from Table *12*. The results were concordant with the decrease obtained by Laude *et al.* (2004) for mean sensitivity estimates between supine (13.0 ms/mmHg) and standing (6.7 ms/mmHg).

There was a 20% decrease in sensitivity for the descending portion of the characteristic *RR*-P_S pattern compared to the ascending portion, in supine position. This trend is justified by the hysteresis behaviour dependence on the direction of pressure change, being usually more efficient when pressure rises. This effect is also reflected in Δ*BRS* in Figure 28, which are positive in 64% of cases for supine position, meaning that the slope of the ascending portion of the cycle is steeper.

In standing position, the differences related to the direction of pressure change are not significant due to the decreased vagal output in response to blood accumulation in peripheral vessels. Δ*BRS* is positive in only 37% of cases in standing position. Additionally, Δ*Setpoint* is decreased by median value in standing position (33.7 ms compared to 45.6 ms in supine). Given the assumption that the ascending portions of the cycle represent expiration phase and the descending portions represent inspiration phase, being the ellipse a representation of a full respiration cycle, this behaviour perfectly reflects the decreased baroreflex modulation of expiration for standing position described by Choy *et al.* (2006).

Studinger *et al.* (2007) found 22% of trials where the value of Δ*Setpoint* was positive and proposed that Δ*BRS* reflects the integrated mechanical and neural ruling in this behaviour while Δ*Setpoint* is governed mainly by neural influence. The results of this work appear to support this hypothesis since there were 6.2% in supine and 8.1% in standing positive Δ*Setpoint* trials, confirming that the hysteresis behaviour is not determined exclusively by vessel mechanics.

Although the ellipse method has the above-mentioned advantages, the quantification of hysteresis is still limited to the number of cycles. Only 7 (A1, A5, A6, B3, B7, B8 and B9) out of 21 subjects have more than 10 cycles (Figure 42) and among those, subject A5 mostly contributed for the number of cycles in supine position. Sequences of common trend did not exist or were less than five in the case of subjects A3, B4, B5, B10, and B13. Although an absence of *BRS* estimates might be linked to baroreflex impairment (Laude *et al.* 2004), it is not possible to affirm that and the unequal distribution of number of sequences/cycles among subjects may have influenced the results.

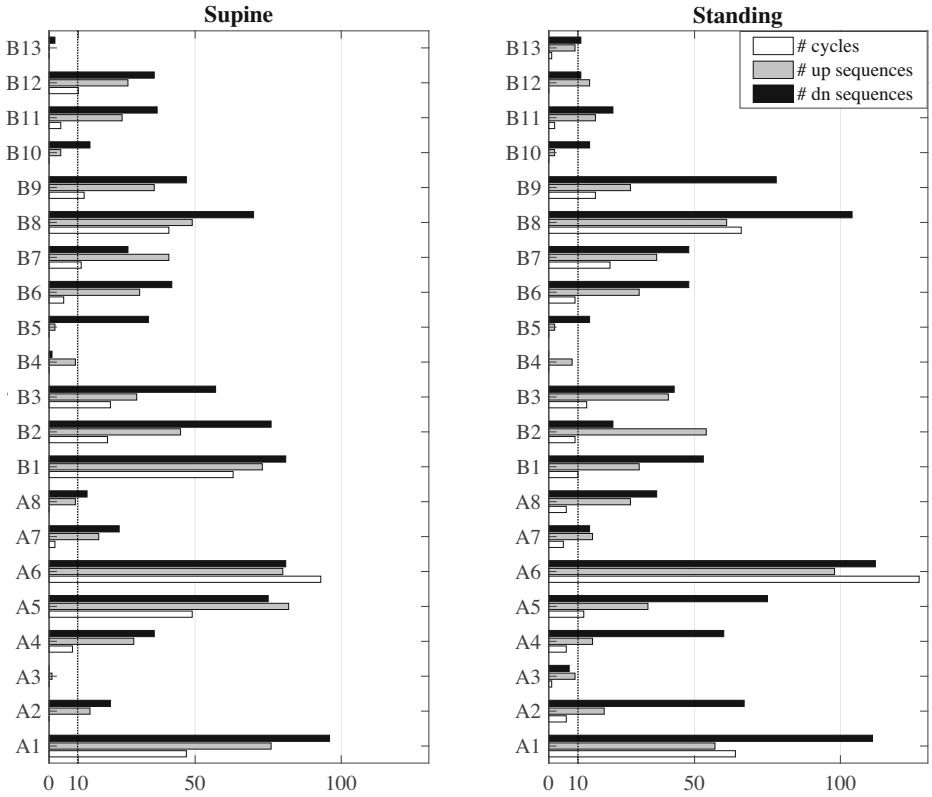

Figure 42 - Number of ascending (up) and descending (dn) sequences and cycles obtained for each subject in the EuroBaVar dataset.

An additional issue found in the course of this work was the difference found in some cases between the mean estimates of *BRS* and the median values (Table *12*) which is probably due to the frequency of outliers (> 10%). The occurrence of outliers is due to the calculation of *BRS* as tangent of the orientation angle of the ellipse. The asymptotic behaviour of the tangent function yields large variations in *BRS* for small orientation variations. This might have influenced the results obtained for this dataset.

Concerning other *BRS* assesment methods investigated in this work, although no direct comparison between ellipse estimates and frequency domain estimates is possible from the results, the trend of decreased *BRS* in standing position is confirmed in the spectral analysis estimates with statistical significance (αHF and LF/HF) in Table *11*. The HF power can be seen as a marker of vagally mediated baroreflex activity while the LF power is thought to reflect the action of both PNS and SNS (Task Force, 1996). The ratio αHF in ms/mmHg is obtained as a frequency domain *BRS* estimate and it showed a 59.1% decrease from supine to standing position, confirming the trend of 50-60% decreased sensitivity observed for all the time domain estimates obtained. Moreover, the αHF changed from 18.1 to 7.4 ms/mmHg, being much closer in absolute value to the time domain estimates in Table *12* than the estimates obtained from LF analysis, which corroborates the results obtained by Laude *et al.* (2004). The increased LF/HF power ratio, from 1.63 in supine to 2.65 in standing denotes the inhibited vagal nerve and promoted sympathetic activity in this position. These results are consistent with Choi *et al.* (2006), who found LF/HF power ratio 1.9 times superior in standing position for EuroBaVar dataset.

In the time domain, the determination of the ideal parameters to use as restriction to the sequences computed using the usual regression method has been subject of discussion (Laude *et al.* 2004, Steptoe & Vögele 1990). For that reason, in this work the effect of applying a lag of one beat between *RR* and P_S series and the average instantaneous variation in pressure were investigated before ellipse fitting.

Unlike the results obtained by Steptoe & Vögele (1990), no significant differences were found in the *BRS* estimates by applying the lag of one beat. Lag 0 sequences are preferable in terms of amount, since 68% for supine and 40% for standing additional sequences without delay were found in supine position (1648 and 1789) in contrast with lagged sequences (981 and 1309). Therefore, sequences concurrent in beat were selected for cycle analysis, also considering that they seem reflect the sensitivity decrease with postural change as accurately as lagged sequences and no significant difference in sensitivity is found by applying the delay (Table 10).

CHAPTER 5.

Conclusion and outlook

In conclusion, the ellipse method proved as efficient as the usual regression method in identifying the cardiovagal sensitivity decrease when moving from supine to standing position. The novelty brought by this method consists on estimating hysteresis from spontaneous (i.e. not induced by vasoactive drugs) fluctuations of P_S, e.g. the ones occurring during the breathing cycle, which can be a valuable advantage in the future study of the characteristic baroreflex *RR*-P_S pattern. Baroreflex sequences identified with the proposed ellipse method characterize hysteretic behaviour correspondent to a shorter range of PS deflections than the classical Oxford method, which can pose as a disadvantage.

Further approval with other datasets is necessary. The GUI app was designed to facilitate the application of the ellipse method in other datasets by any user. Further developments might also investigate the effect on stability of mean results when a different range of P_S and *RR* is selected for each cycle during pixel conversion, increasing the resolution in a personalized manner and cropping the cycle closer to its extremes.

List of Figures

List of Tables

References

Task Force of The European Society of Cardiology and The North American Society of Pacing and Electrophysiology, "Heart rate variability: Standards of measurement, physiological interpretation, and clinical use." (1997), in *European Heart Journal*, vol. 17, pp. 354–381.

E. E. Benarroch, "The arterial baroreflex: functional organization and involvement in neurologic disease." (2008), (in eng), in *Neurology*, vol. 71, no. 21, pp. 1733-8.

I. Bonhay, G. Jokkel, K. Karlocai, R. Reneman, and M. Kollai, "Effect of vasoactive drugs on carotid diameter in humans." (1997) in *American Journal of Physiology*, vol. 273, no. 4, *Heart and Circulatory Physiology*, pp. H1629-H1636.

M. W. Chapleau, "Baroreceptor reflexes " (2012) in *Primer on the Autonomic Nervous System (Third Edition): Academic press* ch. 33, pp. 161-165.

Y. Choi, S. Ko, and S. Ying, "Effect of Postural Changes on Baroreflex Sensitivity: A study on the Eurobavar data set," (2006) in *2006 Canadian Conference on Electrical and Computer Engineering*, pp. 110-114.

B. De Maria *et al.*, "Cardiac baroreflex hysteresis is one of the determinants of the heart period variability asymmetry." (2019), in *Am J Physiol Regul Integr Comp Physiol*, vol. 317, no. 4, pp. R539-51.

D. L. Eckberg and P. Sleight, "Human baroreflexes in health and disease.", (1992) vol. Oxford: Clarendon Press.

W. Feller, "An Introduction to Probability Theory and Its Applications" (1957), vol. 1. John Wiley & Sons.

E. W. Group. "EuroBavar DataSets for BRS Estimation." http://www.eurobavar.altervista.org/ (Last accessed 27 04 2021).

R. L. Hughson, L. Quintin, G. Annat, Y. Yamamoto, and C. Gharib, "Spontaneous baroreflex by sequence and power spectral methods in humans." (1993), in *Clinical Physiology*, vol. 13, no. 6, pp. 663-76.

B. E. Hunt, L. Fahy, W. B. Farquhar, and J. A. Taylor, "Quantification of mechanical and neural components of vagal baroreflex in humans." (2001), in *Hypertension*, vol. 37, no. 6, pp. 1362-1368.

A. V. Incognito *et al.*, "Arterial baroreflex regulation of muscle sympathetic nerve activity at rest and during stress." (2019), in *J Physiology*, vol. 597, no. 18, pp. 4729-4741.

A. V. Incognito *et al.*, "Sympathetic arterial baroreflex hysteresis in humans: different patterns during low- and high-pressure levels.", (2020), in *Am J Physiol Heart Circ Physiol*, vol. 319, no. 4, pp. H787-H792.

E. Kaniusas, "Biomedical signals and sensors, linking physiological phenomena and biosignals." (2012) ed: Springer, Berlin, Heidelberg.

M. T. La Rovere *et al.*, "Baroreflex sensitivity and heart-rate variability in prediction of total cardiac mortality after myocardial infarction. ATRAMI (Autonomic Tone and Reflexes After Myocardial Infarction) Investigators.", (1998), in *Lancet*, vol. 351, no. 9101, pp. 478-484.

D. Laude *et al.*, "Comparison of various techniques used to estimate spontaneous baroreflex sensitivity (the EuroBaVar study)." (2004), in *Am J Physiol Regul Integr Comp Physiol*, vol. 286, no. 1, pp. R226-R231.

A. S. Ler, M. A. Cohen, and J. A. Taylor, "A planar elliptical model of cardio-vagal hysteresis.", (2010), in *Physiol Meas*, vol. 31, no. 6, pp. 857-873.

M. Lowry, J. Windsor, and S. Ashelford, "Orthostatic hypotension 2: the physiology of blood pressure regulation." (2016), in *Nursing Times*, vol. 112, 43/44, pp. 17-19.

H. Malberg *et al.*, "Advanced analysis of spontaneous baroreflex sensitivity, blood pressure and heart rate variability in patients with dilated cardiomyopathy." (2002), in *Clin Sci (Lond)*, vol. 102, no. 4, pp. 465-473.

J. Malmivuo and R. Plonsey, "Bioelectromagnetism - Principles and Applications of Bioelectric and Biomagnetic Fields." (1995), vol. Oxford University Press, New York.

Mathworks, "simplify Documentation." https://de.mathworks.com/help/matlab/ref/polyshape.simplify.html (Last accessed 29 04 2020).

Mathworks, "findpeaks Documentation." https://de.mathworks.com/help/signal/ref/findpeaks.html (Last accessed 30 04 2020).

M. Milic, P. Sun, F. Liu, C. Fainman *et al.* "A comparison of pharmacologic and spontaneous baroreflex methods in aging and hypertension." (2009), in *Journal of hypertension*, vol. 27, 6, pp. 1243–1251.

H. Moellering and J. N. Rayner, "The Harmonic Analysis of Spatial Shapes Using Dual Axis Fourier Shape Analysis (DAFSA)." (1981), in *Geographical analysis*, vol. 13, no. 1, pp. 64-77.

D. D. O'Leary, D. S. Kimmerly, A. D. Cechetto, and J. K. Shoemaker, "Differential Effect of head-up tilt on Cardiovagal and Sympathetic Baroreflex Sensitivity in Humans." (2003), in *Experimental Physiology*, vol. 88, no. 6, pp. 769-774.

G. Parati *et al.*, "Evaluation of the baroreceptor-heart rate reflex by 24-hour intra-arterial blood pressure monitoring in humans." (1988), in *Hypertension*, vol. 12, no. 2, pp. 214-222.

J. Penáz, "Photoelectric measurement of blood pressure, volume and flow in the finger." (1973), in *Digest of the 10th International Conference on Medical Engineering*, vol. 104.

R. Pflanzer, J. C. Uyehara, and W. McMullen, "Physiology Lessons for use with the Biopac Student Lab: ELECTROCARDIOGRAPHY I," vol. BIOPAC Systems Inc.

T. G. Pickering and J. Davies, "Estimation of the conduction time of the baroreceptor-cardiac reflex in man." (1973), in *Cardiovasc Res.*, vol. 7, no. 2, pp. 213-219.

S. W. Porges, R. E. Bohrer, M. N. Cheung, and F. Drasgow, "New time-series statistic for detecting rhythmic co-occurrence in the frequency domain: The weighted coherence and its application to psychophysiological research." (1980), in *Psychological Bulletin*, vol. 88, 3, pp. 580-587.

G. Raczak *et al.*, "Arterial baroreflex modulation of heart rate in patients early after heart transplantation: lack of parasympathetic reinnervation." (2004), in *Clinical Heart Transplantations*, pp. 399-406.

R. F. Rea and D. L. Eckberg, "Carotid baroreceptor-muscle sympathetic relation in humans." (1987), in *The American Journal of Physiology*, vol. 6 pt 2, pp. 929-934.

H. W. J. Robbe *et al.*, "Assessment of baroreceptor reflex sensitivity by means of spectral analysis." (1987), in *Hypertension*, vol. 10, pp. 538-543.

L. Rudas *et al.*, "Human sympathetic and vagal baroreflex responses to sequential nitroprusside and phenylephrine." (1999), in *Am J Physiol*, vol. 276, no. 5 pt 2, pp. H1691-H1698.

E. Santos-Fernández, "Multivariate Statistical Control Using R." (2012), Springer.

A. Steptoe and C. Vögele, "Cardiac baroreflex function during postural change assessed using non-invasive spontaneous sequence analysis in young men.", (1990), in *Cardiovasc Res*, vol. 24, no. 8, pp. 627-632.

P. Studinger, R. Goldstein, and J. A. Taylor, "Mechanical and neural contributions to hysteresis in the cardiac vagal limb of the arterial baroreflex." (2007), in *J Physiol*, vol. 583, Pt 3, pp. 1041-1048.

C. E. Taylor, C. K. Willie, G. Atkinson, H. Jones, and Y. C. Tzeng, "Postural influences on the mechanical and neural components of the cardiovagal baroreflex." (2013), in *Acta Physiol (Oxf)*, vol. 208, no. 1, pp. 66-73.

A. Trzebski and M. Smietanowski, "Non-linear dynamics of cardiovascular system in humans exposed to repetitive apneas modeling obstructive sleep apnea: Aggregated time series data analysis." (2001), in *Autonomic Neuroscience: Basic and Clinical*, vol. 90, pp. 106–115.

B. Wang, W. Shi, and Z. Miao, "Confidence Analysis of Standard Deviational Ellipse and Its Extension into Higher Dimensional Euclidean Space." (2015), in *PLoS ONE*, vol. 10, no. 3.

F. Yasuma and J. Hayano, "Respiratory sinus arrhythmia: why does the heartbeat synchronize with respiratory rhythm?" (2004), in *Chest*, vol. 125, no. 2, pp. 683-690.

D. Zemaityte, "Autonomic regulation of heart rhythm: mechanisms, registration, clinical value." (1997), Kaunas Medical Academy Publisher.

Appendix A

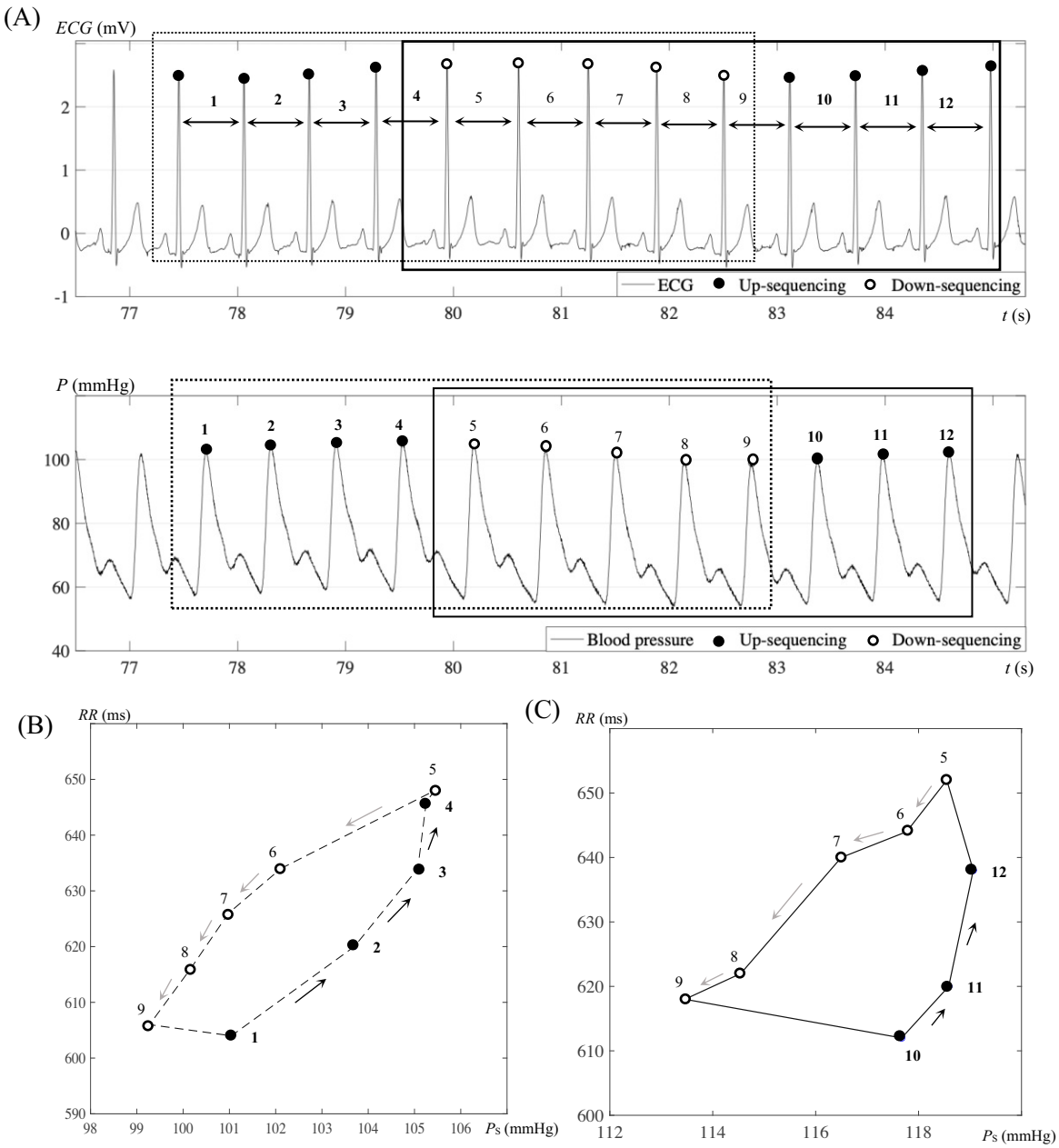

Figure A.1 - Redundancy of the baroreflex cycles. (A) Odd number of consecutive sequences. The descending sequence is simultaneously part of two distinct baroreflex cycles, marked with (C) normal and (B) dotted lines. Data from subject A1 in supine position.

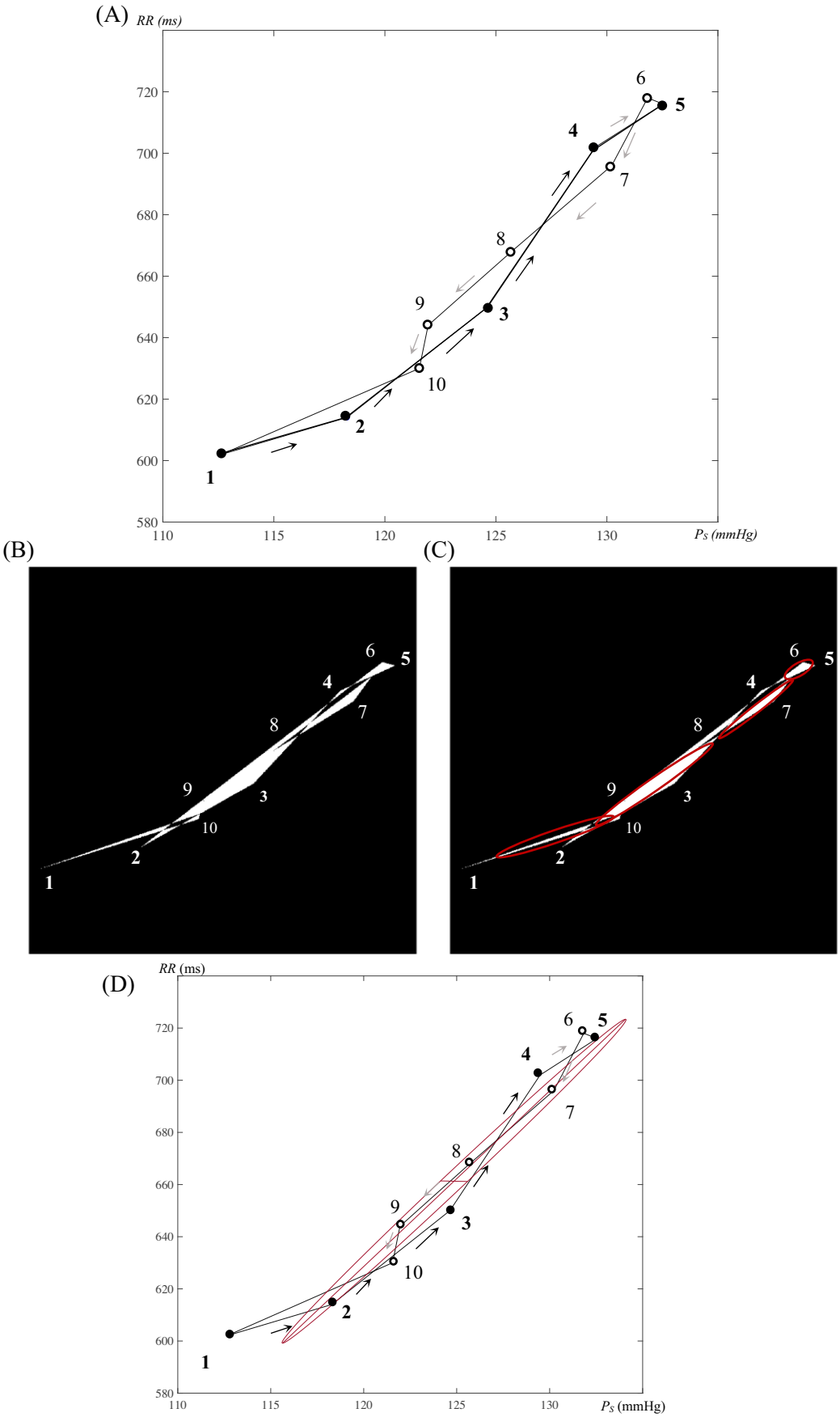

Figure A.2 - Representative example of (A) a baroreflex cycle region with multiple regions. Pixel image of the region in (B) and with ellipse fit from region props in (C). The chosen resolution

was 10 000 x 10 000 px and the image was cropped to facilitate visualization. Final best-fitted ellipse in (D). Data from subject A1 in supine position.

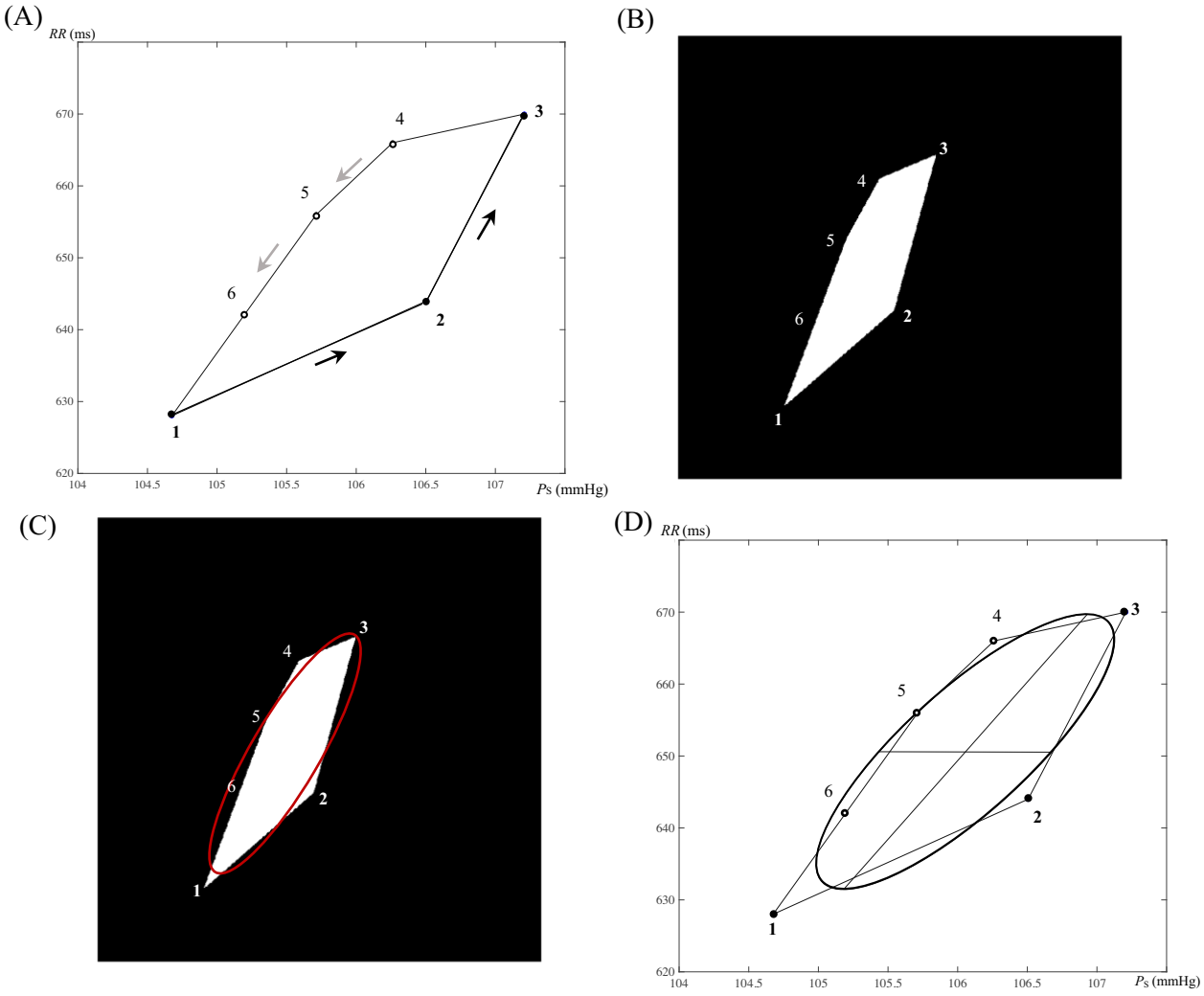

Figure A.3 - Black and white image of a baroreflex cycle region after transformation of (A) its vertices into (B) pixel coordinates. The chosen resolution was 10 000 x 10 000 px and the image was cropped to facilitate visualization. The ellipse fit obtained from *regionprops* is shown in (C) and (D) corresponds to the final product, with the ellipse scaled back to original coordinates. Data from subject A1 in supine position.